Laboratory core flooding experiments for bio-conversion of coal with overburden pressure

by
Arnab Guha

A thesis submitted in partial fulfillment of the requirements for the degree of

Master of Science

Department of Mechanical Engineering
University of Alberta

Abstract

An experimental facility was constructed in order to examine the feasibility of the coal bio-conversion under the application of confining pressure. The main purpose of this work was to investigate the effect of confining pressure on methane generation. Core-flooding experiments were conducted for 180 days using a Hassler type core holder with confining pressure at 6205 kPa(g) and back pressure at 3447 kPa(g). Crushed coal with total mass of 666.5 grams and particle size ranging from 150-250 microns was packed inside the core holder. Calculated porosity and permeability of the porous media were 35.65% and 8.53 mD, respectively. The core was flooded initially with 2.2 pore volumes (*PV*) of mineral salt medium (WR-86) and Tryptone solution to achieve a fully saturated porous media. This was followed by inoculation with 1.3 *PV* of microbial culture solution (QSAF). *In-situ* temperature measurements at different locations of the coal pack were obtained using T type thermocouples. Confining pressure had a positive impact on methane generation. Carbon dioxide production was less in the case of core flood runs operated with confining pressure in comparison to the literature results operated without confining pressure. The metabolites formed during the bio-conversion process confirmed anaerobic biodegradation of coal constituents. The temperature of the coal pack was relatively constant throughout the core flooding experiments.

Preface

Some of the research conducted for this thesis forms part of a research collaboration, led with Dr. Julia Foght of Biological Sciences Department at the University of Alberta, Dr. Karen Budwill at Alberta Innovates Technologies Future (AITF), Dr. David S. Nobes at University of Alberta with Dr. Sushanta K. Mitra being the lead collaborator at the University of Alberta. The technical apparatus referred to in chapter 3 was set up by myself, with the assistance of Aleksey Baldygin. The software with graphical user interface used to carry out experiment in current project and collect data from pressure and temperature data acquisition units were developed by Aleksey Baldygin. Results and Discussions in chapter 4 and the summary of the results obtained from core flooding runs with overburden pressure in chapter 5 are my original work, as well as the literature review in chapter 2. No part of this thesis has been previously published.

To My Parents and Almighty God

Acknowledgements

I would like to thank my supervisor, Dr. Sushanta K. Mitra for his constant guidance and support over the last two years. He introduced within me the professionalism which is very much essential for the research work. I am also thankful to my co-supervisor, Dr. David S. Nobes for his motivation and useful discussions during the course of research.

I would like to thank the external examiners of MSc. Thesis committee: Dr. Marc Secanell and Dr. Hongbo Zeng for reviewing my thesis.

I am also thankful to my colleagues and Micro and Nano-scale Transport Laboratory group members for their help and support. I am really grateful to Aleksey Baldygin and Anil Stephen for their immense help during the course of my research. Aleksey never failed to inspire me during my MSc. program and his helpful nature and guidance often made things simpler for me. I am thankful to him for his valuable assistance in building the set up for my experiments.

I greatly acknowledge Dr. Karen Budwill and Twyla Malcolm at AITF for providing me the inoculum and stimulated formation fluid required for my experiments. I am also thankful to Annie Wong, Anh Dao and Dr. Julia Foght for their assistance in GC and GCMS analyses respectively. I acknowledge Shihong Xu for his help in performing the SEM-EDX analysis. I am thankful to TransAlta and Sherritt coal for providing me the sub-bituminous coal for my experiments. I am also grateful to Carbon Management Canada for providing me the financial support for performing the experiments.

Contents

List of Tables

List of Figures

Chapter 1

Introduction

1.1 Motivation

Fossil fuels comprising of oil, coal and natural gas constitute the major energy sources in the present scenario. Burning of fossil fuels lead to significant amount of carbon dioxide emissions in the environment and can result in severe environmental and health hazards [1]. Global Carbon Project stated that combustion of coal, oil and gas contribute to 43%, 33% and 18% of the global CO_2 emissions respectively in 2012 [4]. Emissions of CO_2 were expected to increase to 36 billion tonnes which is 61% above the emission level in 1990 [4]. Presently, coal is one of the most widely utilised energy resources which has reservoirs across 70 different countries [5]. Coal is mainly consumed worldwide for electricity generation. In 2011, 62% of the globally produced coal was consumed by electricity sector and apart from electricity generation, coal is also used in industrial, commercial and residential sectors respectively [5]. Currently, coal provides 29.7% of the energy produced globally, but is also a major contributor for global carbon dioxide emissions [5]. In order to fulfill the high energy demand and to reduce greenhouse gas emissions, low carbon technologies like *in-situ* bioconversion of coal into methane can be a promising alternative solution.

Coalbed methane (CBM) has gained its popularity as one of the most unconventional natural gas resources across USA, Canada and Australia [6]. Coal seam permeability and gas content are the two most important factors governing the effi-

ciency of CBM production [6]. Coalbed methane is generally recovered by means of primary and enhanced recoveries respectively. Primary CBM production refers to the depletion of reservoir pressure to allow for methane gas desorption from coal. In case of enhanced CBM production, mostly a dissimilar gas like CO_2 is injected into the coal seam. CO_2 displaces CH_4 from the coal seam as it has more affinity towards coal in comparison to CH_4. Such recoveries can eventually lead to dwindling of CBM reserves to such an extent that there will be practically no methane after some point of time. Hence, methane generation in coal beds can also be enhanced by implementing *in-situ* bioconversion of coal in presence of microbial species. Methane recovered during the bioconversion process can be a potential source for a cleaner fuel which can not only meet the high energy demand but also can extend the life of the CBM reservoirs.

The main motive of the present research work is to investigate the potentiality of *in-situ* bioconversion of coal into methane under the application of confining pressure. To the best of our knowledge, there are few published works on coal bioconversion and only one laboratory scale study involving the bioconversion process has been performed so far. But, the experimental study related to coal bioconversion did not take into account the effect of confining pressure on methane recovery [1]. The present experimental study focuses on simulating the actual coal reservoir conditions from the laboratory scale point of view in a more realistic manner compared to the one done earlier without confining pressure. Current experimental setup also gives us the opportunity to examine the temperature changes for the first time during the ongoing bioconversion process.

1.2 Objective

The objective of the current study is to investigate the feasibility of the laboratory core flooding experiments involving bio-conversion of coal under the effect of overburden pressure.

The present experimental setup aims to:

- Implement the concept of confining pressure to the existing core flooding setup for coal bioconversion by using Hassler type core holder [1].
- Compare the methane generation data with and without confining pressure [1].
- Study the effect of overburden pressure on coal methanogenesis.
- Investigate the *in-situ* temperature changes inside the core holder for the first time during the ongoing coal bio-conversion process.
- Examine the coal microbe interaction and consequent permeability changes of the packed coal simulating the actual coal reservoir under the application of overburden pressure .

The thesis consists of five chapters. The first chapter depicts the motivation and the objectives of the current research work. The second chapter of the thesis focusses on the literature survey of the existing work related to coal bioconversion. Literatures related to core flooding experiments under the effect of confining pressure have been given a special emphasis. The experimental setup of the current research work has been described in details in chapter 3. Chapter 3 also provide a thorough idea about the experimental procedure and the measurement techniques involved in quantification of gases and metabolites formed during the bioconversion process. In chapter 4, the methane and carbon dioxide generation rates, consequent changes in permeability of the coal pack, porosity of the coal pack, key metabolic byproducts formed during the bio conversion process and the subsequent changes in effluent pH in presence of overburden pressure have been compared with the case devoid of overburden pressure. Chapter 5 provides a brief summary of the current research work and also paves the pathway for future studies related to the current experimental setup.

Chapter 2

Literature Survey

2.1 Origin of methane

Methane generation in a coal reservoir can occur from either thermal breakdown of kerogen or demethylation of organic molecules via bacterial species or from the reduction of CO_2 [7]. Thermal generation of hydrocarbon gases begin for a coal rank which has an approximate vitrinite reflectance of 0.6 %. Thermal generation of methane increases with an increase in vitrinite reflectance of the coal. Vitrinite reflectance is also related to the coal maturity. Thermogenic methane production is usually linked with coals possessing high maturity like bituminous and anthracite coals which are generally found at sub-bottom depths [8].

Biogenic methane production is usually associated with low maturity coals and also with coal seams of shallow depths [9, 7]. Biogenic methane generation generally starts in the course of peatification process and the production carries on till the coalification process ends. Biogenic methane can be recovered more easily in comparison to the thermogenic methane due to its production in low permeable and shallower coal seams [8]. The origin of methane production in coal seams can be known from the carbon and hydrogen stable isotope analysis of CH_4, CO_2 and formation water respectively [10, 11]. Methane content found in basins as for e.g. Alberta basin [12], Black Warrior basin [13], Illinois basin [11, 14, 15], Colorado basin [10], Powder River basin [16, 17] and San-Juan basin [10, 18] are considered to be of biogenic origin. However,there are basins like Bowen, Sydney and Surat

basins [19, 20] in Australia and San-Juan basin [21, 10, 18] in United States where the methane content has been proven to be a mixture of biogenic and thermogenic origins respectively.

2.2 Biodegradation pathways for coal

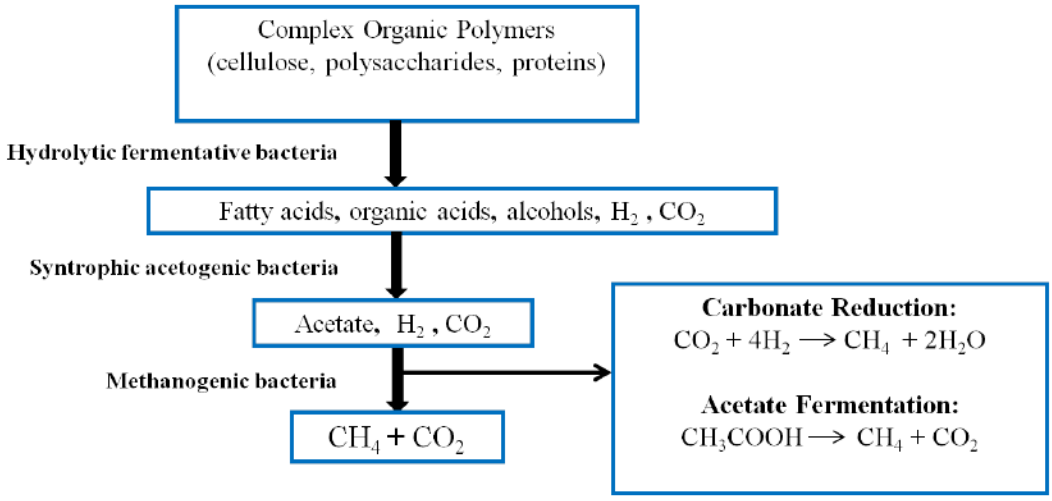

Figure 2.1: Flow diagram dictating the bioconversion pathways (adopted from [2, 3])

.

Coal is considered as a complex polymeric structure comprising of aromatic and polycyclic rings with hydroxyl, carboxyl or methoxy groups attached to it. It is derived from lignin which is also a biologically produced polymer with moderate biodegradability. Three types of bacterial species are mainly involved in the coal biodegradation process namely hydrolytic fermentative bacteria, syntrophic acetogenic bacteria and the methanogenic bacteria respectively.

Fermentative microbes hydrolyses the complex polymeric coal structure into longer chained fatty acids, acetate (CH_3COO^-), carbon dioxide, hydrogen, ammonia (NH_3) and hydrogen sulphur (HS^-) [3]. Low molecular weight fatty acids like propionate and butyrate are the most common byproducts of fermentation process. The role of syntrophic acetogenic bacteria is to oxidise these low molecular weight

acids into acetate and CO_2 in case of propionate. Hydrogen or formate ($HCOO^-$) is also formed as the reduced product during the oxidation process. Methanogens therefore utilise CO_2, H_2 and $HCOO^-$ as the substrates for the methanogenesis [3]. There are basically two main pathways for methane generation namely carbon dioxide reduction pathway and the acetoclastic pathway respectively. Carbon dioxide is reduced into methane by hydrogenotrophic methanogens using hydrogen as the electron source in CO_2 reduction pathway. In acetoclastic reaction, acetoclastic methanogens use acetate as the substrate and produce CH_4 by the transfer of the methyl group.

Experiments suggest that $\frac{2}{3}$ of the methane generation occurs through acetoclastic pathways and the rest (i.e. $\frac{1}{3}$) occurs from CO_2 reduction pathways [22]. Methane generation in both the pathways depend on the availability of H_2. In carbonate reduction process,the source of H_2 is the formation water present in the coal seams. In acetoclastic fermentation process,$\frac{3}{4}$ of H_2 is supplied from the acetate itself and the rest fraction of H_2 is supplied from either formation water or from the fermentation process of the complex coal structure. There are couple of hypotheses regarding the rate limiting step for the coal bioconversion. One hypothesis states that the initial fermentation process leading to the breakdown and solubilisation of complex coal structure into intermediate substrates as for e.g. fatty acids, acetate and CO_2 may be the crucial or rate limiting step for coal biodegradation [23]. Another hypothesis indicates methanogenesis as the predominant step for coal bioconversion when the concentration of trace elements as for e.g. zinc and cobalt are limited and the enzymatic activities cease [24]. Carbon and hydrogen stable isotope analysis can predict the most dominant pathway for methanogenesis in coal basins. Isotope analysis states that carbon dioxide reduction as the dominant pathway for Australian coal basins like Sydney, Bowen and Surat [19, 20], while in powder river basin, isotope analysis suggests that acetoclastic reaction is the dominant pathway for coal methanogenesis [21, 16, 17, 25].

2.3 Microbial species involved in coal biodegradation

Different bacterial and archaeal species are involved in bioconversion of coal into methane. Proteobacteria, Firmicutes as for e.g. *Clostridia* sp., Bacteroides and Actinomycete [26, 27] are involved in breaking down the complex polymeric structures into monomers as for e.g. fatty acids, sugars and acetate. *Desulfobulbus* sp., a sulfate reducing bacteria plays the role of syntrophic acetogenic bacteria in order to aid the bioconversion process [26, 27]. Methanomicrobiales and Methanosarcinales are the two most common forms of methanogenic archaea associated with methanogenesis [26, 27, 28, 29, 25]. Methanosarcinales utilize acetate and methyl group containing compounds as substrates for methanogenesis. Methanomicrobiales uses formate, hydrogen and carbon dioxide as substrates for methanogenesis. Methanogens are strictly anaerobic in nature. 16S rRNA pyrotag sequencing results of the coal core which was initially inoculated with bacterial species and flooded with mineral salts medium along with tryptone for 90 days depict the presence of methanogens like *Methanobacterium* and *Methanosarcina* along the inlet section of the core [1]. *Methanobacteria* and *Methanosarcina* produce methane via hydrogenotrophic and acetoclastic pathways respectively. Different Clostridia species like *Sedimentibacter* and *Peptostreptococcaceae* are found mostly in the inlet section of the core. *Desulfosporosinus* and *Peptococcaceae* are the most abundant Clostridia species found along the central and outlet sections of the core at the end of core flooding experiments [1]. Clostridia are basically fermentative anaerobes which deal with metabolism of aromatic compounds present in the coal.

2.4 Metabolic by products of coal biodegradation

Metabolite analysis of the coal formation water can give us a clear picture regarding the possible bioconversion pathways occurred in a particular coal seam. In general, longer chain alkane, ethers, cyclic aliphatic compounds, fatty acids like hexadecanoic acid, octadecanoic acid etc. are the most common metabolic by products

of coal biodegradation [30, 27]. Water soluble intermediate products like acetate and formate are also found in the effluent produced during the coal bioconversion process. Cyclic aromatic hydrocarbons and their derivatives, benzene derivatives, phenols, aromatic amines etc are also found in coal formation water [31]. Alkyl succinic acid, methyl succinate and p-tolylacetate are detected in the early stage of the core flooding experiment involving bioconversion of coal from the collected effluent sample [1]. Naphthalic acids are also detected in the consequent effluent samples obtained from the core flooding experiments [1].

2.5 Coal incubation studies

Methane generation rate is essentially governed by the presence of methanogenic substrates, electron donors, electron acceptors and the nutrient rich medium respectively. Laboratory incubation studies, also referred as bottle experiments have been carried out by researchers using coal as the only carbon source while some incubation studies have added substances like H_2 and CO_2 [29, 25], formate [29] and acetate [25] in order to increase the methane production rate. Incubation studies predict that addition of such substrates can even reduce the lag phase before the actual methane production starts [29].

Harris et.al. [29] have conducted bottle experiments on coal samples collected from the Fort Union formation at Powder river basin and found that carbon dioxide reduction is the dominant pathway for methanogenesis. Bottle experiments conducted by Green and his co-researchers [25] on the same coal samples have revealed acetoclastic reaction as the dominant pathway for methane production. Bottle experiments also depict that rate of methanogenesis depends on temperature. Incubation studies on coal samples suggest that size of the coal particles also influence the methane generation rate. Decrease in coal particle size in bottle experiments implies increase in coal surface area and hence the dissolution rate of coal also increases. The exposure of coal surface to the microbial species also increases on

account of reduced particle size [25, 19]. The pH of the growth medium in contact with the microbial species has a strong influence on methanogenesis. A pH value ranging between 6 and 7 is favourable for methanogenesis [25, 32].

The salinity of the growth medium can also impact the rate of methanogenesis. Generally lower salinity of the growth medium (i.e. the formation water) is preferable. Bottle experiments report that coals with lower maturity have shown greater potential for methanogenesis in comparison to the highly matured coals [7, 26, 33]. Researchers have also performed bottle experiments by adding nutrients to the microbial species. Yeast extract, milk, vitamins, ammonia, tryptone, carboxylate compounds and Brain-Heart infusion are the various nutrients tested in different coal incubation studies [34, 28, 35]. Use of mineral salts medium along with nitrogen rich nutrient tryptone in coal has been found to be more effective in terms of biogenic methane generation when compared to coal only or nutrient only medium [28]. The headspace pressure used for the bottle experiments ranges form 106-137 kPa [29, 36, 27]. Laboratory incubation studies account for higher loading of growth medium, nutrients and microbial consortium and hence greater surface area of coal becomes exposed to these components [29, 36, 27, 33, 37]. Such studies cannot be projected for the actual coal reservoir condition as the exposure of the coal surface to the microbial consortium and nutrient enriched growth medium is much lower in case of bottle experiments.

2.6 Core flooding experiments in absence of overburden pressure

Researchers have explored core flooding experiments mostly for the purpose of oil and gas recoveries by mimicking the actual reservoir conditions. The natural reservoirs like the sandstone reservoir, coal reservoir, limestone reservoir etc. can be simulated under laboratory conditions by packing the particles appropriate to a particular reservoir [1, 38]. Core flooding experiments have also been done by using

actual samples from the natural reservoirs [39, 40]. The natural reservoirs can be typically represented as a porous medium with the dimension of the pore spaces ranging from nanometers up to certain millimeters [41]. Experiments have been performed by packing sand particles in a three dimensional core holder. The sand pack has been flooded with water in order to recover paraffin oil from the vertical production wells. Oil is recovered from horizontal production wells through water flooding via vertical injection wells after complete extraction from vertical wells [38]. 3D water flooding experiments with different combinations of injection and production wells have been performed [42]. Flow visualisation techniques have also been implemented in three dimensional water flooding experiments with different configurations of horizontal and production wells respectively. The experimental results obtained for various well configurations have been compared by numerical simulations performed in a commercial simulator called Eclipse [43]. One dimensional water flooding experiments for oil recovery have been performed using cylindrical and rectangular Berea sandstone core samples respectively [40].

Alkali flood and salt-water flood experiments have been utilised for recovering oil from the packed limestone core [44]. Crushed limestone sample mixed homogeneously with water and crude oil was packed inside a one dimensional core model made of steel which was tested for 1000 kPa working pressure. The entire core model was kept inside an air bath installed with a thermocouple. The inside of the air bath was covered with glass wool for insulation purpose. Temperature controller was also used for regulating the temperature of the limestone core. The core holder was kept at a temperature of 50°C during the entire flooding operation. Polymer-water flood experiments were also implemented on packed limestone cores for crude oil recovery purposes [45]. Polymer runs were conducted in an unconsolidated one dimensional core holder. Ceramic bead based external heaters were wrapped on the core model. The external part of the core was covered by glass wool. Desired temperature of the sand pack was maintained by means of temperature controller [45]. The effect of different configurations of the injection and production wells on oil recovery were tested in three dimensional core

holder which was packed with crushed limestone samples and flooded with alkaline solution [46]. The efficiency of steam injection on crude oil recoveries from packed limestones cores were also tested using a 3D core holder which was wound by means of external band heaters. A total of 62 thermocouples were installed at the top, bottom and central planes of the core holder in order to examine the 3D temperature distribution during the flooding operation [47]. Steam assisted gravity drainage technique was also used for the purpose of recovering heavy oil. Three dimensional rectangular shaped model was constructed for packing the crushed limestone sample. 25 thermocouples were installed along the central plane in order to record the 3D temperature distribution [48]. Steam flooding technique was also employed for recovering heavy, medium and light oils respectively using a 3D core model of limestone [49, 50]. The efficiency of CO_2 in displacing heavy oil from limestone packs were also examined through core flooding runs [51].

Core flooding experiment has also given important insights regarding *in-situ* bioconversion of coal into methane [1]. 300.4 grams of sub-bituminous coal was packed into a bi-axial core holder. The coal core was initially inoculated with methanogenic microbial solution which was enriched from the coal samples, obtained from a coal seam in Alberta province of Canada. The core model was continuously flooded with mineral salt medium and a nitrogen rich nutrient called tryptone for 90 days. 456.608 μmoles of CH_4 in total was recovered from the entire coal pack at the end of 90 days. Acetic acid, an important substrate for methanogenesis was detected in the effluent samples collected during the course of the experiment. Compounds for e.g. benzoate, salicylic acid, benzylsuccinate, toluate, benzoic acid, succinic acid, glutaric acid, phenylacetic acid, naphthoate and hexadecanoic acid were also detected apart acetic acid from the collected effluent samples. Focused Ion Beam Scanning Electron microscopic studies and 16S rRNA pyrotag sequencing results of the coal-microbe samples, collected from the inlet, middle and outlet position of the core holder at the end of the experiment depict the growth of bacterial colonies responsible for coal bioconversion.

2.7 Overburden pressure

Overburden pressure at a particular depth in a reservoir is given by the weight of the overlying rock matrix and the fluids like water, oil or gas which occupy the pore spaces in case of a porous medium [39]. It is also referred as the lithostatic pressure or the confining pressure. Overburden pressure at a particular depth z is generally expressed as [39] :

$$p_{(z)} = p_0 + g \int_0^z \rho_{(z)} dz, \tag{2.1}$$

where $\rho_{(z)}$ is the density of the overlying rock matrix, p_0 is the datum pressure or the surface pressure and g is the acceleration due to gravity.

In a coal reservoir, coals generally occur within a coal zone along with other rocks like sandstone, mudstone, siltstone etc. For example in Alberta province of Canada, a typical coal zone consists of several coal seams which are grouped in a close proximity over a thin stratigraphic spacing of 20-50 m. Coals typically occur in packages within several coal bearing formations in the Alberta plains like Scollard formation, Paskapoo formation, Horseshoe Canyon formation, Belly river group and Mannville group respectively [52]. Such coal packages are commonly known as coal zones.

The different stratas present in Paskapoo formation above the coal seam consist of successive thick, tabular, buff coloured sandstone beds, siltstone and mudstone. Many thin coal beds like Obed coal zone are found throughout the entire Paskapoo formation. The different layers present in a coal zone in Scollard Formation comprises of thick, grey to buff coloured sandstone, siltstone, thin shale and coal. Ardley coal zone is found within the Scollard formation. The average thickness of Ardley coal zone varies from 14 m at the outcrop to more than 200 m at the western margins of the Alberta plains. The different stratas present in Horseshoe Canyon Formation comprises of 250 m thick successive layers of non-marine sandstone, siltstone, shale, mudstone comprising of coal, coaly shale, ironstone con-

cretions and isolated bentonite beds respectively [52]. Three coal zones are found in Horseshoe Canyon Formation namely Drumheller coal zone, Daly-Weaver coal zone and Carbon-Thompson coal zone respectively. Drumheller coal zone is a relatively thicker coal zone in Horseshoe Canyon Formation and contains up to 18 m local coal accumulations. Average thickness of the coal seams in Carbon-Thompson coal zone ranges from 2-3 m. Belly River Group consists of sedimentary wedge comprising of sand, clay and silt which are deposited in a nonmarine environment. Belly River Group comprises of three coal zones namely McKay coal zone, Taber coal zone and Lethbridge coal zone respectively. The thickness for McKay coal zone varies from 30-50 m. The average thickness of Taber coal zone is 25 m. The average thickness for Lethbridge coal zone ranges from 10-15 m. Mannville coals are deeper in comparison to Horseshoe Canyon coals and their thickness varies from 800-2500 m [52].

2.8 Core flooding experiments in presence of overburden pressure

Core flood experiments were performed with different combinations of pore pressure and overburden pressure in order to examine the variations in coal permeability during primary and enhanced CBM recoveries respectively [53]. Coal core sample of length 85.5 mm and average cross-sectional area of 3.580 mm^2 was collected from Mannville Group in Alberta province of Canada. The solid coal core was kept inside a cylindrical mold made of urethane resin comprising of 50% by volume of curative and 50% by volume of a pre-polymer. The coal core along with urethane resin mold was confined inside a rubber sleeve which was kept inside a high pressure, X-ray transparent core holder. The above arrangements were made in order to keep the coal core intact during the application of radial confining stress. The overburden pressure was varied from 7,100-10,500 kPa(g) during the measurement of permeability with methane.

Core flooding experiments were run using a triaxial core holder in order to examine the effect of overburden, axial and pore pressures on non Darcy flow pattern of nitrogen gas through a sandstone core from Dakota [54]. Dakota sandstone core was kept at 37.78°C and was subjected to 3447.53 kPa(g) pore pressure along with axial and confining pressures ranging from 13790 to 68950 kPa(g). CO_2 core flood and flue gas core flood experiments were conducted for the improvement of coal bed methane production [55]. The coal core was sealed inside a rubber sleeve which was wound with a lead foil in order to avoid issues regarding gas diffusion. The entire rubber sleeve was kept inside a pressure cell which can withstand a maximum radial stress of 20,000 kPa(g) and a maximum temperature of 150°C. The annular space between the rubber sleeve and the core holder was filled with hydraulic oil. Overburden pressure was applied to the coal core through rubber by means of pressurizing the oil. The ratio between the confining pressure and the pore pressure was always maintained between 2:1 to 5:3 [55]. Carbon dioxide sequestration potential was also investigated through core flood runs for recovering oil from fractured Berea sandstone core samples [56]. The overburden pressure was always kept 2068.53 kPa(g) higher than the pore outlet pressure while injecting CO_2 into Berea sandstone core.

Chapter 3

Core flooding Experimental Setup and Methodology

3.1 Experimental Setup

The schematic of the entire experimental set up has been shown in Figure 3.1. The experimental set up comprises of upstream, core block and downstream sections. The upstream section is responsible for driving degassed water, MSM-Tryptone solution and the inoculum solution into the coal core at a constant flow rate. The core block section consists of Hassler core holder and data acquisition units for pressure and temperature measurements. The downstream section is responsible for collection of effluent and maintenance of back pressure for the whole set up.

3.1.1 Upstream section

The schematic of the upstream section of the experimental apparatus has been shown in Figure 3.2. The upstream section of the core flood apparatus consists of a single piston syringe pump or PUMP-1 (500D, Teledyne Isco, Inc.), Formation fluid piston accumulator U-PA-1, Inoculum piston accumulator U-PA-2, inline pressure transducer C-PT-1 (FP2000 series, Honeywell International Inc.), Formation fluid carboy or CARBOY-1, Degassed water carboy or CARBOY-2 and safety valve C-SV-1 (SS-4R3A, Swagelok Co.) respectively. The schematic of the entire experimental set up has been shown in Figure 3.1. PUMP-1 is used for driving fluids like degassed water, formation fluid and inoculum at a constant flow rate into

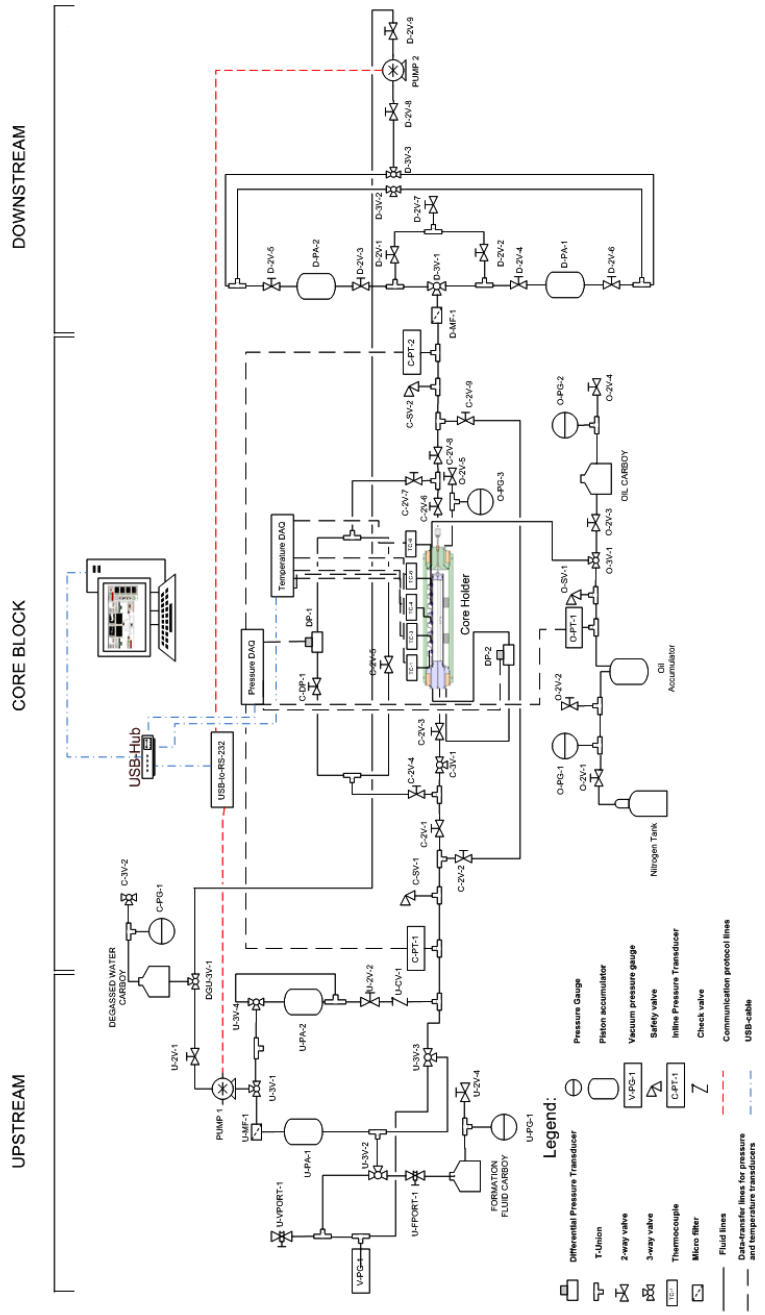

Figure 3.1: Schematic of the core flooding set up with overburden pressure.

the coal core. A 15-μm filter or U-MF-1 (SS-2TF-LE, Swagelock Co.) is installed in the downstream section in order to prevent contamination of the syringe pump during accidental back flow while conducting the core flood runs.

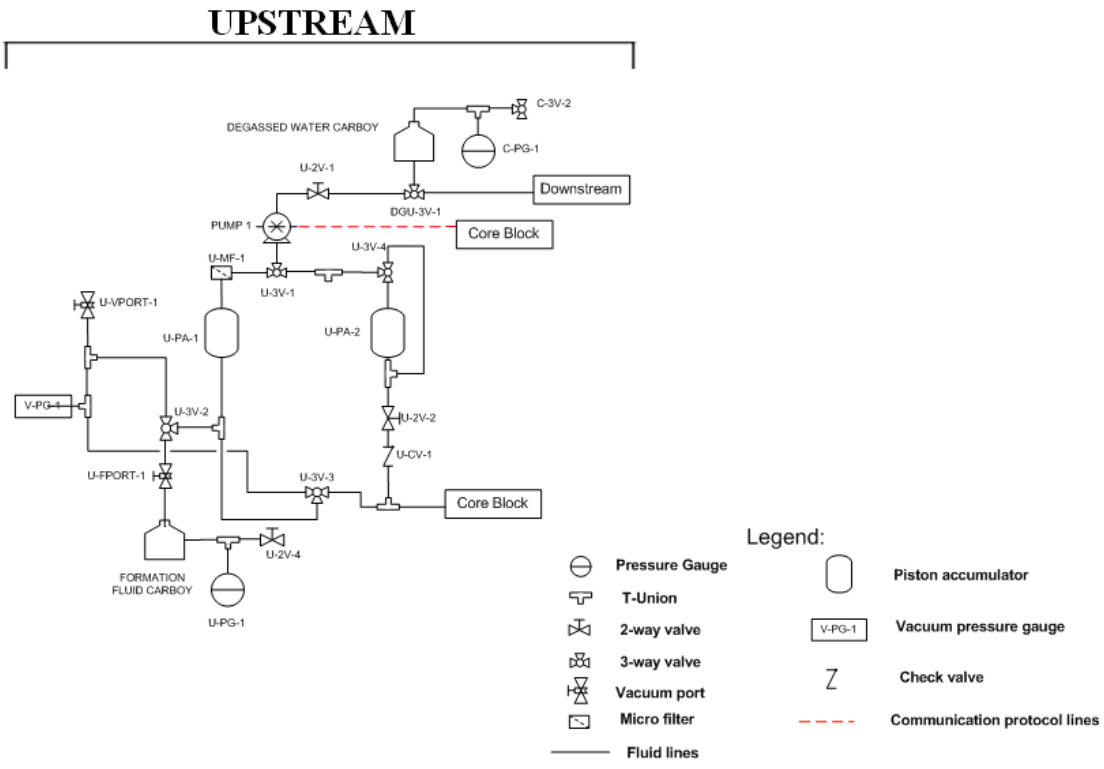

Figure 3.2: Schematic of the upstream section.

Degassed water from CARBOY-2 is injected into the coal pack using PUMP-1, valves U-3V-1, U-3V-4, U-2V-2, U-CV-1, C-2V-1, C-3V-1 and C-2V-3 respectively for porosity and permeability calculations. The valves C-2V-2, C-2V-4 and C-2V-6 are kept closed while flooding the core model with degassed water. Formation fluid or MSM-Tryptone solution is transferred in U-PA-1 from formation fluid carboy or CARBOY-1 using U-FPort-1 and the valve U-3V-2. CARBOY-1 is pressurized to 5 psi in order the facilitate the flow of MSM-Tryptone solution to U-PA-1 which is previously evacuated. U-PA-1 is sterilised with 95% by volume of ethanol before filling it with formation fluid. U-PA-2 is sterilised using an autoclave (3850M-B/L, Tuttnauer) before the anaerobic transfer of inoculum into it. The check valve U-CV-1 is installed between the valve U-2V-2 and C-PT-1 in order to protect U-PA-2 from any back flow of inoculum solution.

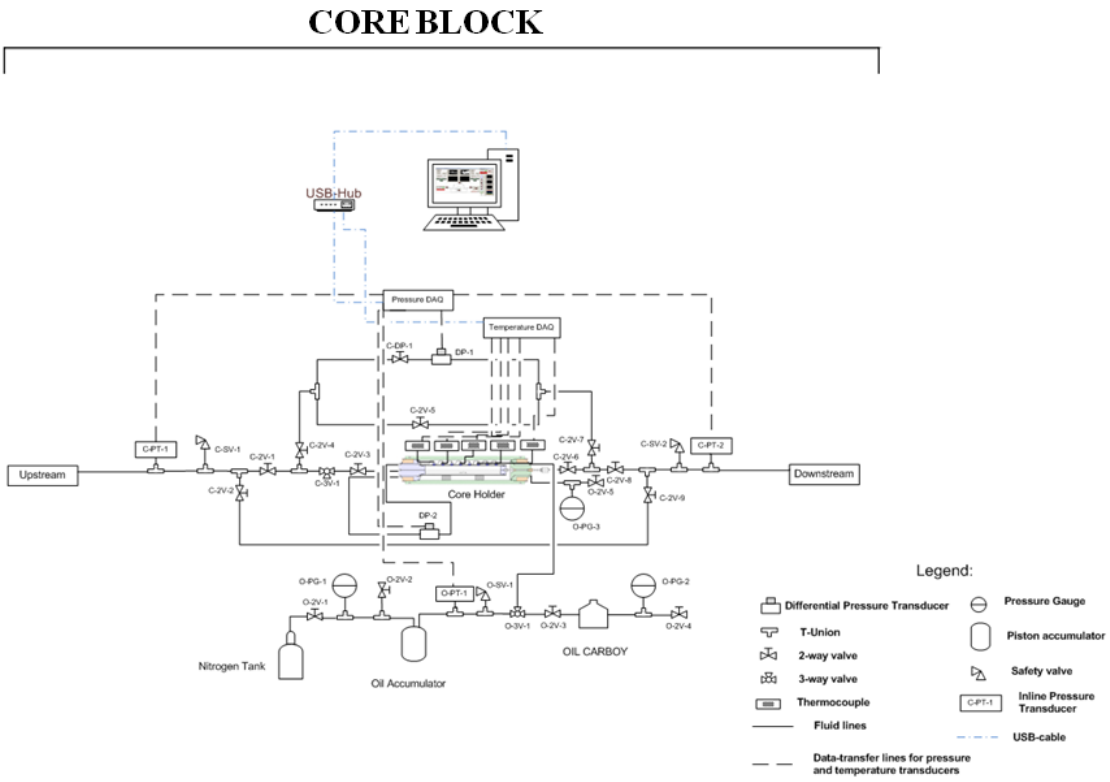

Figure 3.3: Schematic of the core block section.

3.1.2 Core Block section

The schematic of the core block section of the experimental apparatus has been shown in Figure 3.3. The middle section of the core flood apparatus comprises of Hassler type core holder, inline pressure transducer for overburden pressure measurement O-PT-1 (AST4700 series, American Sensor Technologies Inc.), inline pressure transducers C-PT-1 and C-PT-2 (FP2000 series, Honeywell International Inc.), differential pressure transducers C-DP-1 (DP15 series, Validyne Engineering Corp.) and C-DP-2 (P55D series, Validyne Engineering Corp.) safety valves 0-SV-1, C-SV-1, C-SV-2 (SS-4R3A, Swagelok Co.), oil piston accumulator O-PA-1 and oil carboy or CARBOY-3 respectively. Safety valves protect the system from accidental pressure rise by releasing the excess pressure. C-DP-1 is used for measuring the differential pressure across the entire core holder. A signal conditioner (CD15, Validyne Engineering Corp.) is installed to the system for converting the signal obtained from C-DP-1 to Data Acquisition Unit. C-DP-2 is used for measuring the

local differential pressure between two points along the length of the coal pack. An image of the entire experimental system has been shown in Figure 3.4. The outer

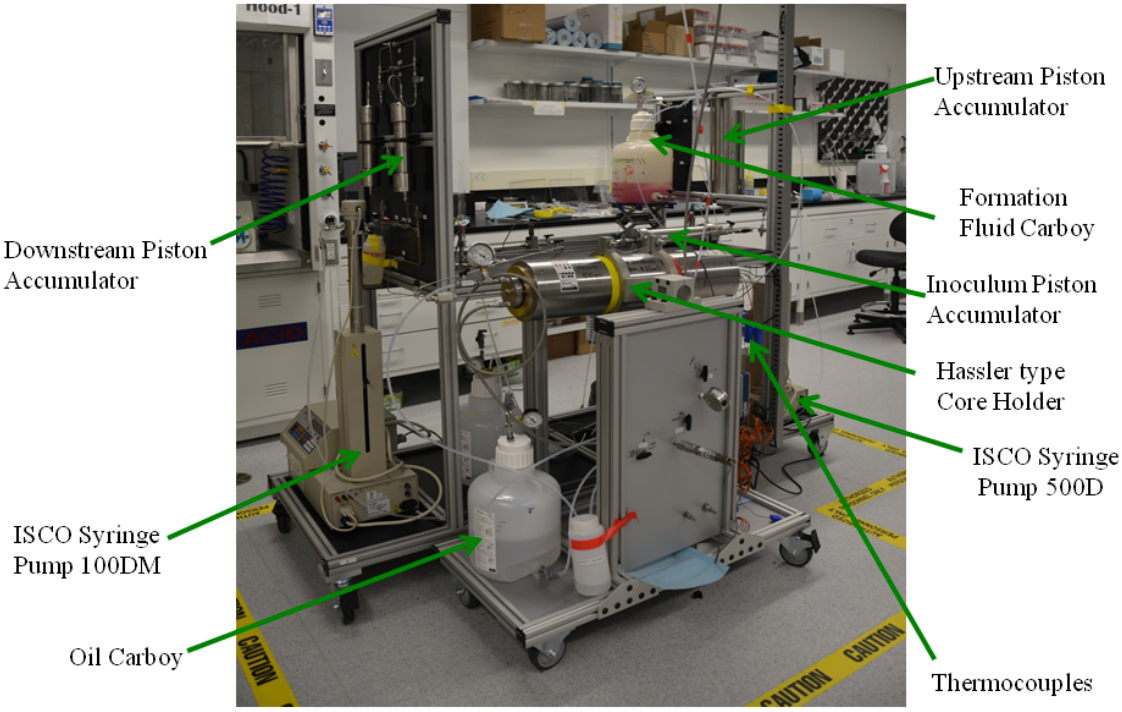

Figure 3.4: Image of the experimental apparatus for core flooding system.

diameter and length of the stainless steel made core holder are 16.256 cm and 66.95 cm respectively. Core holder can handle cores of diameter 5.08 cm and the length of the core can be varied from 30.48-43.18 cm. Core length of 43.18 cm has been used for the current experimental set up. The two ends of the core holder are provided with a ferrule assembly as the brass made end caps are connected to ferrules via screws. The rubber sleeve is fixed around both the ferrules. Core sample is packed inside the rubber sleeve. The rubber sleeve along with the ferrule assembly is inserted from one side of the core holder. The remaining part of the sleeve-ferrule assembly can be fixed and tightened after the rubber sleeve is placed inside the core holder. The end plugs connected with the rubber sleeve are provided with ultra thin polyester filter fabric of particle size 40 μm in order to obtain the optimum radial flow redistribution of the coal core. The rubber sleeve is supported inside the core

holder by means of two dead volume spacers or core supports made of teflon in order to avoid bending of the coal core after the application of radial pressure. The outlet end plug of the core holder is provided with a floating distribution plug made of stainless steel.

The schematic of the Hassler type core holder has been provided in Figure 3.5. Core holder is provided with ports which are installed along the central plane for *in-situ* pressure and temperature measurements. Ports 2 and 7 have been used for *in-situ* pressure measurements and ports 1, 3, 4, 6 and 8 have been used for *in-situ* temperature measurements. The spacing between the successive ports is 5.08 cm. 2 ports have been used for measuring the local differential pressure across two points inside the core holder and 5 ports have been utilised for installing T type thermocouples. The annulus portion between the inner diameter of the steel body and the outer diameter of the rubber sleeve is filled with oil (Drakeol 5, Light Mineral oil, NF Typicals) in order to provide the overburden stress to the coal pack. The rubber sleeve around the end plugs have been fixed by means of clamps in order to avoid entry of oil to the coal pack. The maximum pressure and temperature ratings of the core holder are 103425 kPa and 121°C respectively. The core holder has been provided with an opening around the outlet end plug for applying the radial confining stress around the core block. The overburden pressure is applied to the coal core using high pressure nitrogen cylinder through the overburden lines comprising of valves namely O-2V-1, O-2V-2, 0-3V-1 and O-SV-1, oil piston accumulator O-PA-1 and pressure transducer O-PT-1. 6205.53 kPa(g) overburden pressure has been used for the present experimental set up which can be measured by a pressure gauge named O-PG-2.

3.1.3 Downstream or Effluent section

The schematic of the downstream section of the experimental apparatus has been shown in Figure 3.6. The downstream section of the core flood apparatus comprises of a single piston syringe pump or PUMP-2 (100DM, Teledyne Isco, Inc.), piston accumulators D-PA-1 and D-PA-2 and a 15-μm filter or D-MF-1 (SS-2TF-LE, Swagelock Co.) respectively. PUMP-2 plays the role of a back pressure regu-

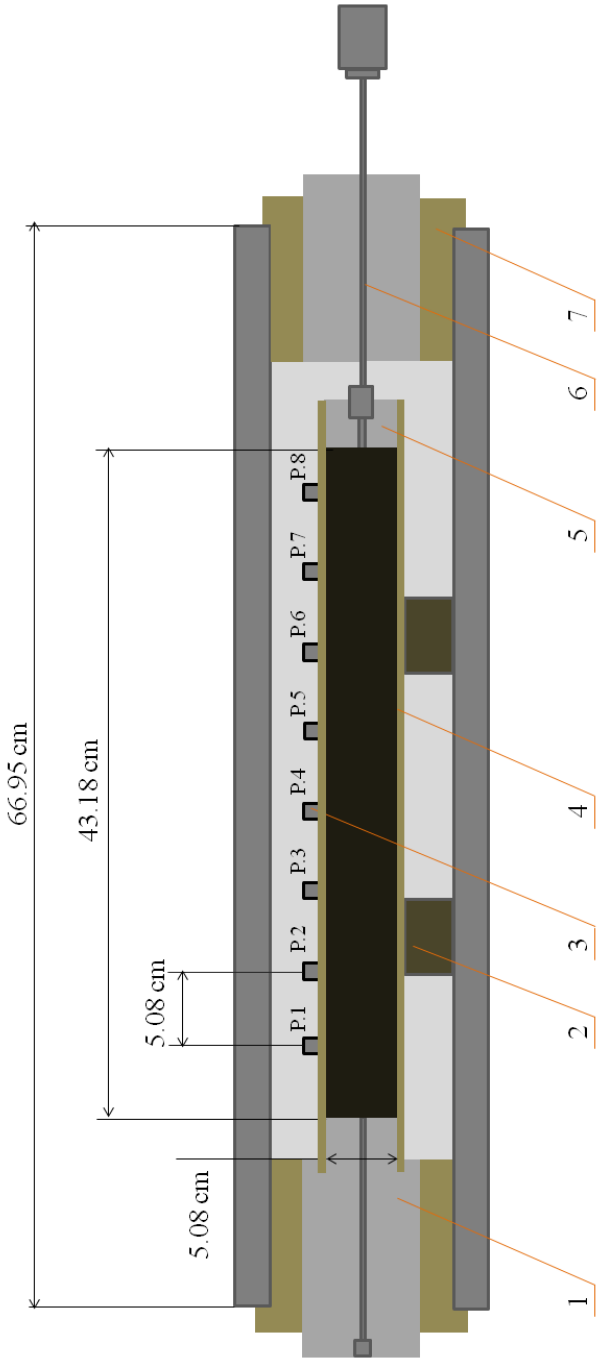

Figure 3.5: Schematic of the Hassler type core holder. 1,2,3,4,5,6 and 7 represent the inlet end plug, core support, port, rubber sleeve, outlet end plug, distribution end plug and end cap respectively.

lator by providing the required back pressure for the entire system. PUMP-2 also provides the pathway for back flow of degassed water from the water side of the

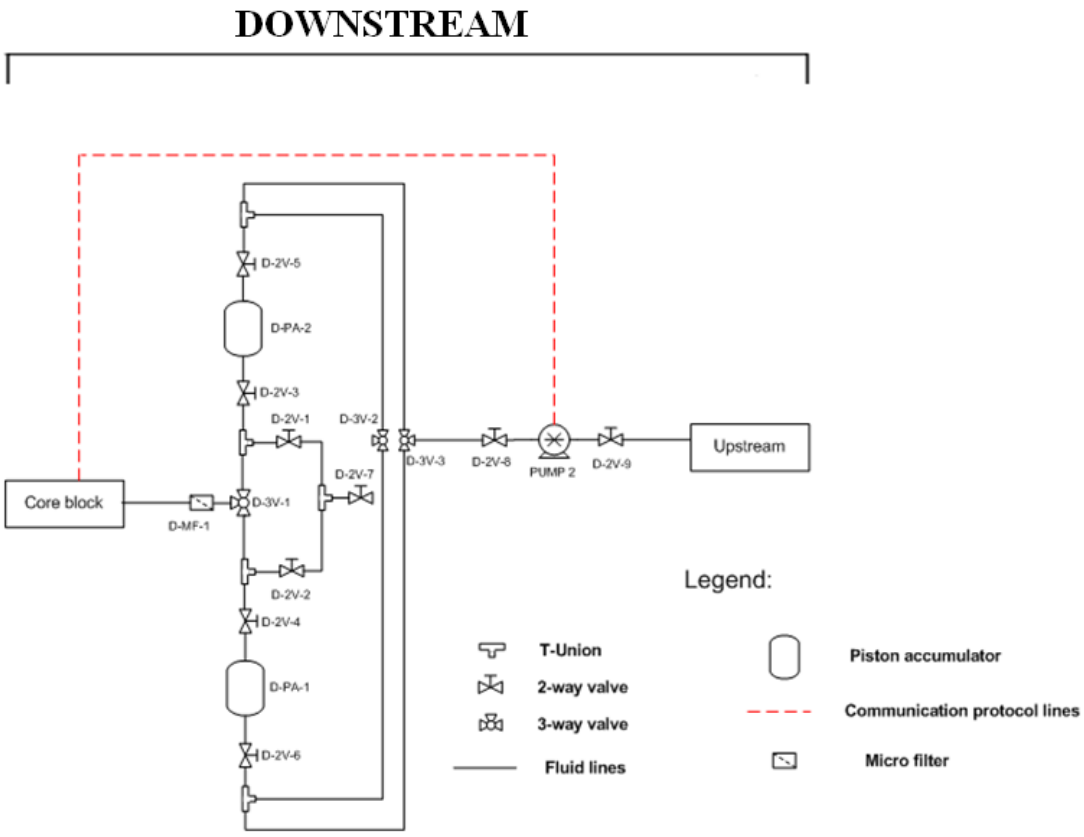

Figure 3.6: Schematic of the downstream section.

downstream piston accumulator to the degassed water carboy during effluent collection. The back pressure for the experiment is chosen as 3447.53 kPa(g) for each effluent collection. The capacity of the individual piston accumulator (D-PA-1 or D-PA-2) is 125 cc. Effluent produced during the experiment is collected in one of the downstream piston accumulators and in case if one of them are full, the effluent collection can be switched to another one without actually stopping the core flooding system. D-PA-1 and D-PA-2 are sterilised by using an autoclave (3850M-B/L, Tuttnauer) before each effluent collection. D-MF-1 is used to filter the coal particles from the effluent coming from the coal core and to prevent the contamination of the downstream piston accumulators.

3.1.4 Evacuation of the experimental system

Maintenance of anaerobic environment is one of the pre-requisites for the current experimental set up. Evacuation of the entire set up has been done using an industrial vacuum pump (Model:117, Labconco Corp.). The upstream side of U-PA-1 is evacuated for 15 minutes by connecting the vacuum pump with the flow lines containing the valve U-3V-2 and UV-Port-1 and keeping the valve U-3V-3 closed. The downstream side of U-PA-1 is evacuated for 15 minutes by using the flow lines comprising of the valves U-2V-1 and U-3V-1, PUMP-1 and the filter U-MF-1.

The main flow line including the by pass lines are evacuated for an hour by connecting the vacuum pump with UV-Port-1 and keeping the valves C-2V-1, C-2V-2, C-2V-4, C-2V-5, C-2V-7, C-2V-8, C-2V-9 and C-DP-1 opened and the valves C-2V-3, C-2V-6, C-3V-1 and D-3V-1 closed during the evacuation process. The coal pack inside the rubber sleeve is evacuated for 30 minutes by connecting the vacuum line with valves C-3V-1 and C-2V-3 respectively. The annulus portion between the outer steel body and the rubber sleeve is evacuated for 30 minutes by connecting the vacuum pump with valve O-2V-1 and keeping the valve O-3V-1 opened in the direction of the core holder. Degassed water carboy, formation fluid carboy and the oil carboy are evacuated by connecting the vacuum pump separately with the valves C-3V-2, U-2V-4 and O-2V-4 respectively.

The downstream section of the system including the flow lines and the piston accumulators are evacuated for 20 minutes by connecting the vacuum pump with the valves D-3V-2 and D-2V-7 and keeping the valve D-3V-1 closed. D-PA-1 is evacuated through the valves D-2V-4, D-2V-6, D-2V-2, D-2V-7 and D-3V-2. D-PA-2 is evacuated through the valves D-2V-3, D-2V-5, D-2V-1, D-2V-7 and D-3V-2. The vacuum level inside the system is maintained at 6.5 kPa(a) which is measured by a pressure gauge named U-VPG-1. The leak tests were conducted using a soap solution during the evacuation process in order to ensure the level of vacuum achieved.

3.1.5 System monitoring and control

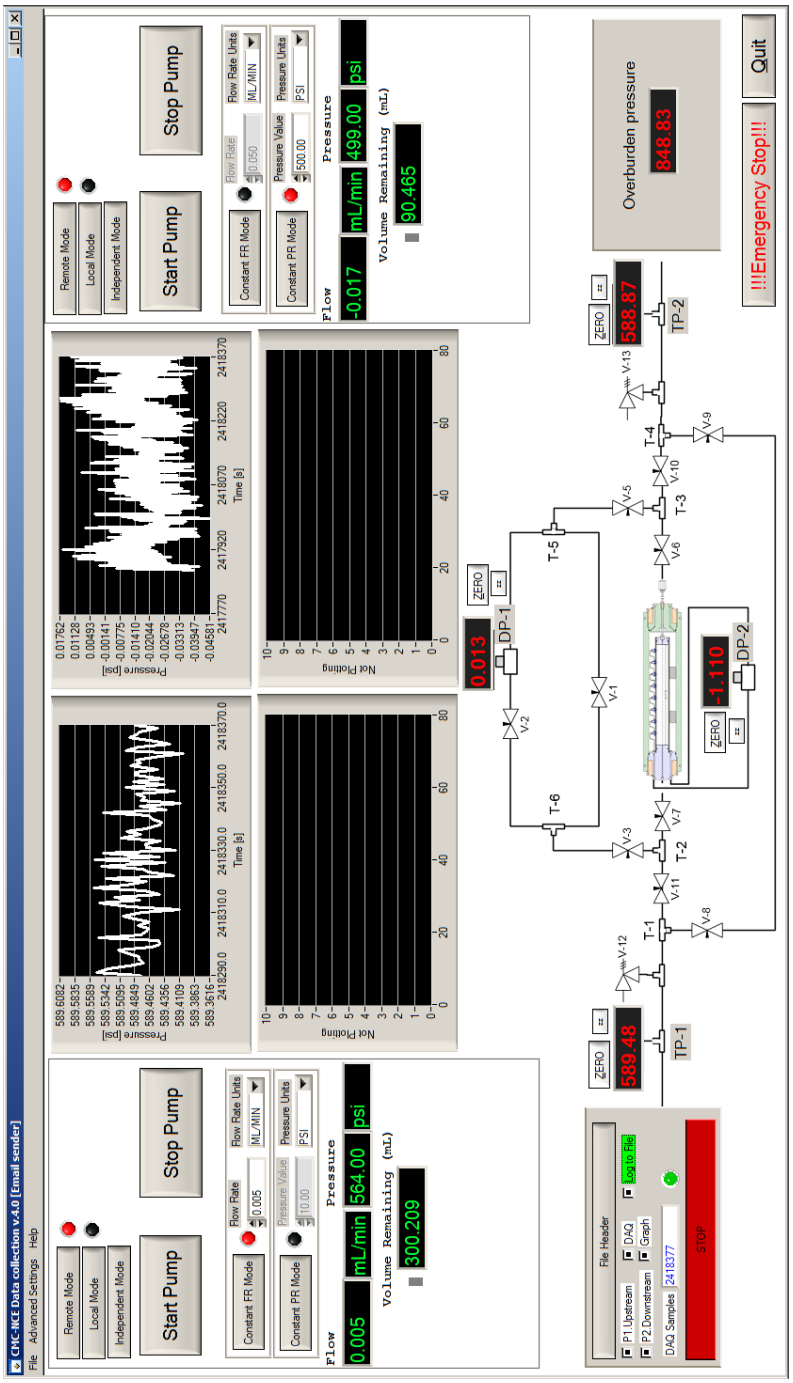

Figure 3.7: Image of Graphic user interface for monitoring and control of system pressure.

The image of GUI for pressure DAQ unit has been shown in Figure 3.7. Collection of data manually for such an experimental system is a cumbersome job

and hence, data acquisition units are installed in order to facilitate monitoring and control of the system. DAQ unit (NI USB-6009, National Instruments Corp.) has been installed for recording the real time data from inline and as well as differential pressure transducers. DAQ systems for pressure sensors and thermocouples were connected to a USB hub (Model: DUB-H4, D-Link Corp.). USB hub was directly connected to a USB port of a computer device. A signal conditioner (Model: USB-232/2, National Instruments Corp.), connected to the USB hub has been used for communicating with the syringe pumps through RS-232 serial protocol. Graphical user interface (GUI) for pressure monitoring of the entire system has been made using a custom design software (Lab Windows/CVI, National Instruments Corp.). The pressure of the entire set up can also be controlled by using the GUI. The left and right sections of the GUI related to pressure measurements were involved in communication with the syringe pumps while the central part was involved in plotting the transient responses of the pressure sensors. Pressure data can be easily stored using the graphical user interface. The image of GUI for temperature DAQ unit has been shown in Figure 3.8. DAQ system for temperature measurements comprises of a DAQ module and a DAQ chassis. DAQ module (NI9213, National Instruments Corp.) along with DAQ chassis (Model: cDAQ-9171, National Instruments Corp.) have been used for recording the real time data from T type thermocouples. Graphical user interface (GUI) for temperature monitoring of the entire system has been made using a custom design software (Lab Windows/CVI, National Instruments Corp.). GUI related to temperature measurements were responsible for plotting the transient responses of the thermocouples installed at different locations along the central plane of the core holder. Temperature fluctuations inside the core holder during the ongoing experiments can be compared with the room temperature reading obtained from a T type thermocouple hanging outside the system. Temperature data can be easily stored using the graphical user interfaces.

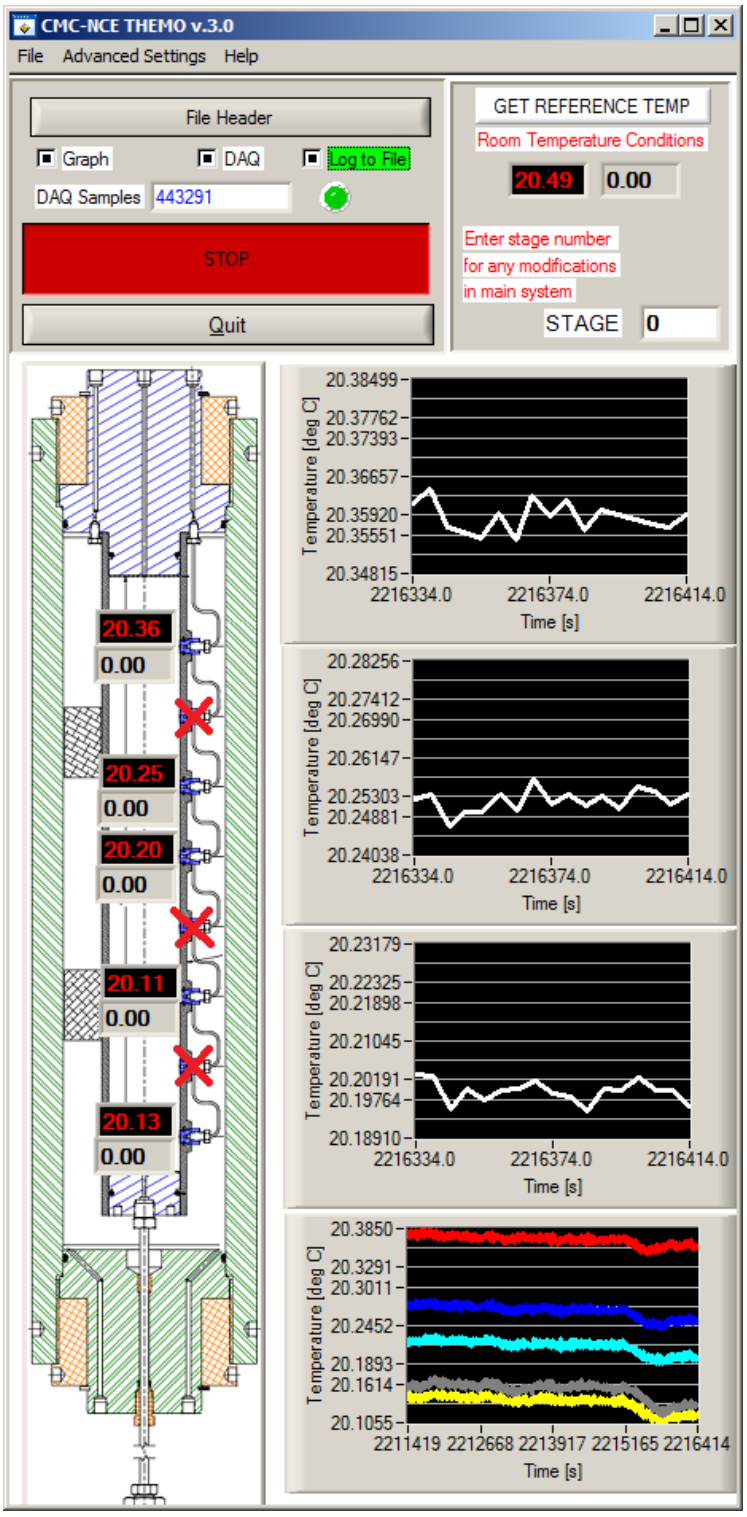

Figure 3.8: Image of Graphic user interface for monitoring of system temperature.

3.2 Experimental Methodology

This section depicts the experimental procedure followed for successful running of the system. Freshly crushed coal particles of size ranging from 150-250 microns was tightly packed inside the core holder. The entire experimental set up was evacuated and frequent leak tests were performed using leak detectors during the evacuation process. The overburden chamber present inside the core holder along with the overburden lines were filled with oil. The oil was pressurized using high pressure nitrogen cylinder in order to apply the radial confining pressure to the coal pack.

Permeability of the coal pack was calculated under 3447.53 kPa(g) overburden pressure by flooding the coal core with nitrogen and after that the coal core was saturated with degassed water. Pore volume or porosity of the coal pack was estimated during water saturation process. Permeability of the coal core was also estimated during water flooding. 800 ml or 2.56 pore volume (PV) of water in total was injected to the system. The coal core was flooded with 2.21 PV of MSM-Tryptone solution or formation fluid after water injection in order to push the accumulated water inside the coal pack to the downstream side. The system pressure was slowly increased to 3447.53 kPa(g) by simultaneously decreasing the flow rate in PUMP-1 and increasing the downstream pressure in steps using PUMP-2 before inoculum injection. The overburden pressure was also successively increased from 3447.53 kPa(g) to 6205.53 kPa(g) during inoculum flooding of the coal core. 1.28 PV of microbial solution was flooded into the system at a flow rate of 0.1 ml/min in order to push the accumulated formation fluid inside the coal core to the downstream section. The system was stopped for two weeks after the inoculum flooding in order to provide sufficient time for microbes to get themselves accustomed inside the coal pack. Valves C-2V-3 and C-2V-6 were kept closed during the incubation period. The system was flooded with formation fluid at a flow rate of 0.005 ml/min after two weeks of gestation period in order to provide nutrients to the microbes for their growth. The resulting effluent formed was collected in one of the downstream pis-

ton accumulators (D-PA-1 or D-PA-2).

100 ml of effluent was collected during each sampling point. The gases were separated from the effluent by pressure reduction method and were analysed using a GC. Metabolites analysis were conducted after gas separation for the remaining effluent using a GCMS. The flow rate of the formation fluid was increased to 0.008 ml/min after four sampling points in order to increase the frequency of sample collection and investigate the effect of methane recovery at higher flow rates. The pressure and temperature measurements for each sample were recorded using the appropriate DAQ's. The coal pack was flooded with 5.77 PV of MSM-Tryptone solution in total for a time span of 180 days.

3.3 Materials and Methods

3.3.1 Coal preparation and Packing

Subbituminous coal was used for the experiments. Coal samples were obtained from the mine face of TransAlta's Highvale coal mine which is situated at the south of Wabamun Lake in Alberta province of Canada. Bigger size coal chunk obtained directly from the mine was at first broken into smaller pieces using a hammer and a chisel. Smaller blocks of coal were further crushed with the help of a mortar and a pestle before the actual grinding operation.

A bench-top planetary ball mill (PM 100, Retsch GmbH) was used to obtain further finer coal particles. Finely crushed coal particles obtained from the grinding operation were separated into two distinct groups of mesh sizes ranging from 60-70 (250-210 μm)and 70-100 (210-149 μm) with the help of a Ro-Tap sieve shaker (RX-29, W.S.Tyler Industrial Group). Test sieves (Fisher Scientific Co.) of ASTM E-11 specifications were used during the sieving operation. Coal particles belonging to mesh sizes 60-70 were homogeneously mixed with coal particles belonging to mesh sizes 70-100 before packing. The coal particles were tightly packed inside the rubber sleeve, connected to a ferrule assembly on one side by using a vibrator

table (VP-181, FMC Technologies, Inc.) along with a vibration controller (Syntron Power Pulse AC, FMC Technologies, Inc.).

The freshly crushed coal particles were cautiously poured inside the rubber sleeve in order to avoid spills when the sleeve-ferrule assembly was kept in a vertical position on the vibration table during continuous vibrations. The coal pack consisted of 206.7 gm of coal particles belonging to mesh sizes 60-70 and 459.8 gm of coal particles belonging to mesh sizes 70-100. The weighted average particle size of the coal pack inside the core holder was 194.59 μm and the estimated packing density was 761.71 Kg/m^3.

3.3.2 Degassed water preparation

The preparation of degassed water was necessary in order to maintain anaerobic environment as far as possible during flooding the coal core with water. Degassed water was also utilised for pressurizing the piston accumulators in the upstream and downstream sections respectively. The gases dissolved in the water are usually removed using a membrane module (PDMSXA 1.0, PermSelect) [2]. The membrane module comprises of various hydrophobic silicone hollow fibres which play the role of membrane. The gases dissolved in the water generally percolate through the hollow fibres by means of diffusion. Water required for degassification is passed through the inlet of the membrane module and is collected in a carboy in the outlet section of the membrane module. The outlet side of the membrane module and the degassed water collecting carboy are connected to a vacuum pump (Model 117, Labconco Corp.) in order to prevent dissolution of oxygen in freshly prepared degassed water [2]. In order to achieve high accuracy in experiments, Degassed water carboy or CARBOY-1 was further purged with nitrogen and the pressure inside the carboy was maintained at 20 kPa(g).

3.3.3 MSM-Tryptone solution preparation

Mineral salt medium (WR-86) in combination with the nutrient, tryptone was prepared as per the procedure described in [57, 1, 2]. MSM-Tryptone medium is also

referred as the formation fluid. Mineral salt medium comprises of distilled water, mineral I, mineral II, vitamin B, phosphate, sulfide and a redox indicator named as resazurin. The composition of the components along with their concentrations in distilled water are shown in Table 3.1 [2].

5 litres of formation fluid was prepared in a carboy and was autoclaved for approximately 45 minutes. The carboy was cooled by purging nitrogen gas through a needle valve connected to the cap of the carboy. Purging of nitrogen was necessary to remove the dissolved oxygen from the medium. The pressure inside the carboy was maintained at 27.61 Kpa(g). Sodium sulphite, a reducing agent was added to the medium after the autoclaving operation. Nitrogen rich nutrient tryptone was added to the medium after sulphite addition. The concentration of the added tryptone was 5 g/l. Formation fluid medium was ultimately transferred from the carboy to a glove bag which was previously purged with nitrogen gas.

3.3.4 Inoculum preparation

Quick Silver Resources Ardley Formation or QSAF methanogenic culture was used in preparing the inoculum for the core flooding experiment. QSAF is originally cultured from the coal cuttings obtained from a coal seam in Alberta province of Canada [58, 1]. QSAF culture was further sub-enriched in many serum bottles consisting of subbituminous coal from Highvale mine of Alberta, resazurin, MSM and Tryptone ($Bacto^{TM}$ Tryptone (Becton, Dickinson and Co.) with a concentration of 5 g/l of MSM respectively.

The serum bottles were incubated for 5 weeks in a dark place at 30°C [1, 28, 57]. Methane generation was observed during the incubation period and it comprised of 30-40 % of the headspace volume of the serum bottles. Inoculum for the core flooding set up was prepared by feeding equal volumes of MSM-tryptone solution and inoculum media to a clean and autoclaved U-PA-2. In total, 400 ml was transferred to inoculum piston accumulator. U-PA-2 was evacuated before inoculum introduction by using a vacuum pump through a valve and a Luer lock fitting which was

Table 3.1: MSM composition

Solution	Constituents	Quantity (g) in 5 litres of distilled water
Mineral I	NaCl	250
	$CaC4l_2$. $2H_2O$	50
	NH_4Cl	250
	$MgCl_2$. $6H_2O$	50
Mineral II	$(NH_4)Mo7O_{24}$. $4H_2O$	50
	$ZnSO_4$. $7H_2O$	0.5
	H_3BO_3	1.5
	$FeCl_2$. $4H_2O$	7.5
	$CoCl_2$. $6H_2O$	50
	$MnCl_2$. $4H_2O$	0.15
	$NiCl_2$. $6H_2O$	0.15
	$AlK(SO_4)_2$. $12H_2O$	0.5
Vitamin B	Nicotinic Acid	0.5
	Cyanocobalamine	0.5
	Thiamine	0.25
	p-Aminobenzoic acid	0.25
	Pyridoxine	1.25
	Pantothenic acid	0.125
Phosphate	KH_2PO_4	250
Resazurin	Resazurin	0.5
Sulfide	Na_2S. $9H_2O$	125

flushed beforehand with MSM. MSM-Tryptone media and the inoculum culture were injected into U-PA-2 in an alternative fashion by using a sterile syringe.

3.3.5 Gas recovery from the effluent side

The effluent produced during the on going bio-conversion process was collected in the downstream piston accumulators (D-PA-1 or D-PA-2). Effluent filled piston accumulator along with its fittings were disconnected from the experimental set up. The valves associated with the water and the effluent sides of the piston accumulator were kept closed while dismantling the piston accumulator from the set up.

The water side of the piston accumulator was connected to an accumulator containing water while the high pressure side or the effluent side of the PA was connected to a Tedlar bag (Model 22049, Restek Co.). A mass flow controller (Model

32907-71, Cole-Parmer) was connected to the accumulator on one side and nitrogen tank on the other side. The Tedlar bag and its associated fittings were evacuated using a vacuum pump (Model 117, Labconco Co.) before the effluent collection. Valve connected to the effluent side of the piston accumulator was opened slowly in order to release the pressure and allow some effluent to go inside the Tedlar bag. The nitrogen tank was set at a pressure of 482.68 kPa(g). After this, the valve connected to the water side of the PA was opened slowly and the required mass flow rate (0.05 ml/min) for the nitrogen gas was set on the mass flow controller.

Finally, the water side of the PA was pressurized with the help of nitrogen gas in order to push the effluent to the Tedlar bag. Such, a rapid decline in the pressure of the effluent paved the pathway for gas desorption and the gas bubbles started to appear on the top of the effluent in the Tedlar bag. During the process of gas recovery, the pressure inside the mass flow controller started to increase until it reached the pre-set pressure of the nitrogen tank while the mass flow rate started to decrease from the pre-set value. Zero mass flow rate value in the mass flow controller indicated that no more effluent was left in the piston accumulator. The gas bubbles formed inside the Tedlar bag was collected and measured by means of a sterile syringe before the gas analysis in a GC.

3.3.6 Measurement of recovered gases from core flooding setup

The gas bubbles appearing on the top of the effluent inside the Tedlar bag were usually collected in a 10 ml syringe and the volume of the total collected gas was recorded. The gas from the syringe was shifted to a 12.5 ml vial which was previously evacuated. The gas was transferred to the vial by means of inserting the syringe needle into a PTFE septum associated with the screw cap of the vial. The level of vacuum inside the vial was noted down before the transferring of the gas.

100 μl or 0.1 ml of gas was collected from the headspace of the vial by using a 500 μl disposable syringe and was directly injected into a gas chromatograph (GC). 0.1 ml of headspace gas was injected into a GC for three times for improving

the accuracy of gas measurements. The peak area obtained during individual injections were recorded. The volume percentage of a particular gas like CH_4, CO_2 etc. from a known volume of a collected gas mixture during each sampling point was calculated by comparing the average of the obtained peak areas with the prepared calibration standards for the respective gases. In the current experimental set up, only CH_4 and CO_2 were analysed from the samples. The details regarding making of calibration standards have been provided in the appendix section. Methane was analysed using a GC (Model 5700A, Hewlett-Packard Co.) which consists of a flame ionisation detector (FID). The length and diameter of the GC column associated with FID were 1.83 m and 3.17 mm respectively. N_2 was used as the carrier gas for methane measurements and the flow rate of nitrogen was 46.1 ml/min. The peak area associated with an injection of 0.1 ml headspace gas from a 12.5 ml vial into a methane GC column was provided by an integrator (Model 3390A, Hewlett-Packard Co.) [1].

Methane measurements are limited to 30% by volume for the methane GC. Hence, the gas samples were diluted sometimes if the peak area obtained after the gas injection exceeded the saturation limit of the machine. CO_2 was analysed using a GC (Model 5890 series II, Hewlett-Packard Co.) consisting of a thermal conductivity detector (TCD). Helium was used as the carrier gas for carbon dioxide measurements. The peak area required for volume percentage calculations related to CO_2 was provided by an integrator (Model 3396 series III, Agilent Technologies). H_2 and air flow rates during the GC measurements were 30.7 ml/min and 260 ml/min respectively. The detectors were always set at a temperature of 200°C while the temperature of the injectors corresponded to the room temperature [1].

3.3.7 Sample preparation and the associated technique for analysis of metabolites

Samples for metabolite analysis were prepared as per the procedure depicted in [1, 2]. Three 5 ml sub samples were collected during each sampling point from the remaining effluent in a Tedlar bag after the recovery of gas bubbles. Each of the

triplicates were transferred in a 20 ml glass scintillation vial and were acidified by adding five drops of concentrated HCl using a glass pasteur pipette. Acidified sample's pH should be less than 2 for prevention of microbial activities and protonation of acidic intermediates. 100 μl of 4-fluoro-1-naphthoic acid was added to the acidified triplicates as an internal or surrogate standard for extraction and derivatization efficiency.

5 ml of ethyl acetate of HPLC grade (Fisher Scientific Co.) were added to each of the triplicates after the addition of internal standard. Samples were shaken by hand after ethyl acetate addition in order to facilitate the mixing. Vials were set aside for approximately 30 minutes to allow phases to separate at room temperature. The upper or the organic solvent layer noticed after half an hour in each vial was transferred to a new scintillation vial. The extraction of the aqueous phase in old vials were repeated for two more times in the same manner as discussed above. The solvent extracts were pooled out in the same vial for each of the triplicates. The solvent volume in every new scintillation vials were allowed to reduce by placing the vials in a fume hood with their caps off. The solvent volume in each of the new scintillation vials was ultimately concentrated to approximately 2 ml. Ethyl acetate volume of less than equal to 0.5 ml was added to each of the concentrated samples and the sides of the vials were rinsed in order to ensure a homogeneous solution. Finally, 0.5 ml of the concentrated sample was transferred to a glass labeled auto-sampler GCMS vial. 100 μl of N,O-Bis (trimethylsilyl) trifluoroacetamide (Thermo Scientific Co.), a derivatizing agent was added to each of the GCMS vials and the contents were mixed thoroughly using a vortex mixer. GCMS vials were heated in 70°C water bath for 30 minutes and were cooled to room temperature before the metabolite analysis was done.

GCMS analysis for each of the triplicate samples was conducted by means of a GC (6890N, Agilent Technologies) associated with an inert mass selective detector (5973, Agilent Technologies) which was connected to a capillary column (HP-5MS, Agilent). The length, internal diameter and film thickness of the column were 30 m,

0.25 mm and 0.25 μm respectively. The carrier gas utilised during GCMS analysis was helium. Metabolites corresponding to a particular sample was detected on the basis of the retention time and the ion fragmentation number corresponding to the surrogate standard used during the extraction. The response obtained for each detected compounds were normalized with the response of the internal standard for a semi quantitative analysis. GCMS analysis for the uninoculated formation fluid samples in triplicated were also performed. Response ratios of the detected compounds for each of the triplicates pertaining to a particular sampling point were represented using a heat map which was constructed using a commercial software [1, 59].

Chapter 4

Results and Discussion

4.1 Coal pack Characterization

4.1.1 Porosity of the coal core

Porosity of the coal pack was evaluated by flooding the evacuated coal core with degassed water using PUMP 1. PUMP 1 was operated at constant flow rate mode. The coal pack was flooded by using the valves U-3V-1, U-3V-4, U-2V-2, C-2V-1, C-3V-1 and C-2V-3. The valves C-2V-2, C-2V-4 and C-2V-6 were kept closed during the water injection process.

Table 4.1: Parameters used for the calculation of porosity with 3447.53 kPa(g) overburden pressure and without overburden pressure

Porosity from experiments with 500 psi overburden pressure		**Porosity from experiments without overburden pressure [1]**	
Core length (cm)	43.18	Core length (cm)	30.5
Core diameter (cm)	5.08	Core diameter (cm)	3.81
Bulk volume (ml)	875	Bulk volume (ml)	347.5
Pore volume (ml)	311.95	Pore volume (ml)	131.95
Porosity (%)	35.65	Porosity(%)	38

Firstly, the amount of degassed water injected until the valve C-3V-1 was recorded using PUMP 1 and the recorded volume was given the name RV-1. Secondly, the valves C-3V-1 and C-2V-3 were opened and the degassed water from C-3V-1 was allowed to flow through the core holder keeping the valve C-2V-6 closed. The

PUMP 1 was stopped when there was sudden increase in pressure inside the system which indicated that the coal pack was fully saturated with water. The volume indicated by PUMP 1 at this stage was recorded and was given the name RV-2. The pore volume (PV) was calculated by subtracting the value of RV-2 from RV-1. Porosity of the coal core was estimated using the formula stated below:

$$\varepsilon(\%) = \frac{PV}{BV} \times 100 \tag{4.1}$$

where, BV is the bulk volume.

It can be inferred from Table 4.1 that the porosity of the coal pack decreases due to the application of overburden pressure.

4.1.2 Permeability of the coal core

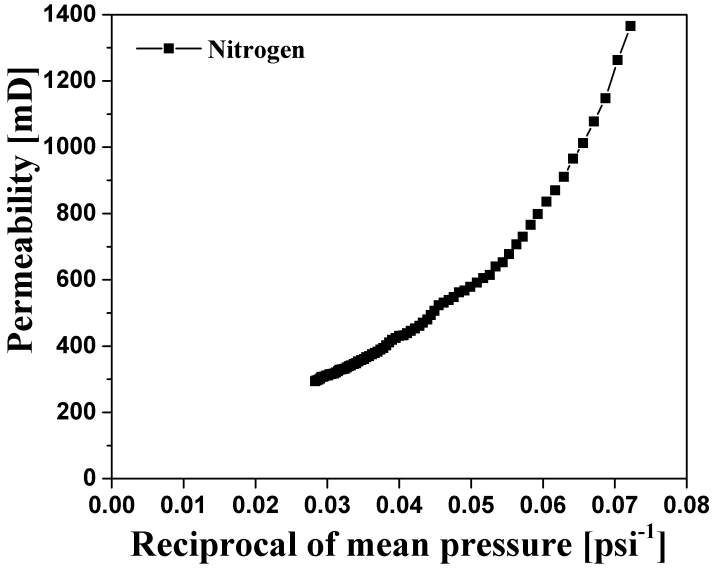

Figure 4.1: Variation of the nitrogen permeability for different values of reciprocal of mean pressure.

Permeability of the coal pack were estimated using nitrogen and degassed water as the working fluids. Nitrogen permeability was calculated at first followed by water permeability. Permeability The coal pack was subjected to 3447.53 kPa(g)

overburden pressure during the permeability measurements.

The core holder was connected to a nitrogen supply and mass flow controller (Model 32907-71, Cole-Parmer) on the upstream section and a pressure gauge on the downstream section. The flow rate of the nitrogen gas through the core holder was controlled by the mass flow controller. The upstream and downstream side pressures (P_1 and P_2) for a particular flow rate were recorded using the mass flow controller and the pressure gauge respectively. The volume flow rate was varied from 100 ml/min to 2000 ml/min for the permeability calculations. The dynamic viscosity value of 1.7654x10^{-5} Pa.s was considered for nitrogen permeability calculations. Permeability measurements were carried out at a temperature of 23.84°C and the pressure of the room during the measurements was 93.08 kPa. Nitrogen permeability was estimated by taking into account the compressibility effect. The formula used for permeability computations is stated below [60, 1]:

$$K_g = \frac{Q_g}{A}\mu_g L \frac{2P_2}{P_1^2 - P_2^2} \tag{4.2}$$

where, K_g is the gas permeability in m^2; A is the cross sectional area of the coal pack in m^2; L is the coal pack length in m; μ_g is the dynamic viscosity of the gas in Pa.s and P_1 and P_2 are the absolute upstream and downstream pressures respectively in Pa.

The absolute value of the mean pressure P_m (i.e. $\frac{P_1+P_2}{2}$) was also computed using the experimental data. Figure 4.1 shows the effect of the mean pressure on nitrogen permeability. The nitrogen permeability data can be exponentially fitted as follows:

$$K_g = 113.3 \times \exp\frac{33.16}{P_m} \tag{4.3}$$

Klinkenberg effect states that at infinite pressure gas behaves as a perfect liquid [61]. Klinkenberg permeability value obtained after setting the mean pressure (P_m)

to infinity in Eq. 4.3 was 113.3 mD. The discrepancy in the values of permeability obtained by water injection and Klinkenberg methods could not be addressed. The absolute permeability for water was calculated after nitrogen flooding. Pres-

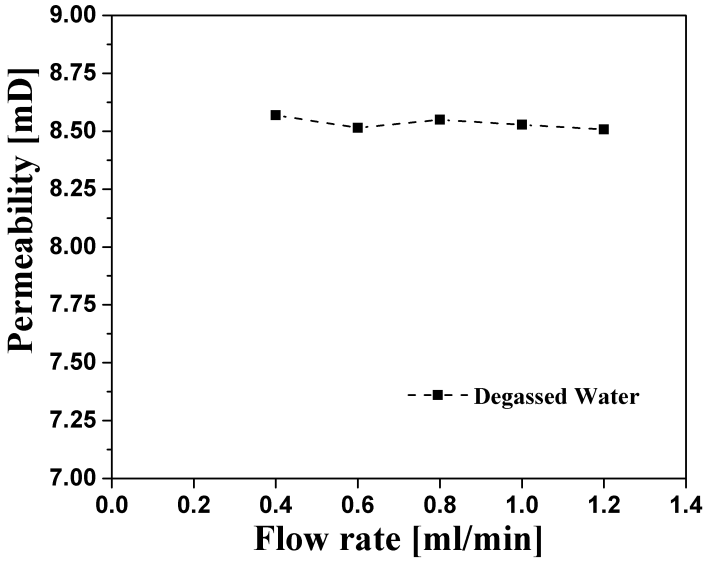

Figure 4.2: Variation of degassed water permeability for different values of volume flow rate.

sure drop across the core holder was computed using the inline pressure transducers (FP2000 series, Honeywell International Inc.). The dynamic viscosity value of 0.001 Pa.s was considered for water permeability calculations. Darcy's law was used for the permeability calculations which is stated as follows:

$$K_w = \frac{Q_w}{A}\mu_w\frac{L}{\Delta P} \tag{4.4}$$

where, K_w is the degassed water permeability in m^2; A is the cross sectional area of the coal pack in m^2; L is the coal pack length in m; μ_w is the dynamic viscosity of the degassed water in Pa.s and ΔP is the pressure difference across the coal pack in Pa. Figure 4.2 shows that the water permeability values remain more or less constant for different flow rate values. The average water permeability value obtained from water flooding is 8.53 mD. Permeability can also be calculated analytically using Kozeny-Carman equation which is given by [62, 1]:

$$K = \frac{\phi^2 d^2 \varepsilon^3}{180(1-\varepsilon)^2} \tag{4.5}$$

where K is the theoretically obtained permeability value, ϕ is the particle sphericity, d is the particle size in micron and ε is the porosity. The sphericity for the coal

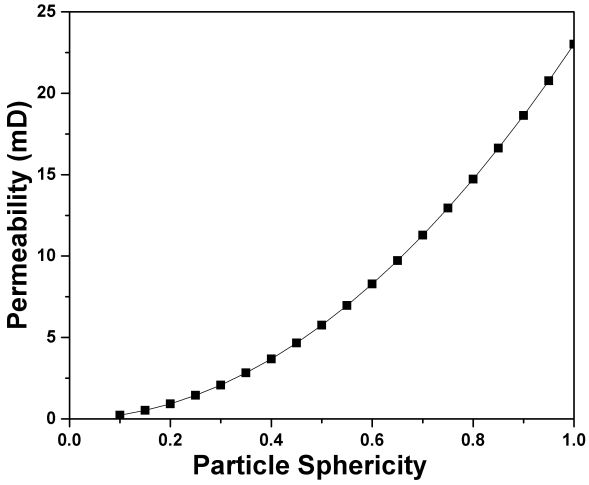

Figure 4.3: Variation of permeability for different values of particle sphericity. The values of porosity and particle size have been considered as 0.3565 and 194.59 μm.

pack obtained using Kozeny-Carman equation and the water injection permeability value of 8.53 mD was 0.61. The weighted average particle size for the coal pack was 194.59 μm and the porosity value used for the calculation was 0.3565. However, based on the particle sphericity value of 0.65 obtained from the literature [1], the permeability of the coal pack came out to be 9.72 mD.

Permeability of the coal pack subjected to a confining stress as observed from

Table 4.2: Permeability values obtained for two sets of experiments using water injection method.

Permeability from experiments with 500 psi overburden pressure		**Permeability from experiments without overburden pressure [1]**	
Water flooding technique (mD)	8.53	Water flooding technique (mD)	13.28

Table 4.2 depicts that the overburden pressure has a stronger influence on the permeability of the coal pack. Application of confining pressure leads to the blockage of pores and hence the pore space decreases, thereby resulting in permeability reduction.

4.2 Variation of coal pack permeability

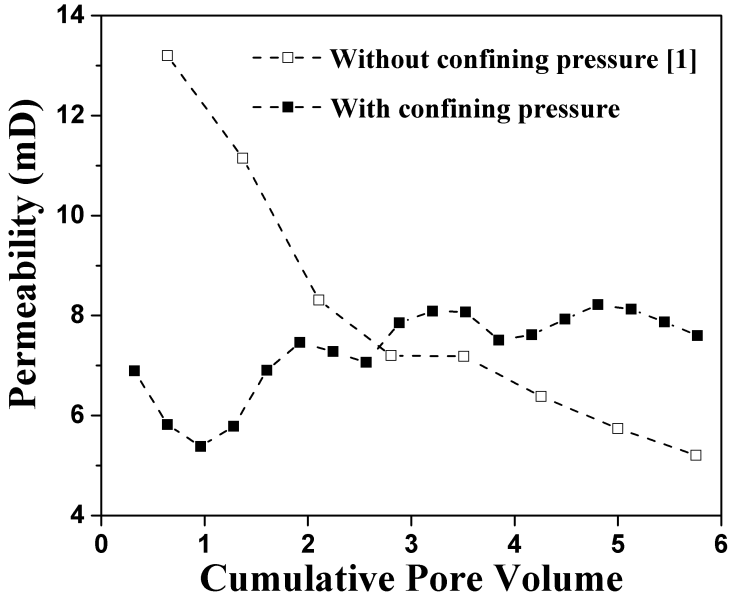

Figure 4.4: Changes in coal permeability with the cumulative pore volume of formation fluid fed to the coal core.

Variations in coal pack permeability were observed due to continuous flooding of MSM-Tryptone solution for 180 days. Figure 4.4 shows the variation of the coal permeability corresponding to the cumulative pore volume of formation fluid flooded through the coal core in presence of confining pressure. Cumulative *PV* of formation fluid pertaining to each sampling point referred to the summation of all the previously injected pore volumes of formation fluid preceding that sampling point with the flooded pore volume of formation fluid pertaining to that sampling point. Cumulative *PV* is chosen as a reference parameter because for different experimental systems, the pore volumes are generally different and hence in order to make comparison between two systems, cumulative *PV* is used. It also depicts the changes in coal permeability in absence of confining pressure. Permeability of the coal pack pertaining to a sample was calculated by taking the average of the pressure drop readings obtained from inline pressure transducers, C-PT-1 and C-PT-2 during the period of collection of that sample. Table 4.3 lists the parameters used during the current core flooding experiments. The parameters used for the exper-

iments conducted without confining pressure [1] have been tabulated in Table 4.4.

During, formation fluid flooding the back pressure of the system was 3447.53

Table 4.3: Experimental Parameters for core flood runs in presence of confining pressure.

Sample No.	Back pressure (kPa(g))	Average differential pressure (kPa)	Flow rate (ml/min)	Cumulative formation fluid injected (PV)
1	3447.53	2.5743	0.005	0.32
2	3447.53	3.0494	0.005	0.641
3	3447.53	3.2984	0.005	0.962
4	3447.53	3.0673	0.005	1.282
5	3447.53	4.1125	0.008	1.603
6	3447.53	3.8072	0.008	1.923
7	3447.53	3.9026	0.008	2.244
8	3447.53	4.0208	0.008	2.564
9	3447.53	3.6161	0.008	2.885
10	3447.53	3.5121	0.008	3.206
11	3447.53	3.5187	0.008	3.526
12	3447.53	3.7839	0.008	3.847
13	3447.53	3.7305	0.008	4.167
14	3447.53	3.5833	0.008	4.488
15	3447.53	3.4572	0.008	4.808
16	3447.53	3.4950	0.008	5.129
17	3447.53	3.6096	0.008	5.45
18	3447.53	3.7368	0.008	5.77

kPa(g) for each sampling cycle. The coal pack was always subjected to 6306.85 kPa(g) confining pressure during MSM-Tryptone flooding. The permeability of the coal pack was 6.8964 mD after flooding the coal pack with 0.32 *PV* of formation fluid. Hence, there was approximately 19.1% reduction in permeability value after the water injection process. Permeability value was further reduced to 5.82 mD after flooding the coal pack with 0.64 *PV* of formation fluid. The volume of gas generated after 0.64 *PV* injection of formation fluid was more than the volume of gas produced after 0.32 *PV* injection of formation fluid. Increase in gas production results in saturation of the coal pack which leads to gas adsorption. Coal matrix starts to swell on account of gas adsorption. Thus, coal swelling may also decrease

Table 4.4: Experimental parameters for core flood runs in absence of confining pressure [1].

Sample No.	Back pressure (kPa(g))	Average differential pressure (kPa)	Flow rate (ml/min)	Cumulative formation fluid injected (PV)
1	3447	2.027	0.006	0.64
2	3447	2.000	0.005	1.37
3	3447	3.757	0.007	2.107
4	1724	3.716	0.006	2.804
5	1724	3.723	0.006	3.507
6	3447	4.192	0.006	4.257
7	3447	4.66	0.006	5.000
8	69	5.136	0.006	5.757

the permeability of the coal pack [63, 64, 55, 53]. Permeability of the coal pack was 5.79 mD after 1.328 *PV* injection of formation fluid. Permeability of the coal pack was increased to 6.9071 mD after 1.6 *PV* injection of formation fluid on account of increase of flow rate from 0.005 to 0.008 ml/min after the first four samples. Thus, flow rate has a positive impact on coal pack permeability.

4.3 CH_4 and CO_2 production

Variations of cumulative productions of methane and carbon dioxide respectively as a function of cumulative pore volume (*PV*) of formation fluid injected into the coal core have been shown in Figure 4.5. Figure 4.5 reports the variation of solubility uncorrected cumulative gas generation data with and without confining pressure. Gas generation data considering solubility of gases in the effluent have been shown in Figure 4.6. Continuous flooding of 0.32 *PV* of formation fluid into the coal pack was considered during each sampling point. Cumulative productions of CH_4 and CO_2 along with their molar ratios have been provided in a tabular form in Table 4.5. Solubility uncorrected data was calculated by considering the quantity of gases recovered from the effluent during each sampling point. The quantity of gas (CH_4

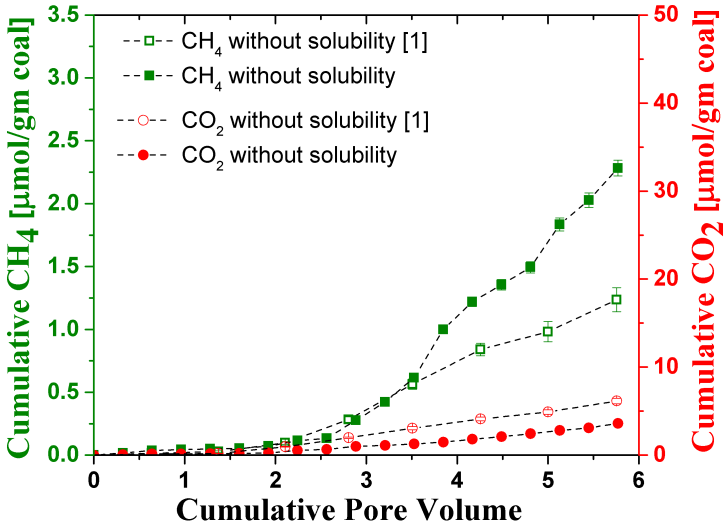

Figure 4.5: Variation of solubility uncorrected cumulative CH_4 and CO_2 generation with the cumulative pore volume of formation fluid fed to the coal pack.

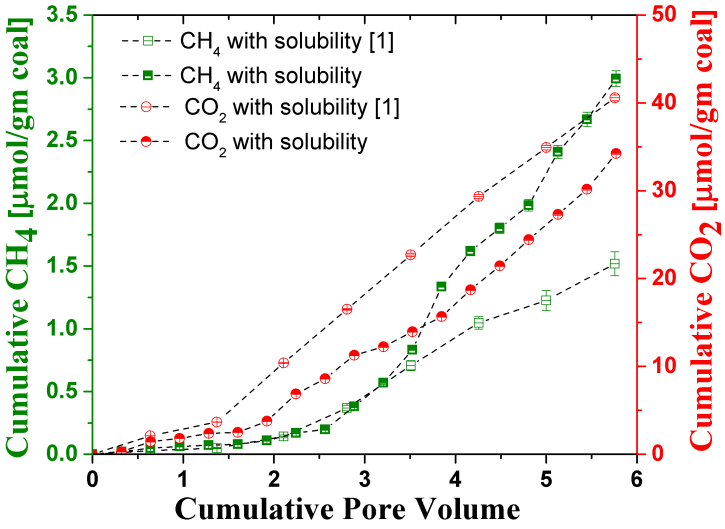

Figure 4.6: Variation of solubility corrected cumulative CH_4 and CO_2 generation with the cumulative pore volume of formation fluid fed to the coal pack.

or CO_2) dissolved in the effluent during each sampling point was added with the recovered gas data in order to obtain the solubility corrected gas generation data. The solubility of the gases in the effluent was calculated using Henry's law which states that quantity of a gas dissolved in a certain volume of liquid at a particular temperature is proportional to the partial pressure of the gas present above the liquid [1, 65, 66]. Cumulative gas generation data pertaining to each sampling point

referred to the summation of all the gas generation data preceding that sampling point with the gas generation data corresponding to that sampling point.

CH_4 production under the application of confining pressure was less in comparison to CO_2 production after flooding the coal pack with 1.28 *PV* of formation fluid. Carbon dioxide production increased from 4.11% after 0.32 *PV* injection of formation fluid to 17.79% after 0.64 *PV* injection of formation fluid . Maximum CH_4 production among the sampling points till 1.28 *PV* injection of formation fluid was only 3.64%. Acetoclastic reaction, i.e. conversion of acetate to methane was the probable dominant pathway for methanogenesis in comparison to carbonate reduction pathway till 1.28 *PV* injection of formation fluid and it can be explained by means of Le Chatelier's principle [67]. Le Chatelier's principle states that for the reactions involving gases, the application of pressure shifts the position of equilibrium in such a way that the effect of pressure is reduced. The number of moles involved in the product side of an acetoclastic reaction (refer to Figure 2.1) are more in comparison to the reactant side. The application of confining pressure shifted the direction of equilibrium towards the left hand side of the reaction and hence, methane generation was not favoured. The flow rate of MSM-Tryptone solution through the coal pack was increased from 0.005 to 0.008 ml/min in order to investigate the effect of flow rate on methanogenesis. Methane production started to increase in case of higher flow rate. Highest methane production from the recovered gas volume among the sampling points was 7.48% till 2.56 *PV* injection of formation fluid. However, CO_2 generation was also relatively higher after the flow rate was increased. Maximum CO_2 production was limited to 47.4% among the sampling points till 2.56 *PV* injection of formation fluid . Percentage of CH_4 and CO_2 recovered from the effluent samples have been listed in Table 4.6. Hence, acetate fermentation pathway was still dominant till 2.56 *PV* injection of formation fluid. The rate of methanogenesis increased significantly after 2.56 *PV* of formation fluid was injected into the coal pack. Cumulative methane production was almost twice after 2.88 *PV* injection of formation fluid as compared to that after 2.56 *PV* injection of formation fluid. Percentage of CO_2 produced was less in comparison to that

Table 4.5: Solubility corrected cumulative CH_4 and CO_2 production data

Sample No.	Cumulative PV injected	Effluent pH	Gas Volume Collected (ml)	Cum. CH_4 (μmol)	Cum. CO_2 (μmol)	Molar ratio CH_4/CO_2
1	0.32	n/a	2.6	14	187.953	0.074
2	0.641	5.97	3	32.66	953.76	0.024
3	0.962	6.05	1.4	41.99	1207.03	0.037
4	1.282	6.18	2.2	47.99	1579.6	0.016
5	1.603	6.38	1.2	53.32	1660.92	0.065
6	1.923	6.26	3.4	72.65	2512.7	0.023
7	2.244	6.3	6.8	113.3	4569.52	0.02
8	2.564	6.3	3.5	131.97	5275.9	0.016
9	2.885	6.6	7.2	253.94	7518.79	0.068
10	3.206	6.75	6.2	379.24	8155.29	0.197
11	3.526	6.62	7.6	554.53	9295.67	0.154
12	3.847	6.61	9	889.78	10444.72	0.292
13	4.167	6.66	10	1079.06	12482.21	0.092
14	4.488	6.4	8.2	1200.37	14287.1	0.067
15	4.808	6.3	8.4	1322.34	16283.26	0.061
16	5.129	6.12	12.2	1605.6	18192.12	0.148
17	5.45	5.85	8	1778.22	20116.97	0.09
18	5.77	5.79	10.6	1994.83	22809.63	0.08

of CH_4 for the samples ranging between 3.2 to 3.84 *PV* injection of formation fluid. Highest methane production (51.92%)pertaining to a particular sampling point was observed after 3.84 *PV* injection of formation fluid. Carbonate reduction pathway was the most dominant pathway for the gas samples analysed between 2.88 to 3.84 *PV* injection of formation fluid and it can be explained by means of Le Chatelier's principle [67]. The number of moles involved in the product side of carbon dioxide reduction pathway (refer to Figure 2.1) are less in comparison to the reactant side. The application of confining pressure shifted the direction of equilibrium towards the right hand side of the reaction and hence, methane generation was favoured. The molar ratio (CH_4/CO_2) as a function of cumulative pore volume of injected formation fluid has been provided in Figure 4.7. CO_2 percentage among the respective sampling points started to increase again after 3.84 *PV* injection of formation fluid. Methane production in a particular sample reduced to 19.51% after 4.8 *PV* injection of formation fluid and reached a maximum value of 36.7% after 5.12 *PV*

Table 4.6: Percentage of CH_4 and CO_2 obtained from the collected gas volume in each sample.

Sample No.	Collected gas volume (ml)	CH_4 (%)	CO_2 (%)
1	2.6	1.85	4.11
2	3	3.64	17.79
3	1.4	2.95	6.19
4	2.2	1.76	8.98
5	1.2	1.48	1.971
6	3.4	4.73	20.28
7	6.8	7.48	47.4
8	3.5	4.18	27.28
9	7.2	16.89	39.74
10	6.2	19.37	14.34
11	7.6	30	26.05
12	9	51.92	25.9
13	10	27.67	45.55
14	8.2	19.83	41.02
15	8.4	19.51	45.21
16	12.2	36.7	41.83
17	8	28.85	43.83
18	10.6	30.64	59.81

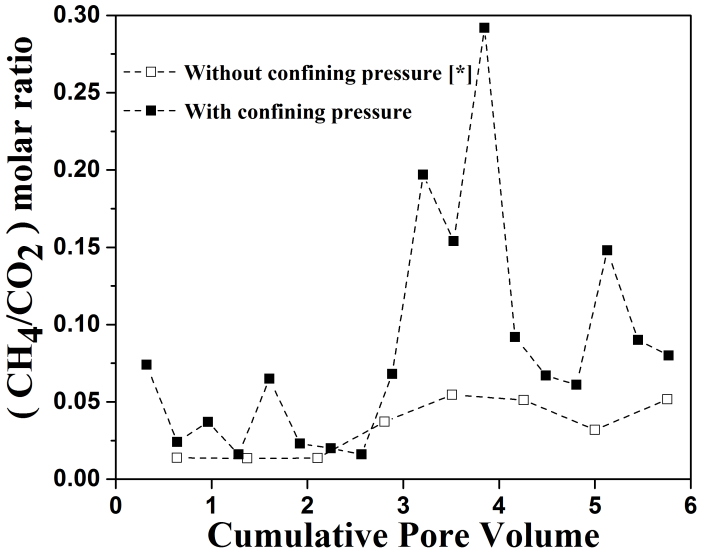

Figure 4.7: Variation of solubility corrected molar ratio (CH_4/CO_2) for each sample with the cumulative pore volume of formation fluid fed to the coal pack.

injection of formation fluid.. However,it is difficult to predict from Table 4.6 that which of the pathways among acetoclastic reaction and carbonate reduction were dominant for the samples analysed between 4.16 to 5.77 *PV* injection of formation fluid.

Table 4.7: Quantity of CH_4 and CO_2 recovered after depressurizing the coal pack.

Cumulative CH_4 (without solubility) (μmol)	Cumulative CH_4 (with solubility) (μmol)	Cumulative CO_2 (without solubility) (μmol)	Cumulative CO_2 (with solubility) (μmol)	Molar ratio CH_4/CO_2
28.01	28.86	17.85	50.43	1.6

Interesting phenomenon occurred during depressurizing the coal pack at the end of the experiments. 687.26 ml of gas was recovered after flooding the coal pack with 1 *PV* injection of formation fluid at 68.98 kPa(g) back pressure. Solubility corrected molar ratio (CH_4/CO_2) was more than one which signifies that methane recovery can be more if the fluid pressure or the back pressure of the system is reduced.

4.4 Temperature variation inside the coal pack

Variations of temperature across the different ports of the core holder along with room temperature as a function of cumulative pore volume (*PV*) of formation fluid injected into the coal core have been shown in Figure 4.8. Five T type thermocouples (Omega Co.) were installed along the central plane of the core sleeve for measuring the temperature during *in-situ* bio-conversion process. Thermocouples TC-1, TC-3, TC-4, TC-6 and TC-8 were installed in ports 1, 3, 4, 6 and 8 respectively. Thermocouple TC-RTC was installed outside the core holder in order to keep a track of the room temperature during the core flooding experiments. The details of thermocouple calibration has been given in Appendix. Temperature pertaining to a particular thermocouple for each sampling point as shown in Figure 4.8 was calculated by taking the average value of the temperature readings during the period of collection of that sample. Table 4.8 lists the temperature reading obtained

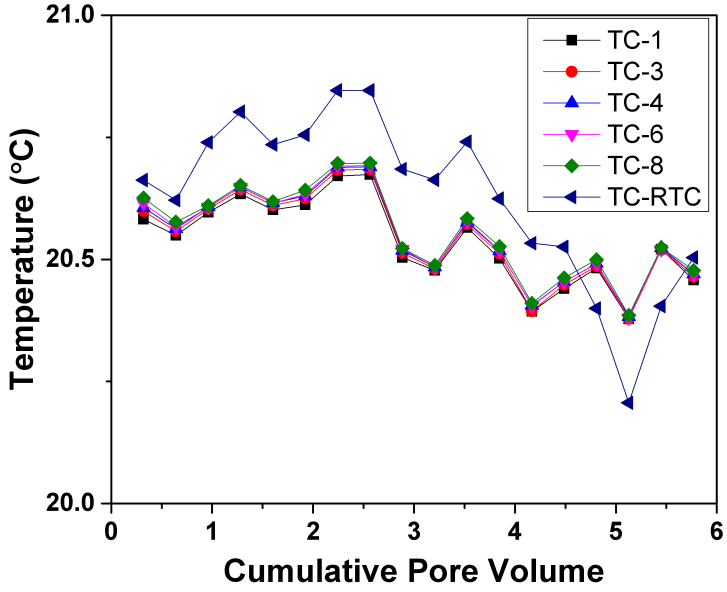

Figure 4.8: Variation of room temperature and *in-situ* temperature at different ports inside the core holder with the cumulative pore volume of formation fluid fed to the coal pack.

Table 4.8: Temperature data at different locations inside the core holder and also inside the room for each sampling point

Sample No.	TC-1 (°C)	TC-3 (°C)	TC-4 (°C)	TC-6 (°C)	TC-8 (°C)	TC-RTC (°C)
1	20.5822	20.5987	20.6063	20.6145	20.6257	20.6624
2	20.5492	20.5577	20.5631	20.5668	20.5765	20.6214
3	20.5966	20.6032	20.6077	20.6072	20.6102	20.7395
4	20.6342	20.6432	20.6483	20.6484	20.6516	20.8025
5	20.6016	20.6105	20.6155	20.6149	20.6185	20.7352
6	20.6115	20.6245	20.6302	20.6336	20.6416	20.7552
7	20.6710	20.6829	20.6886	20.6912	20.6965	20.8461
8	20.6740	20.6845	20.6898	20.6919	20.6971	20.8463
9	20.5036	20.5132	20.5183	20.5206	20.5255	20.685
10	20.4774	20.4802	20.4843	20.4845	20.4878	20.663
11	20.5653	20.5714	20.5762	20.5781	20.5836	20.741
12	20.5019	20.5114	20.5171	20.5182	20.5267	20.6245
13	20.3933	20.3997	20.4057	20.4047	20.4104	20.533
14	20.4398	20.4479	20.4541	20.4541	20.4620	20.5256
15	20.4823	20.4859	20.4915	20.4914	20.4996	20.3995
16	20.3778	20.3779	20.3824	20.3803	20.3853	20.2062
17	20.5205	20.5194	20.5238	20.5207	20.5242	20.4043
18	20.4579	20.4644	20.4701	20.4696	20.4773	20.5039

from the thermocouples installed across different locations along the mid plane of the coal pack for each sampling point. Table 4.8 also gives the room temperature reading associated with each sampling point. Figure 4.8 depicts that the temperature variation inside the core holder followed the same pattern as that of the room temperature.

Figures 4.9, 4.10, 4.11 and 4.12 represent the variation of the temperature of the coal pack along with that of outside temperature for 1 minute, 1 hour, 1 day and 1 week during the collection of sixth sample respectively. The *in-situ* temperature profiles followed the pattern of the room temperature profile with an offset. Temperature of the room was relatively higher as compared to that inside the core holder which suggested that there was heat transfer from room to the core holder during the collection of sixth effluent sample.

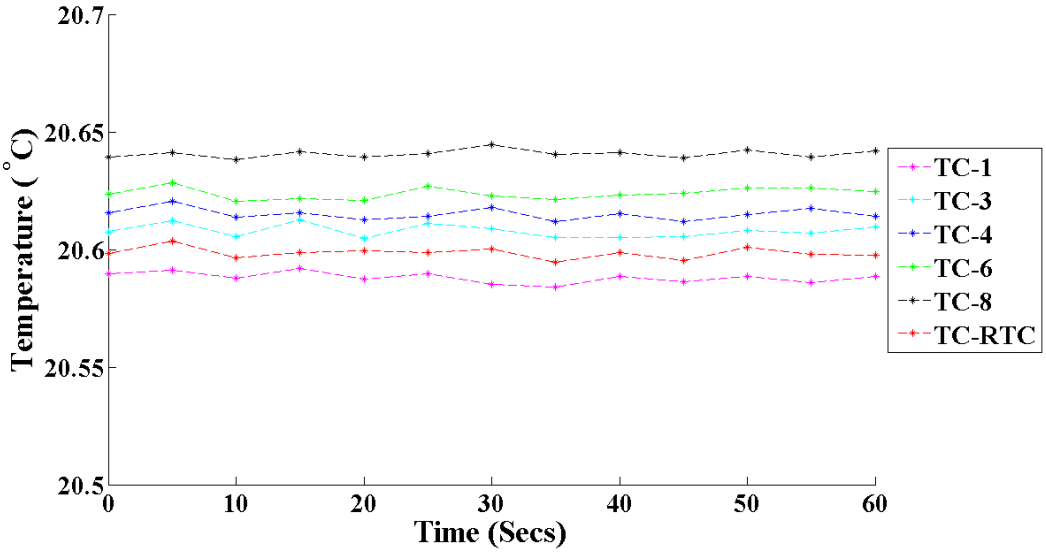

Figure 4.9: Variation of room temperature and *in-situ* temperatures at different ports for a minute during 6^{th} sampling point.

Figures 4.13, 4.14, 4.15 and 4.16 represent the variation of the temperature of the coal pack along with that of outside temperature for 1 minute, 1 hour, 1 day and 1 week during the collection of sixteenth sample respectively. The *in-situ* temperature profiles followed the pattern of the room temperature profile. Temperature inside the core holder was sometimes higher as compared to that inside the room

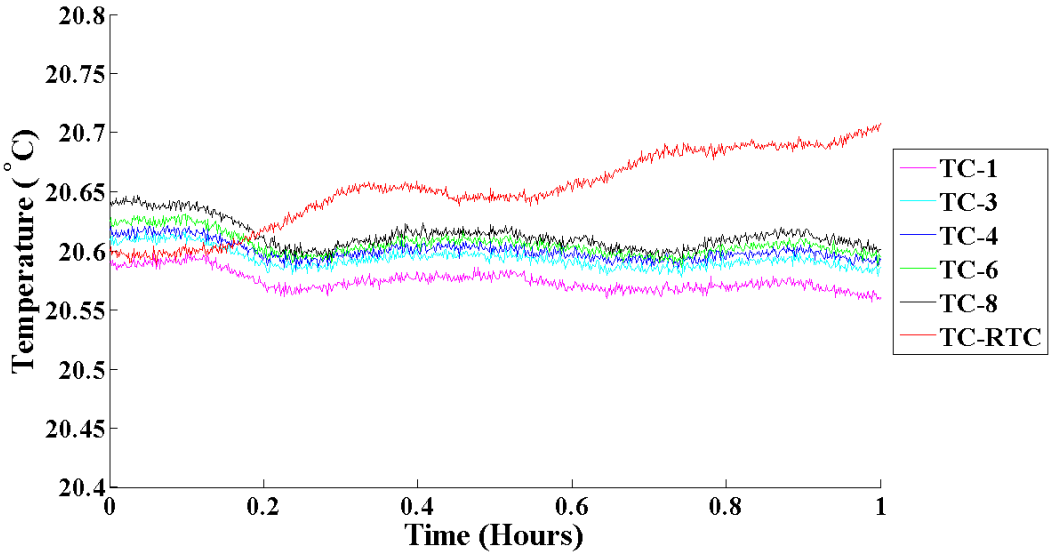

Figure 4.10: Variation of room temperature and *in-situ* temperatures at different ports for an hour during 6^{th} sampling point.

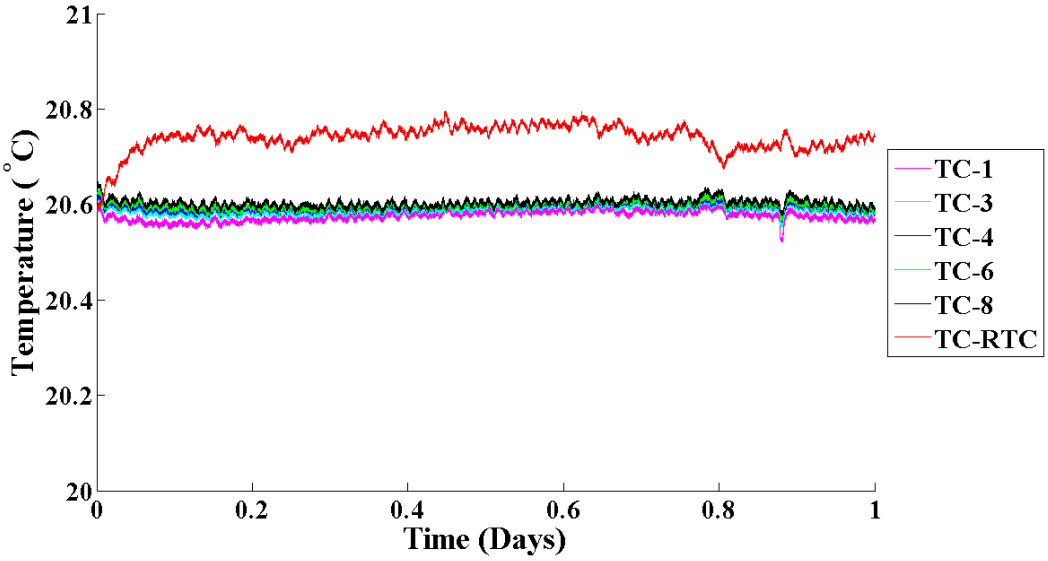

Figure 4.11: Variation of room temperature and *in-situ* temperatures at different ports for a day during 6^{th} sampling point.

which suggested that there was heat transfer from core holder to the room during the collection of sixteenth sample.

The core holder was not insulated and hence the chances of heat transfer between the room and the core holder could not be ruled out. Fluctuation of the room

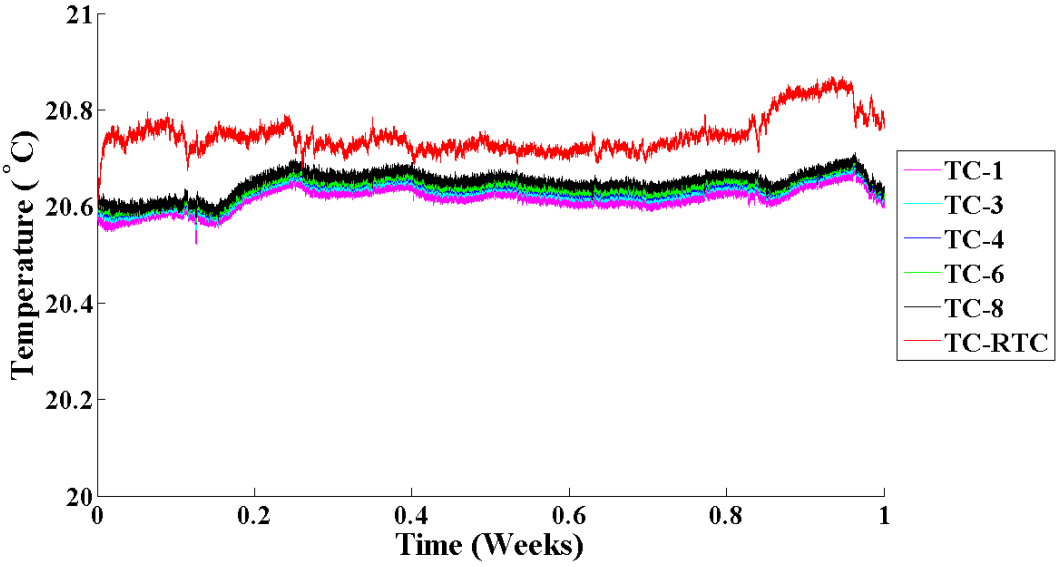

Figure 4.12: Variation of room temperature and *in-situ* temperatures at different ports for a week during 6^{th} sampling point.

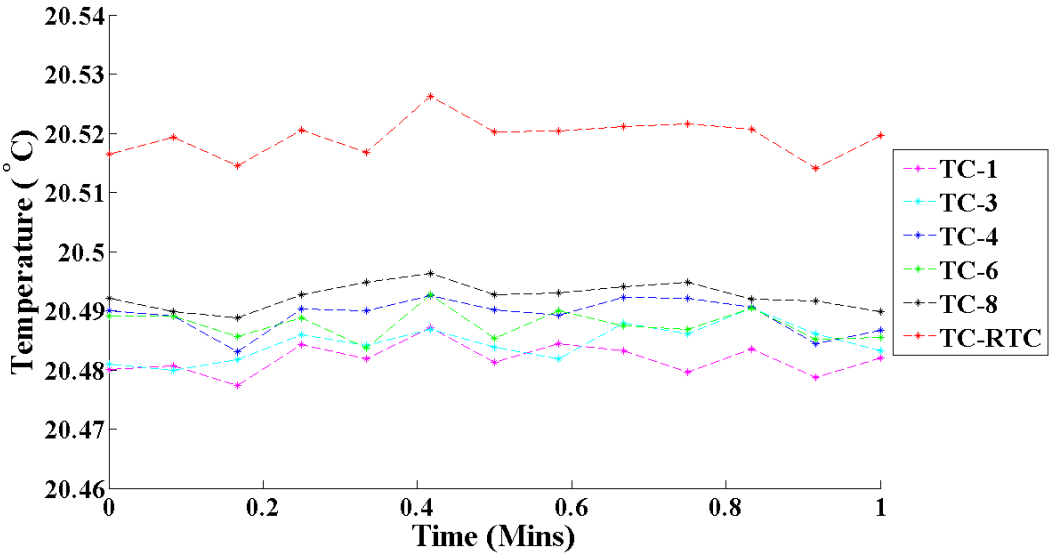

Figure 4.13: Variation of room temperature and *in-situ* temperatures at different ports for a minute during 16^{th} sampling point.

temperature during the day of collection of the sample suggested that the *in-situ* readings obtained from the thermocouples were influenced by the room temperature readings. Ideally, a temperature rise would have been observed if the core holder was perfectly insulated. Calculated enthalpies of the reactions (ΔH) for the acetate fermentation and carbon dioxide reaction pathways under the experimental

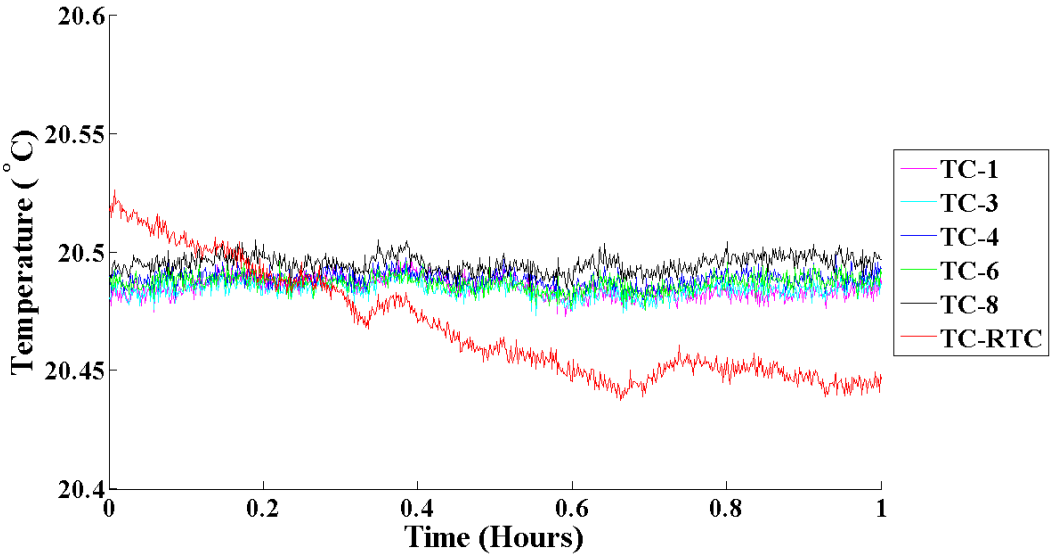

Figure 4.14: Variation of room temperature and *in-situ* temperatures at different ports for an hour during 16^{th} sampling point.

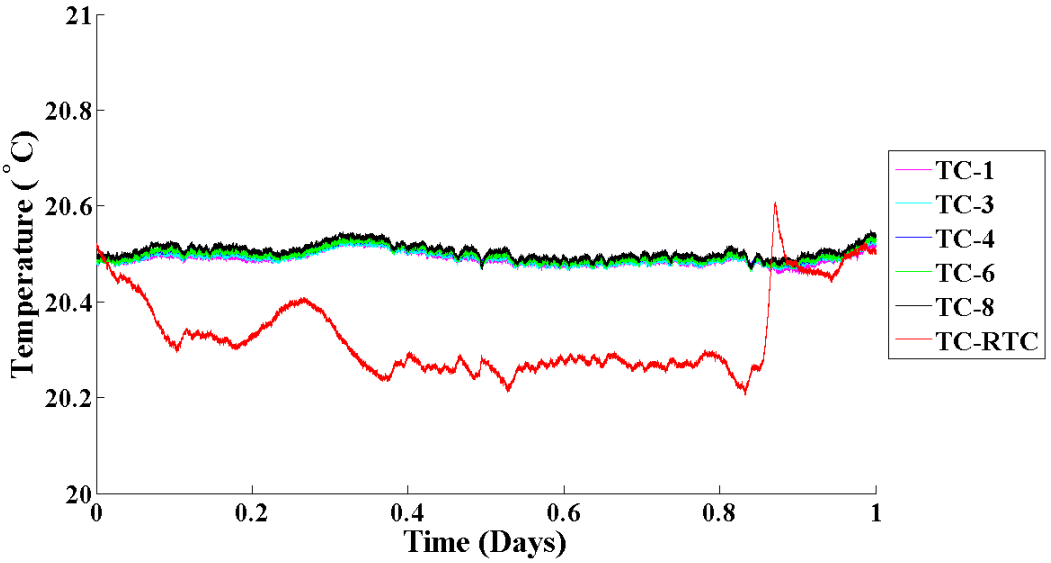

Figure 4.15: Variation of room temperature and *in-situ* temperatures at different ports for a day during 16^{th} sampling point.

conditions (6205.28 kPa(g) confining pressure and 20°C temperature) were -474.22 KJ and -9.13 KJ respectively [68, 69, 70, 71]. The enthalpy values suggested that for an ideally insulated system the reactions leading to methane generation were exothermic in nature. Hence, core holder should be insulated and a temperature controller should be installed for the betterment of the temperature readings.

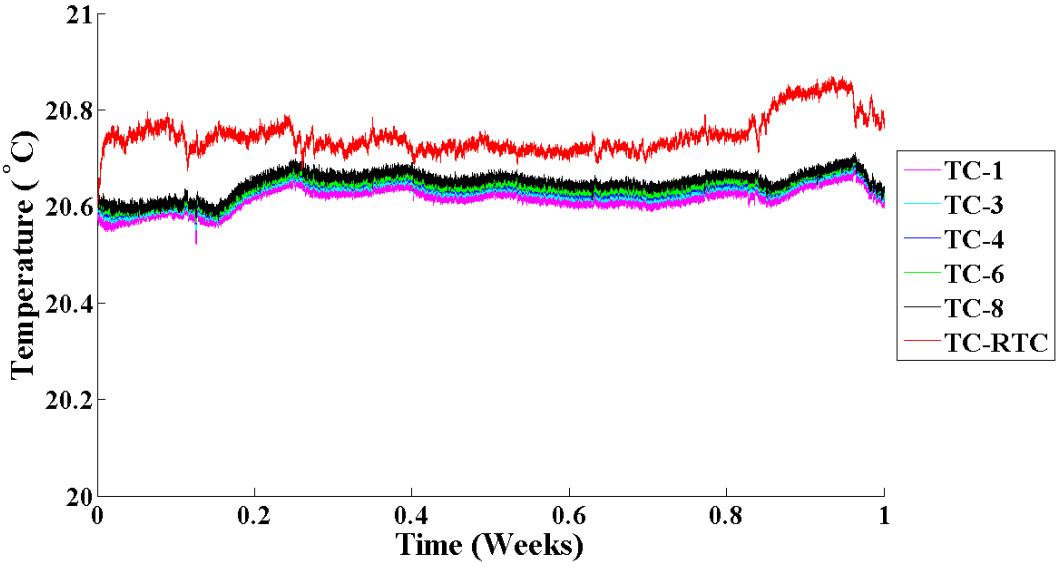

Figure 4.16: Variation of room temperature and *in-situ* temperatures at different ports for a week during 16^{th} sampling point.

4.5 Elemental analysis of coal microbe samples

Coal microbe samples were collected aseptically from the inlet, middle and outlet positions of the core holder after running the core flooding experiments for 180 days. Control coal sample and the coal-microbe samples collected from three different positions were fixed in 15 ml centrifuge tubes using electron microscopy fixative consisting of 2.5% gluteraldehyde and 2% paraformaldehyde in 0.1 M phosphate buffer for a single day at room temperature. Solutions in the centrifuge tubes were washed in 0.1 M phosphate buffer two times for 10 minutes.

Dehydration was the next step after the phosphate buffer wash. All the samples underwent a series of ethanol washes. Solutions were at first washed with 50% ethanol for 5 minutes followed by 70% ethanol for 5 minutes and then 90% ethanol for 5 minutes respectively. Next, the samples were washed twice with 100% ethanol for 5 minutes followed by 5 minutes sequential ethanol:HDMS series washes comprising of the ratio 75:25, 50:50 and 25:75 respectively. After that, the samples were washed with 100% HDMS (Hexamethyldisilazane) for about 5 minutes. Samples were centrifuged in between the washes for 1 minute using a centrifuge (Thermo

Scientific Co.)which was operated at 10,000 rpm. Maximum HDMS was poured off in the last wash for each samples. Finally, after the series of washes the centrifuge tubes containing the samples were left in the fume hood for overnight with caps opened for the purpose of air drying. The air dried samples were kept on

Table 4.9: Elemental analysis of the control and coal-microbe samples collected from inlet, middle and outlet positions of the core holder.

	Weight (%)			
Element	Control	Inlet	Middle	Outlet
C	65.67	62.69	62.61	65.23
O	31.24	32.97	31.85	30.25
Na	0.63	0.95	0.93	0.83
Mg	n/d	0.06	0.05	n/d
Al	0.46	0.41	0.83	0.37
Si	0.81	0.75	1.61	1.14
S	0.1	0.17	0.10	0.09
Ca	0.61	1.01	1.06	1.13
Fe	0.12	0.1	0.1	0.14
P	0.35	0.88	0.87	0.83

carbon conductive adhesive tabs and the elemental analysis was performed using a Scanning Electron Microscope (Vega-3, Tescan Orsay Holding, a.s.) connected to an EDXS detector (Oxford Instruments plc). The elements detected during the analysis have been shown in Table 4.9. Decrease in carbon concentration at inlet, middle and outlet sections of the core holder suggested that bio-conversion occurred throughout the length of the coal pack.

4.6 Variation of Effluent pH

Figure 4.17 reports the variation of pH of core flooding effluent fluid with the cumulative pore volume of injected formation fluid under the application of confining pressure. Figure 4.17 also gives us information regarding the variation of effluent pH in absence of confining pressure as well. The pH measurements of the collected effluent samples were performed using a pH meter (AB15, Accumet Engineering Co.) which was integrated to an electrode (13-620-104A, Accumet Engineering

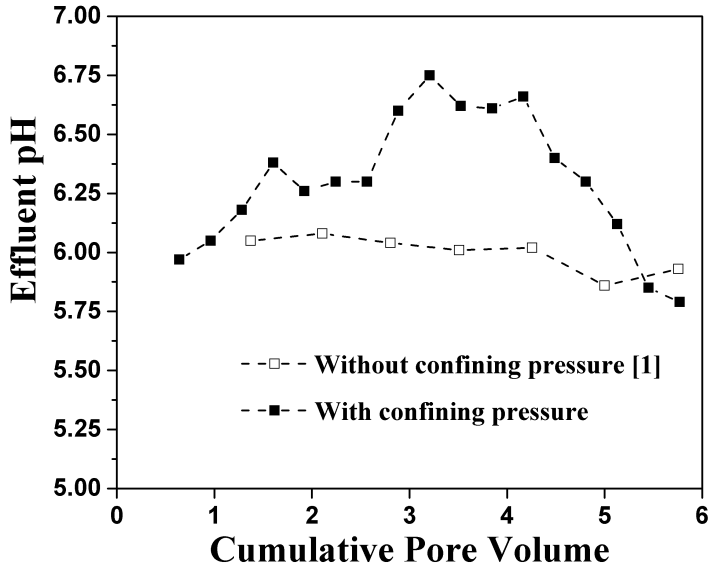

Figure 4.17: Variation of effluent pH with the cumulative pore volume of formation fluid fed to the coal pack.

Co.). The pH of the effluent samples have been reported in Table 4.5. The pH value of the uninoculated formation fluid was 7.05. The pH of the effluent had an increasing trend till 3.2 *PV* of formation fluid was flooded to the coal pack. However, a decrease in pH value was noticed after the coal pack was flooded with 4.48 *PV* of formation fluid and it continued till 5.77 *PV* injection. Methane is generated as a result of many enzymatic reactions. Each enzymatic reaction has its own optimum pH value during which the rate of the reaction is maximum [72]. The optimum pH for the current experiment appeared to be 6.75. The variation of Gibbs energy as a function of pH can give us valuable insight regarding the spontaneity of the enzymatic reactions [73].

4.7 Metabolites detected in the effluent samples

Figure 4.18 depicts the relative concentrations of the compounds detected in uninoculated MSM-Tryptone medium and the core flooding effluent samples through a representation of a heat map constructed using a statistical package software [1, 59]. Samples are listed in the heat map in a chronological manner starting from control

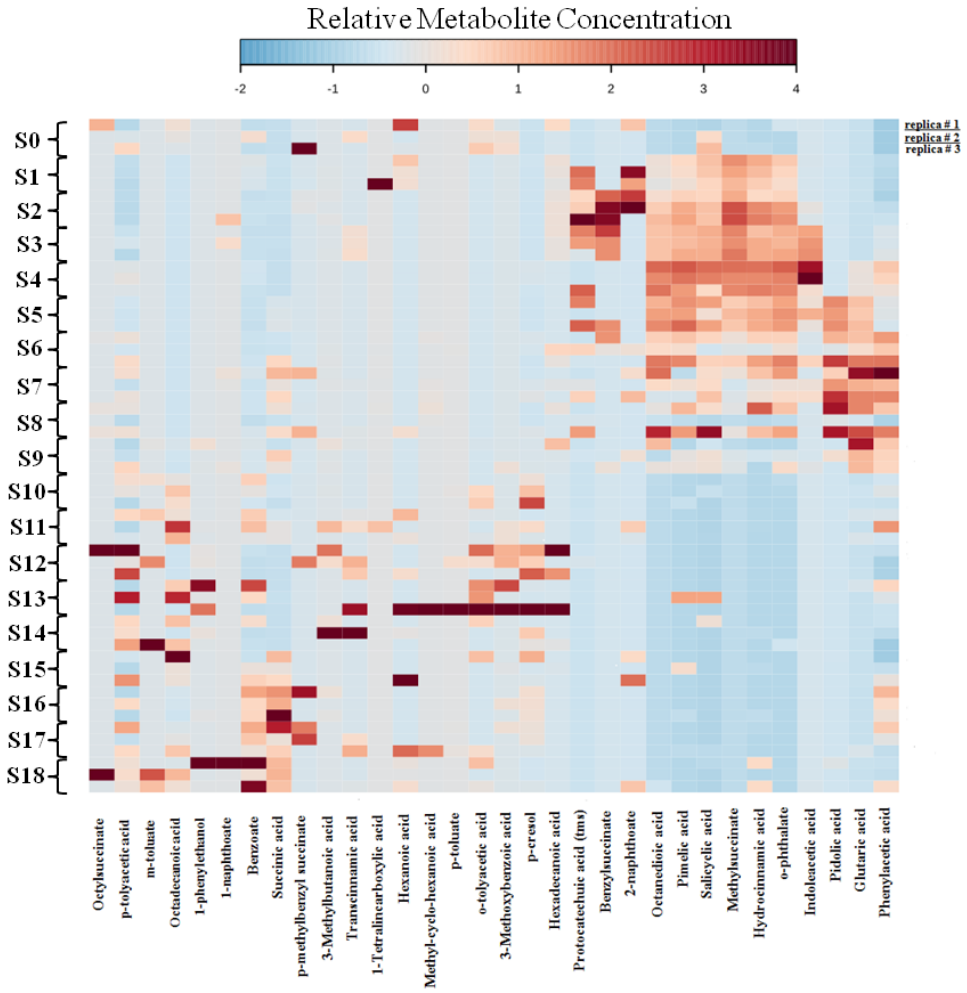

Figure 4.18: Heat map showing the relative concentration of the metabolites in the control sample (S0) and as well as in the collected effluent samples (S1-S18). S1 represents the first core flood sample and S18 represents the eighteenth or the last effluent sample. The relative concentration increases from blue to red in the heat map.

sample (S0) and terminating with the last core flood sample (S18). A graded colour code starting from -2 to +4 is used for representing the relative concentration of the detected compounds. Blue colour corresponding to a particular metabolite in any sample predicts that the metabolite is present in low concentration in that sample. The deep red colour corresponding to a particular metabolite in any sample denotes the probability of the metabolite to be present in high concentration in that sample.

The metabolic products of larger molecular weight hydrocarbons like mono, di and aromatic carboxylic acids [1, 30, 74, 27] were found in the effluent samples. Benzyl succinate was detected in high concentration in S2 and S3. Methyl succinate was also detected in high concentration in samples S1 to S6. However, p-tolyacetic acid and o-tolyacetic acid concentrations started to increase from S11 onwards. The presence of alkyl succinates like methyl succinate and benzyl succinate and tolyacetic acids in the effluent samples were indicator of bio degradation of simple coal constituents like alkanes and mono aromatic acids [1]. Detection of methyl succinate ensured the transformation of alkane groups in coal through addition of fumarate [75, 76, 1].The presence of p-cresol, toluic acids like m-toluate and p-toluate and phthalic acid like o-phthalate also indicated that the aromatic constituents of coal underwent biodegradation. Detection of naphthoates in the effluent sample showed the evidence of naphthalene degradation. Phenylalanine present in Tryptone can undergo anaerobic catabolism to produce phenyl acetate [77]. The enzymes associated with the degradation of phenylalanine to phenyl acetate are L-phenylalanine:2-oxoglutarate transaminase (Pat), phenylpyruvate decarboxylase (Pdc) and phenylacetaldehyde oxidoreductace (AOR). Phenyl acetate in presence of enzymes can be changed to benzyl - CoA which undergoes anaerobic degradation in presence of fermentative microbes to produce acetate (see supporting information of [1]). The acetate can be utilised by acetoclastic methanogens to produce methane. The relative concentration of phenyl acetate was higher till 9^{th} sampling point which proved that microorganisms could be utilizing tryptone as the substrate for methane production. However, for the last nine sampling points, the relative concentration of phenyl acetate decreased which proved that microbes were utilizing coal as a substrate for methanogenesis.

Succinic acid, a value added byproduct [78] obtained during methanogenesis was found in higher concentration in samples S16 to S18. Low methane production till 8^{th} sample was probably due to slower rate of transformation of amino acids, fatty acids and alcohols into acetates, formate, butyrate, H_2 and CO_2 by acetogenic bacteria which are important substrates for methanogenesis. Three kinds of bacteria

are needed ultimately for methanogenesis. Hydrolytic fermentative bacteria breaks the complex polymeric structure of coal into simpler substrates as for e.g. organic acids, fatty acids and alcohols. Hence, the rate of the reaction during primary fermentation process is affected by the concentration of the hydrolytic fermentative bacteria. Syntrophic acetogenic bacteria converts the substrates obtained during primary fermentation process into further simpler substrates as for e.g. acetate, hydrogen and carbon dioxide in presence of enzymes secreted by fermentative microbes. Hence, the rate of the reaction during the secondary fermentation process is affected by the concentration of the enzymes which act as catalysts [79], acetogenic bacteria and substrates which are formed due to anaerobic degradation of complex polymers of coal. The substrates produced during secondary fermentation process are finally consumed by methanogenic bacteria to generate methane. Hence, the rate of methanogenesis are affected by the concentration of substrates formed after secondary fermentation process. Methanogens act like a catalyst during acetoclastic and carbonate reduction reactions. Acetic acid, an important substrate for methanogenesis was also found in the effluent samples. But, overlap of multiple unknown compound peaks from coal between 0 to 10 minutes while performing GCMS analysis gave inaccurate acetic acid readings and hence the data for acetic acid was not collected.

4.8 Comparison with the core-flooding experiment in absence of overburden pressure

Core flooding experiments devoid of overburden pressure[1] yielded 38% porosity while the porosity was 35.65% in case of core flooding with overburden pressure. The permeability value based on water injection was 13.5 mD in absence of overburden pressure while the experiments in presence of 3447.53 kPa(g) confining pressure yielded a permeability value of 8.53 mD. Hence, there was a reduction in permeability of the coal pack under the application of overburden pressure. The permeability of the coal pack decreased by 56.7% from the initial value of 13.27

mD after continuous flooding of MSM-Tryptone solution for 90 days in absence of confining pressure [1]. It is evident from Figure 4.4 that the permeability of the coal pack did not vary significantly with the cumulative pore volume of formation injected to the coal pack in comparison to the experiments performed without overburden pressure.

The core-flooding results without overburden pressure yielded a maximum of 13.51% CH_4 from a collected gas sample. Cumulative methane generation without confining pressure was 1.52 μmol per gram of coal at the end of the experiment [1]. There was a significant increase in methane production for the current experimental set up after 2.6 PV of formation fluid was injected into the coal pack. A total of 2.993 μmol of CH_4 was produced per gram of coal after flooding 5.77 PV of formation fluid into the coal pack at a constant back pressure of 3447.53 kPa(g). 25.73 μmol of CH_4 was recovered at the end after reducing the back pressure of the system to almost 68.98 kPa(g). Hence, it indicates that more methane can be recovered at reduced back pressure. Maximum percentage of CH_4 recovered in a collected gas sample was 51.92%. Cumulative CO_2 production was less in case of experiments conducted with overburden pressure.

The average pH of the effluent sample for the experimental set up with overburden pressure was 6.3 while the core flood runs in absence of overburden pressure yielded a pH of 6 [1]. Hence, it shows that pH has a positive effect on methane generation. The metabolites detected under the current experimental set up were consistent with those detected without overburden pressure. There was a significant decrease in weight (%) of carbon in the inlet section of the core holder compared to the control coal sample for the experiments devoid of overburden pressure. Hence, it showed that coal bio-conversion occurred mostly at the inlet section of the coal pack [1]. The elemental analysis of the coal microbe samples for the present experimental set up as seen from Table 4.9 did not show such a significant decrease in weight (%) of carbon in the inlet section of the core holder.

Chapter 5

Conclusion and Future Work

5.1 Conclusion

The concept of confining pressure was employed to an existing core flooding set up [1]. A special type of core holder named as Hassler type core holder was used for applying overburden pressure to the coal pack. The core flooding experiments were performed under 6205.53 kPa(g) confining pressure using crushed sub-bituminous coal samples. The core flooding set up was consistently operated at 3447.53 kPa(g) back pressure. The core flooding set up was run continuously for 180 days. Cumulative pore volume of formation fluid injected into the coal pack was kept the same as in case of core flood runs without confining pressure in order to make comparisons between the two core flooding systems. The above experimental set up is an attempt to mimic the actual coal reservoir conditions in a laboratory scale.

Porosity of the coal pack subjected to confining stress was 0.3565 while coal core porosity in absence of confining stress was 0.38 [1]. The flooding of formation fluid and microbial solution into the coal core resulted in 32.12 % decrease in coal pack permeability at the end of 180 days. However, permeability of the coal pack in absence of overburden pressure decreased by 57.4 % at the end of 90 days due to flooding of formation fluid and microbial solution [1]. A total of 28.86 μmol of methane was generated from per gram of coal while performing the core flooding runs with confining pressure for 180 days. Core flooding experiments in absence of confining pressure yielded only a total of 1.52 μmol of methane at the end of

90 days [1]. The pH of the collected effluent samples for the current experiments were relatively higher when compared to that of the experiments without confining pressure. The metabolites detected in the current core flooding runs were consistent with those found during performing the experiments without confining stress [1].

Slower rate of methanogenesis for the first eight sampling points indicated that acetate fermentation was the preferred pathway for methane production during that period. However, carbon dioxide reduction appeared to be the most dominant pathway for methane generation after 2.88 *PV* injection of formation fluid into the coal pack. There was an increase in the molar ratio of CH_4 to CO_2 in the subsequent samples. Molar ratio exceeded one after the coal core was depressurized for gas desorption and the carbon dioxide content in the recovered gas sample was less in comparison to methane. Hence, it suggested that heat of adsorption for CO_2 has a higher value in comparison to that of CH_4. The concept behind the adsorption of gases in the coal matrix can be studied with the help of Langmuir isotherm [80]. Gas bubbles were found when the core flooding system was decommissioned which indicated that the coal pack was fully saturated with the gases formed during methanogenesis.

The existing core flooding set up would have yield more methane if the experiments were continued beyond 180 days. The feasibility of coal bio-conversion under the application of confining pressure was tested for the first time. *In-situ* temperature measurements during the coal bio-conversion process was monitored for the first time. Methane generation data obtained from the existing core flooding set up predicts that the technology of *in-situ*bio-conversion is scalable and can be applied in the actual coal reservoir.

5.2 Future Work

The current core flooding set up has shown lot of potential for biogenic methane production. Some further studies will facilitate in clear understanding of the bio

conversion process. Some of the future research work is stated below:

- The present experimental set up focuses on methane generation at 6205.53 kPa(g) confining pressure. Cumulative methane production can be studied for different sets of overburden pressure by keeping the back pressure of the system constant. Conversely, methane generation can be studied for different sets of back pressure by keeping the confining pressure constant.
- Nutrients apart from tryptone can used to study the potential of *in-situ* methane generation.
- AFM characterization of the coal-microbe samples can be done in order to study the interaction between the coal particles and the microbes.
- Intermittent flooding of the combination of mineral salts medium and nutrient solution into the coal pack with overburden pressure can be done in order to study the methane generation potential.
- 16S rRNA pyrotag sequencing of the current coal core samples obtained from the inlet, middle and outlet sections of the core holder can be done and the results can be compared with that of the experiments performed without confining pressure.

References

[1] A. Stephen, A. Adebusuyi, A. Baldygin, J. Shuster, G. Southam, K. Budwill, J. Foght, D.S. Nobes, and S.K. Mitra. Bioconversion of coal: New insights from a core flooding study. *RSC Advances*, 4(43):22779–22791, 2014.

[2] A. Stephen. Comprehensive study of the bioconversion of coal using laboratory core flooding experiments. *MSc. Thesis*, 2014.

[3] Karen Budwill. Microbial methanogenesis and its role in enhancing coalbed methane recovery. *Canadian Coals) CSEG Recorder (Nov. 2003) pp*, pages 41–43, 2003.

[4] Global Carbon Project. Emissions from fossil fuels. *See also: http://www.globalcarbonproject.org*, 2014.

[5] Center for Climate and Energy Solutions. Quick facts. *See also: http://www.c2es.org/energy/source*, 2014.

[6] T.A. Moore. Coalbed methane: A review. *International Journal of Coal Geology*, 101:36–81, 2012.

[7] J.L. Clayton. Geochemistry of coalbed gas - a review. *International Journal of Coal Geology*, 35(1-4):159–173, 1998.

[8] A.R. Scott. Hydrogeologic factors affecting gas content distribution in coal beds. *International Journal of Coal Geology*, 50(1-4):363–387, 2002.

[9] D.D. Rice and G.E. Claypool. Generation, accumulation, and resource potential of biogenic gas. *American Association of Petroleum Geologists Bulletin*, 65(1):5–25, 1981.

[10] A.R. Scott, W.R. Kaiser, and W.B. Ayers Jr. Thermogenic and secondary biogenic gases, san juan basin, colorado and new mexico - implications for coalbed gas producibility. *American Association of Petroleum Geologists Bulletin*, 78(8):1186–1209, 1994.

[11] D. Strapo, M. Mastalerz, C. Eble, and A. Schimmelmann. Characterization of the origin of coalbed gases in southeastern illinois basin by compound-specific carbon and hydrogen stable isotope ratios. *Organic Geochemistry*, 38(2):267–287, 2007.

[12] K. Cheung, P. Klassen, B. Mayer, F. Goodarzi, and R. Aravena. Major ion and isotope geochemistry of fluids and gases from coalbed methane and shallow groundwater wells in Alberta, Canada. *Applied Geochemistry*, 25(9):1307–1329, 2010.

[13] J.C. Pashin. Hydrodynamics of coalbed methane reservoirs in the black warrior basin: Key to understanding reservoir performance and environmental issues. *Applied Geochemistry*, 22(10):2257–2272, 2007.

[14] D. Strapo, F.W. Picardal, C. Turich, I. Schaperdoth, J.L. Macalady, J.S. Lipp, Y.-S. Lin, T.F. Ertefai, F. Schubotz, K.-U. Hinrichs, M. Mastalerz, and A. Schimmelmann. Methane-producing microbial community in a coal bed of the illinois basin. *Applied and Environmental Microbiology*, 74(8):2424–2432, 2008.

[15] M.E. Schlegel, J.C. McIntosh, B.L. Bates, M.F. Kirk, and A.M. Martini. Comparison of fluid geochemistry and microbiology of multiple organic-rich reservoirs in the illinois basin, usa: Evidence for controls on methanogenesis and microbial transport. *Geochimica et Cosmochimica Acta*, 75(7):1903–1919, 2011.

[16] C.A. Rice, R.M. Flores, G.D. Stricker, and M.S. Ellis. Chemical and stable isotopic evidence for water/rock interaction and biogenic origin of coalbed

methane, fort union formation, powder river basin, wyoming and montana u.s.a. *International Journal of Coal Geology*, 76(1-2):76–85, 2008.

[17] Romeo M. Flores, Cynthia a. Rice, Gary D. Stricker, Augusta Warden, and Margaret S. Ellis. Methanogenic pathways of coal-bed gas in the Powder River Basin, United States: The geologic factor. *International Journal of Coal Geology*, 76(1-2):52–75, 2008.

[18] Z. Zhou, C.J. Ballentine, R. Kipfer, M. Schoell, and S. Thibodeaux. Noble gas tracing of groundwater/coalbed methane interaction in the san juan basin, usa. *Geochimica et Cosmochimica Acta*, 69(23):5413–5428, 2005.

[19] S.L. Papendick, K.R. Downs, K.D. Vo, S.K. Hamilton, G.K.W. Dawson, S.D. Golding, and P.C. Gilcrease. Biogenic methane potential for surat basin, queensland coal seams. *International Journal of Coal Geology*, 88(2-3):123–134, 2011.

[20] John W. Smith, Keith W. Gould, Glenn H. Hart, and Don Rigby. Isotopic studies of australian natural and coal seam gases. *AIMM bulletin*, 290(6):43–51, 1985.

[21] D.D. Rice. Composition and origins of coalbed gas. in: Law, b.e., rice, d.d. (eds), hydrocarbons from coal. *American Association of Petroleum Geologists Studies in Geology*, 38:159–184, 1993.

[22] M. T. Madigan, J. M. Martinko, and J. Parker. *Brock Biology of Microorganisms*. Pearson Education, Inc., 2003.

[23] R.M. Fakoussa and M. Hofrichter. Biotechnology and microbiology of coal degradation. *Applied Microbiology and Biotechnology*, 52(1):25–40, 1999.

[24] Burcu Unal, Verlin Ryan Perry, Mili Sheth, Vicente Gomez-Alvarez, Kuk-Jeong Chin, and Klaus Nüsslein. Trace elements affect methanogenic activity and diversity in enrichments from subsurface coal bed produced water. *Frontiers in microbiology*, 3:175, 2012.

[25] M.S. Green, K.C. Flanegan, and P.C. Gilcrease. Characterization of a methanogenic consortium enriched from a coalbed methane well in the powder river basin, u.s.a. *International Journal of Coal Geology*, 76(1-2):34–45, 2008.

[26] D. Strapoc, M. Mastalerz, K. Dawson, J. MacAlady, A.V. Callaghan, B. Wawrik, C. Turich, and M. Ashby. Biogeochemistry of microbial coalbed methane. *Annual Review of Earth and Planetary Sciences*, 39:617–656, 2011.

[27] B. Wawrik, M. Mendivelso, V.A. Parisi, J.M. Suflita, I.A. Davidova, C.R. Marks, J.D. Van Nostrand, Y. Liang, J. Zhou, B.J. Huizinga, D. Strapo, and A.V. Callaghan. Field and laboratory studies on the bioconversion of coal to methane in the san juan basin. *FEMS Microbiology Ecology*, 81(1):26–42, 2012.

[28] T. J. Penner, J.M. Foght, and K. Budwill. Microbial diversity of western canadian subsurface coal beds and methanogenic coal enrichment cultures. *International Journal of Coal Geology*, 82(1-2):81–93, 2010.

[29] S. H. Harris, R. L. Smith, and C. E. Barker. Microbial and chemical factors influencing methane production in laboratory incubations of low-rank subsurface coals. *International Journal of Coal Geology*, 76(1-2):46–51, 2008.

[30] W.H. Orem, C.A. Tatu, H.E. Lerch, C.A. Rice, T.T. Bartos, A.L. Bates, S. Tewalt, and M.D. Corum. Organic compounds in produced waters from coalbed natural gas wells in the powder river basin, wyoming, usa. *Applied Geochemistry*, 22(10):2240–2256, 2007.

[31] W.H. Orem, M.A. Voytek, E.J. Jones, H.E. Lerch, A.L. Bates, M.D. Corum, P.D. Warwick, and A.C. Clark. Organic intermediates in the anaerobic biodegradation of coal to methane under laboratory conditions. *Organic Geochemistry*, 41(9):997–1000, 2010.

[32] Katherine A. Taconi, Mark E. Zappi, W. Todd French, and Lewis R. Brown. Methanogenesis under acidic ph conditions in a semi-continuous reactor system. *Bioresource Technology*, 99(17):8075 – 8081, 2008.

[33] E. J. P. Jones, M. A. Voytek, P. D. Warwick, M. D. Corum, A. Cohn, J. E. Bunnell, A. C. Clark, and W. H. Orem. Bioassay for estimating the biogenic methane-generating potential of coal samples. *International Journal of Coal Geology*, 76(1-2):138–150, 2008.

[34] S. Jin, A. E. Bland, and H. S. Price. Biogenic methane production enhancement systems. (20090246849), 2009.

[35] R. S. Pfeiffer, G. A. Ulrich, and M. Finkelstein. Chemical amendments for the stimulation of biogenic gas generation in deposits of carbonaceous material. (US7696132 B2), 2010.

[36] G. Ulrich and S. Bower. Active methanogenesis and acetate utilization in powder river basin coals, united states. *International Journal of Coal Geology*, 76(1-2):25–33, 2008.

[37] L.K. Gallagher, A.W. Glossner, L.L. Landkamer, L.A. Figueroa, K.W. Mandernack, and J. Munakata-Marr. The effect of coal oxidation on methane production and microbial community structure in powder river basin coal. *International Journal of Coal Geology*, 115:71–78, 2013.

[38] N. Hadia, L. Chaudhari, S.K. Mitra, M. Vinjamur, and R. Singh. Experimental investigation of use of horizontal wells in waterflooding. *Journal of Petroleum Science and Engineering*, 56(4):303–310, 2007.

[39] ME Shafiee, A Kantzas, et al. Investigation on the effect of overburden pressure on vuggy carbonate oil reservoir core properties. *Canadian International Petroleum Conference*, 2009.

[40] N. Hadia, L. Chaudhari, A. Aggarwal, S.K. Mitra, M. Vinjamur, and R. Singh. Experimental and numerical investigation of one-dimensional waterflood in

porous reservoir. *Experimental Thermal and Fluid Science*, 32(2):355–361, 2007.

[41] P.D. Gamson, B.B. Beamish, and D.P. Johnson. Coal microstructure and micropermeability and their effects on natural gas recovery. *Fuel*, 72(1):87–99, 1993.

[42] N. Hadia, L. Chaudhari, S.K. Mitra, M. Vinjamur, and R. Singh. Waterflood profiles and oil recovery with vertical and horizontal wells. *Energy Sources, Part A: Recovery, Utilization and Environmental Effects*, 30(17):1604–1618, 2008.

[43] V. Santosh, S.K. Mitra, M. Vinjamur, and R. Singh. Experimental and numerical investigations of waterflood profiles with different well configurations. *Energy and Fuels*, 21(6):3353–3359, 2007.

[44] S. Bagci, M.V. Kok, and U. Turksoy. Determination of formation damage in limestone reservoirs and its effect on production. *Journal of Petroleum Science and Engineering*, 28(1-2):1–12, 2000.

[45] S. Bagci and H. Hodaie. An investigation of polymerflooding in limestone reservoirs with a bottom water zone. *Energy Sources*, 25(3):253–264, 2003.

[46] S. Bagci. 3-d model studies of alkaline flooding using horizontal wells. *Energy Sources*, 26(8):783–793, 2004.

[47] S. Bagci. Seven-spot steam injection experiments in heavy oil reservoirs having a bottom water zone. *Energy and Fuels*, 19(3):1037–1046, 2005.

[48] S Bagci, S Dogay, Y Pamukcu, Y Yilmaz, et al. Investigation of surfactant-sagd process in fractured carbonate reservoirs. *Canadian International Petroleum Conference*, 2004.

[49] S. Baci and F. Gmrah. An examination of steam-injection processes in horizontal and vertical wells for heavy-oil recovery. *Journal of Petroleum Science and Engineering*, 8(1):59–72, 1992.

[50] S. Baci, E.P. Turna, and U. Altmi. Steamflooding of medium and light oils in limestone using 3-d laboratory model. *Chemical Engineering Research and Design*, 76(A5):604–611, 1998.

[51] S Bagci, E Tuzunoglu, et al. 3d model studies of the immiscible co process using horizontal wells for heavy oil recovery. *Annual Technical Meeting*, 1998.

[52] A. Beaton, W. Langenberg, and C. Pan. Coalbed methane resources and reservoir characteristics from the alberta plains, canada. *International Journal of Coal Geology*, 65(1-2):93–113, 2006.

[53] R. Guo, K. Mannhardt, and A. Kantzas. Laboratory investigation on the permeability of coal during primary and enhanced coalbed methane production. *Journal of Canadian Petroleum Technology*, 47(10):27–32, 2008.

[54] Z. Zeng, R. Grigg, and S. Ganda. Experimental study of overburden and stress influence on non-darcy gas flow in dakota sandstone. *Proceedings - SPE Annual Technical Conference and Exhibition*, pages 377–386, 2003.

[55] S. Mazumder, K.H.A.A. Wolf, P. Hemert, and A. Busch. Laboratory experiments on environmental friendly means to improve coalbed methane production by carbon dioxide/flue gas injection. *Transport in Porous Media*, 75(1):63–92, 2008.

[56] Japan Jitendrabhai Trivedi, Tayfun Babadagli, et al. Experimental analysis of co2-sequestration efficiency during oil recovery in naturally fractured reservoirs. *SPE Eastern Regional/AAPG Eastern Section Joint Meeting*, 2008.

[57] P.M. Fedorak and S.E. Hrudey. The effects of phenol and some alkyl phenolics on batch anaerobic methanogenesis. *Water Research*, 18(3):361–367, 1984.

[58] K. Budwill, S. Koziel, and J. Vidmar. Advancements in understanding and enhancing biogenic methane production from coals. *Society of Petroleum Engineers - Canadian Unconventional Resources Conference 2011, CURC 2011*, 2:1621–1629, 2011.

[59] J. Xia, R. Mandal, I.V. Sinelnikov, D. Broadhurst, and D.S. Wishart. Metaboanalyst 2.0-a comprehensive server for metabolomic data analysis. *Nucleic Acids Research*, 40(W1):W127–W133, 2012.

[60] Adrian E. Scheidegger. *The physics of flow through porous media*. University of Toronto Press, Toronto, third edition, 1974.

[61] L.J. Klinkenbeg. The permeability of porous media to liquids and gases, drilling and production practice. *American Petroleum Institution*, pages 200–213, 1941.

[62] P. C. Carman. Permeability of saturated sands, soils and clays. *The Journal of Agricultural Science*, 29:262–273, 1939.

[63] W. Lin, G.-Q. Tang, and A.R. Kovscek. Sorption-induced permeability change of coal during gas-injection processes. *SPE Reservoir Evaluation and Engineering*, 11(4):792–802, 2008.

[64] S Mazumder and K Wolf. Differential swelling and permeability change of coal in response to CO2 injection for ECBM. *International Journal of Coal Geology*, 74(2):123–138, 2008.

[65] D.A. Wiesenburg and N.L. Guinasso Jr. Equilibrium solubilities of methane, carbon monoxide, and hydrogen in water and sea water. *Journal of Chemical and Engineering Data*, 24(4):356–360, 1979.

[66] E. Wilhelm, R. Battino, and R.J. Wilcock. Low-pressure solubility of gases in liquid water. *Chemical Reviews*, 77(2):219–262, 1977.

[67] Chemguide. Le chatelier's principle. *See also: http://www.chemguide.co.uk/physical/equilibria/lechatelier.html*, 2014.

[68] Peace software. Thermodynamic state variables of methane. *See also: http://www.peacesoftware.de/einigewerte/methane.html*, 2014.

[69] Peace software. Thermodynamic state variables of carbon dioxide. *See also: http://www.peacesoftware.de/einigewerte/co2.html*, 2014.

[70] Peace software. Thermodynamic state variables of water. *See also: http://www.peacesoftware.de/einigewerte/wasserdampf.html*, 2014.

[71] Wikipedia. Thermodynamic properties of acetic acid. *See also: http://en.wikipedia.org/wiki/acetic acid(datapage)*, 2014.

[72] Worthington Biochemical Corporation. Effects of ph. *See also: http://www.worthington-biochem.com/introbiochem/effectsph.html*, 2014.

[73] A. Flamholz, E. Noor, A. Bar-Even, and R. Milo. Equilibrator - the biochemical thermodynamics calculator. *Nucleic Acids Research*, 40(D1):D770–D775, 2012.

[74] K.E. Duncan, L.M. Gieg, V.A. Parisi, R.S. Tanner, S.G. Tringe, J. Bristow, and J.M. Suflita. Biocorrosive thermophilic microbial communities in Alaskan North Slope oil facilities. *Environmental Science and Technology*, 43(20):7977–7984, 2009.

[75] L.M. Gieg and J.M. Suflita. Detection of anaerobic metabolites of saturated and aromatic hydrocarbons in petroleum-contaminated aquifers. *Environmental Science and Technology*, 36(17):3755–3762, 2002.

[76] V.A. Parisi, G.R. Brubaker, M.J. Zenker, R.C. Prince, L.M. Gieg, M.L.B. Da Silva, P.J.J. Alvarez, and J.M. Suflita. Field metabolomics and laboratory assessments of anaerobic intrinsic bioremediation of hydrocarbons at a petroleum-contaminated site. *Microbial Biotechnology*, 2(2 SPEC. ISS.):202–212, 2009.

[77] M. Carmona, M.T. Zamarro, B. Bizquez, G. Durante-Rodrguez, J.F. Jurez, J.A. Valderrama, M.J.L. Barragn, J.L. Garca, and E. Daz. Anaerobic catabolism of aromatic compounds: A genetic and genomic view. *Microbiology and Molecular Biology Reviews*, 73(1):71–133, 2009.

[78] J.G. Zeikus, M.K. Jain, and P. Elankovan. Biotechnology of succinic acid production and markets for derived industrial products. *Applied Microbiology and Biotechnology*, 51(5):545–552, 1999.

[79] Chemistry for Biologists. Function of enzymes. *See also: http://www.rsc.org/Education/Teachers/Resources/cfb/enzymes.htm*, 2014.

[80] C.M. White, D.H. Smith, K.L. Jones, A.L. Goodman, S.A. Jikich, R.B. LaCount, S.B. DuBose, E. Ozdemir, B.I. Morsi, and K.T. Schroeder. Sequestration of carbon dioxide in coal with enhanced coalbed methane recovery - a review. *Energy and Fuels*, 19(3):659–724, 2005.

Appendix

A.1 Pressure Transducers

A.1.1 Calibration procedure for Differential Pressure Transducers

Differential pressure transducers, C-DP-1 (DP15 series, Validyne Engineering Corp.) and C-DP-2 (P55D series, Validyne Engineering Corp.) were calibrated using a calibration device (Druck PACE5000, General Electric Company). The maximum differential pressure ratings for C-DP-1 and C-DP-2 transducers were 3.2 psi(d) and 2 psi(d) respectively. C-DP-1 was used for measuring the pressure drop across the whole length of the coal pack while C-DP-2 was used for measuring the local differential pressure in the coal pack.

The rear part of the calibration equipment was connected to an IEC power connector. The calibration device was connected to the computer by means of RS232 cable. The positive connection port of the differential transducers was connected to a nitrogen supply line while the negative connection port was open to atmosphere. C-DP-1 transducer was connected to a signal conditioner (CD15) via PTA02A-10-6P connector. The front section of the signal conditioner were provided with red and black output binding posts. The red output binding post was attached to one of the positive connection terminals (AIX+) of the DAQ card (NI USB-6009) through a red electric re. The black output binding post was attached to a negative connection terminal (AIX-) of the DAQ card (NI USB-6009) through a black electric wire. USB cable was used to connect the DAQ unit with the computer. In case of C-DP-2 differential transducer, the positive and negative connection ports were directly connected to DAQ.

Pressure calibrations were performed using NI Measurement and Automation Explorer (National Instruments Corp.) and the custom operated Pressure Calibration Project (PCP) software respectively [2]. Minimum differential pressure (0 psi) for each of the transducers corresponded to 0 V. The maximum differential pressure for C-DP-1 transducer corresponded to 10 V while the maximum differential

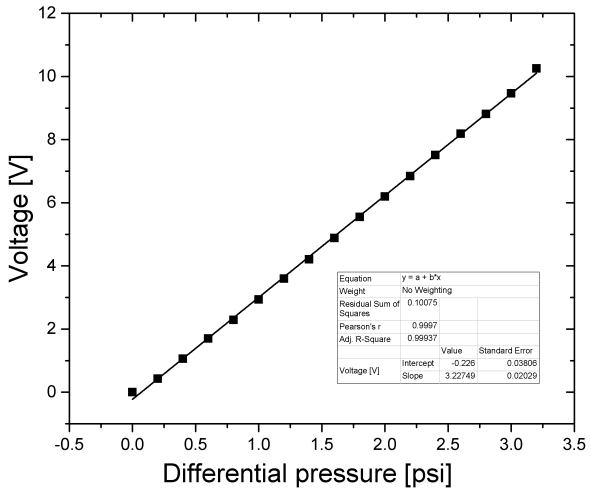

Figure A.1: Calibration curve for C-DP-1 showing the variation of voltage with differential pressure

pressure for C-DP-2 transducer corresponded to 5 V. In case of C-DP-1 transducer, zero setting was done by adjusting the zero knob present on the signal conditioner, CD15. Zero knob was adjusted till the voltage reading reached a value close to zero. Span setting of C-DP-1 was done by adjusting the span knob and the adjustments were carried on till the DC voltage reading indicated a value of 10 V. The voltage readings for pressure ranging from 0 to 3.2 psi were taken at an interval of 0.2 psi for C-DP-1. The pressure was set directly in C-DP-2 transducer using the calibration software and the voltage readings for differential pressure varying from 0 to 2 psi at an interval of 0.25 psi were taken.

A.1.2 Calibration procedure for Inline Pressure Transducers

The inline pressure transducers, C-PT-1 and C-PT-2 (FP2000 series, Honeywell International Inc) were previously calibrated by Honeywell Company. The maximum pressure ratings for the inline pressure transducers (C-PT-1 or C-PT-2) was 750 psi(g) which corresponded to a maximum voltage of 10 V.

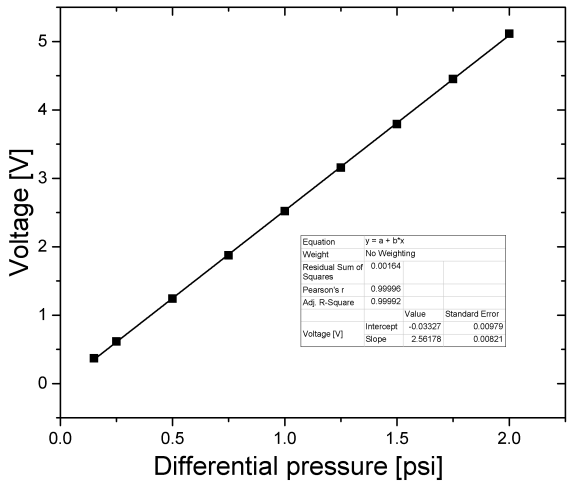

Figure A.2: Calibration curve for C-DP-2 showing the variation of voltage with differential pressure

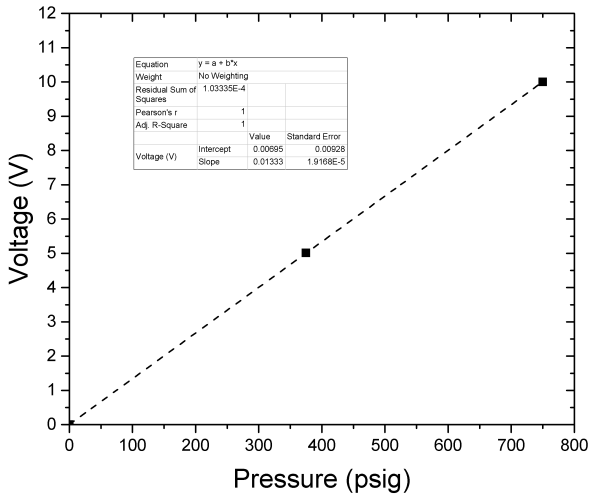

Figure A.3: Calibration curve for C-PT-1 and C-PT-2 showing the variation of voltage with pressure

A.1.3 Variation of differential pressure readings for all the sampling points

This section shows the variation in differential pressure readings obtained using inline pressure transducers(C-PT-1 and C-PT-2) and differential pressure transducer

(C-DP-1) during the collection of subsequent samples.

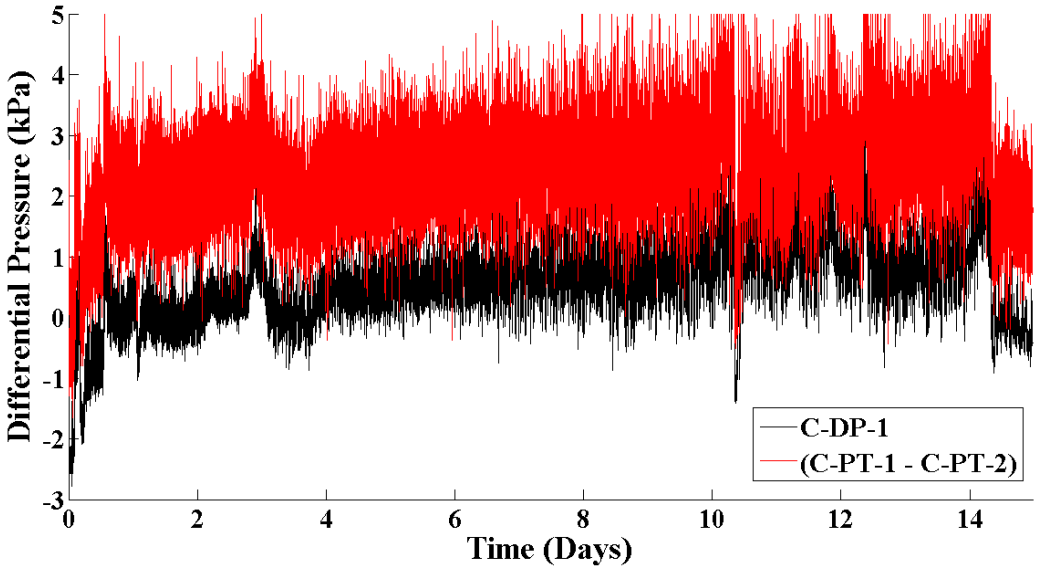

Figure A.4: Variation of differential pressure during the collection of Effluent Sample No. 1.

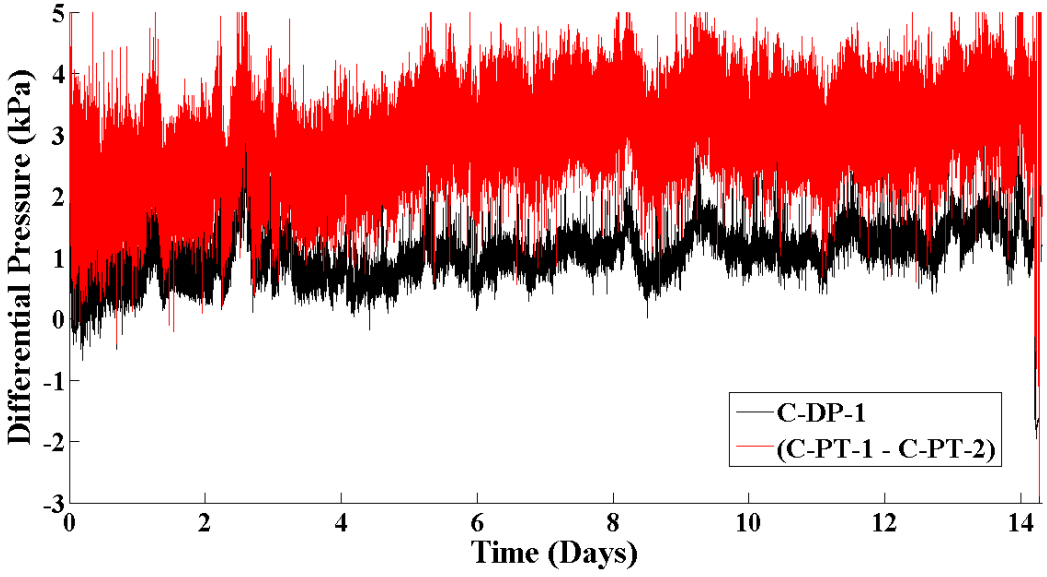

Figure A.5: Variation of differential pressure during the collection of Effluent Sample No. 2.

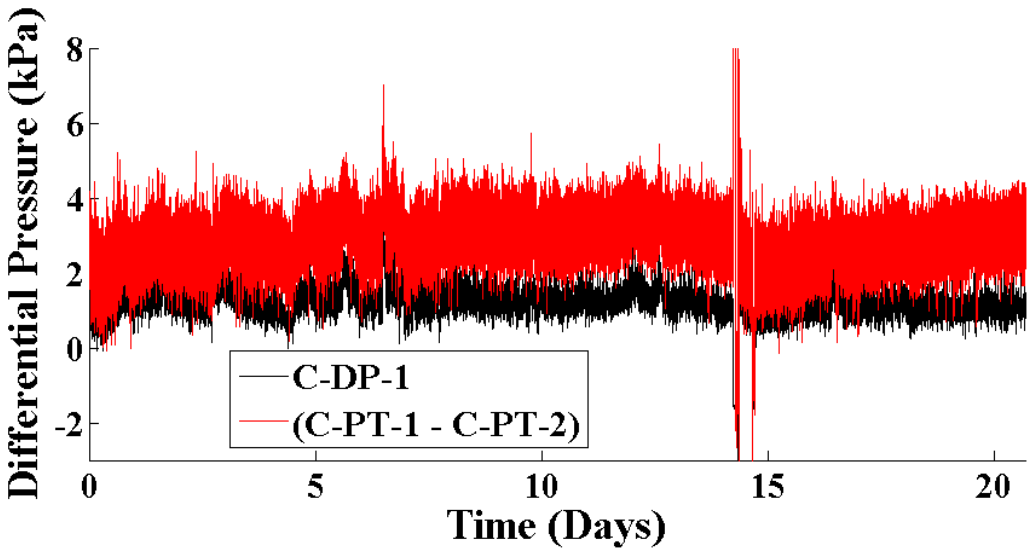

Figure A.6: Variation of differential pressure during the collection of Effluent Sample No. 3.

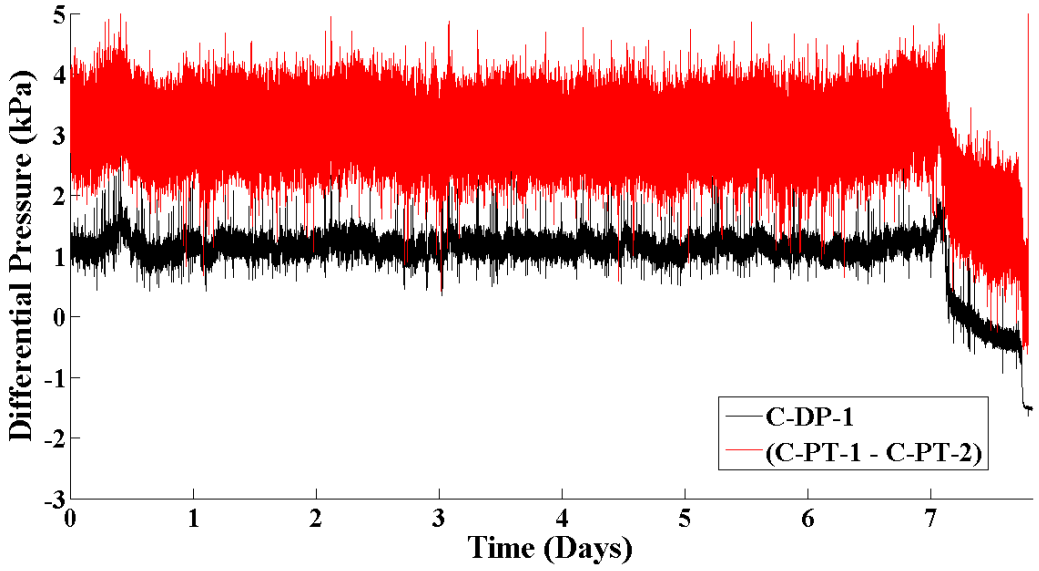

Figure A.7: Variation of differential pressure during the collection of Effluent Sample No. 4.

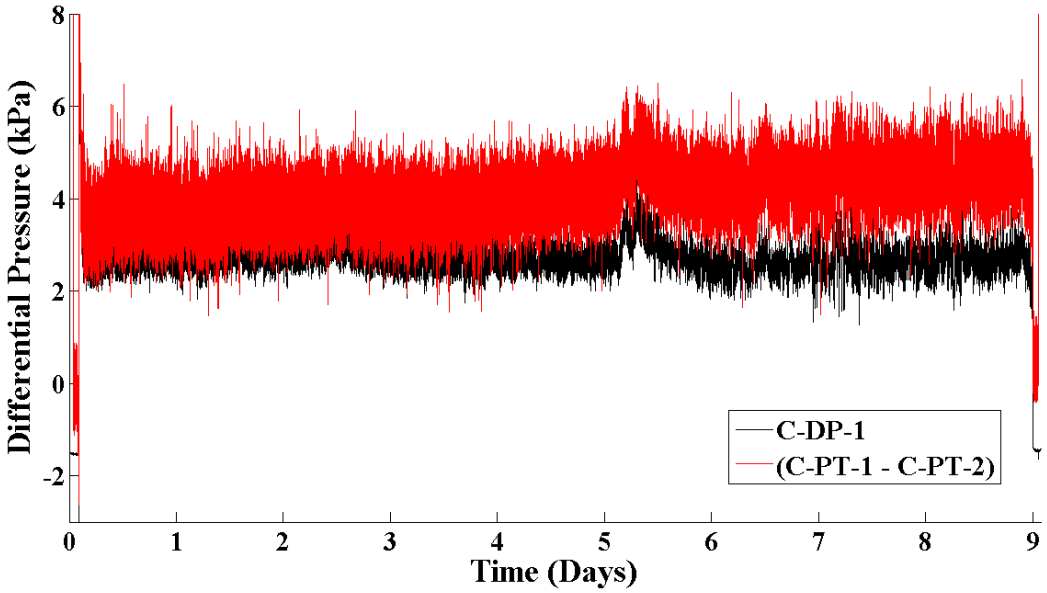

Figure A.8: Variation of differential pressure during the collection of Effluent Sample No. 5.

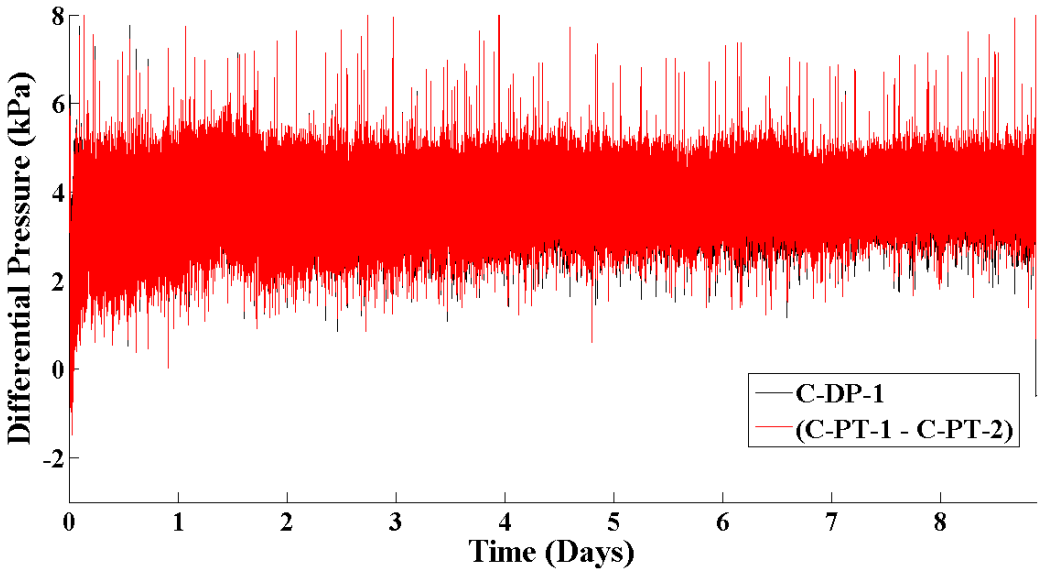

Figure A.9: Variation of differential pressure during the collection of Effluent Sample No. 6.

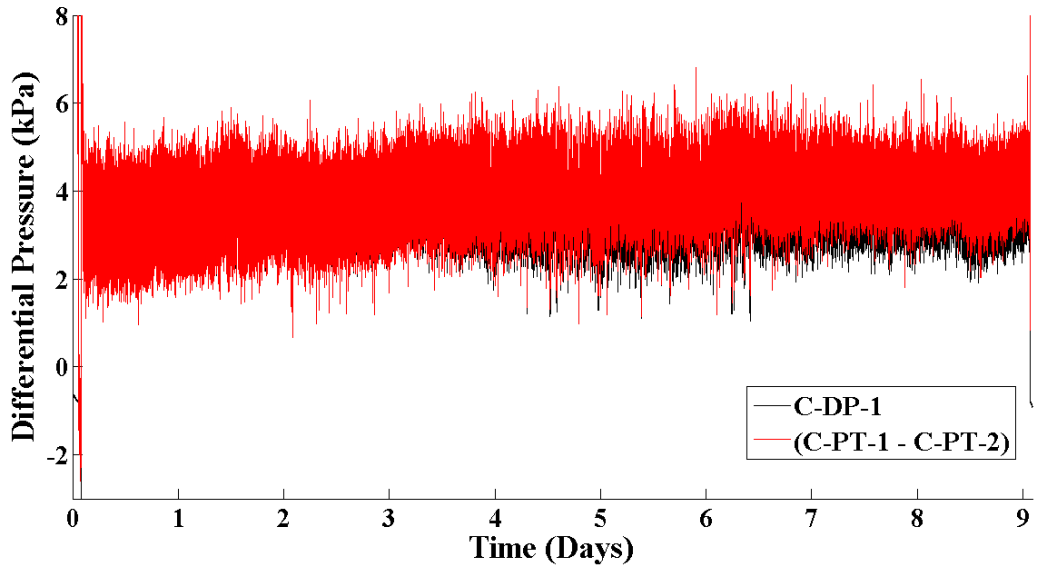

Figure A.10: Variation of differential pressure during the collection of Effluent Sample No. 7.

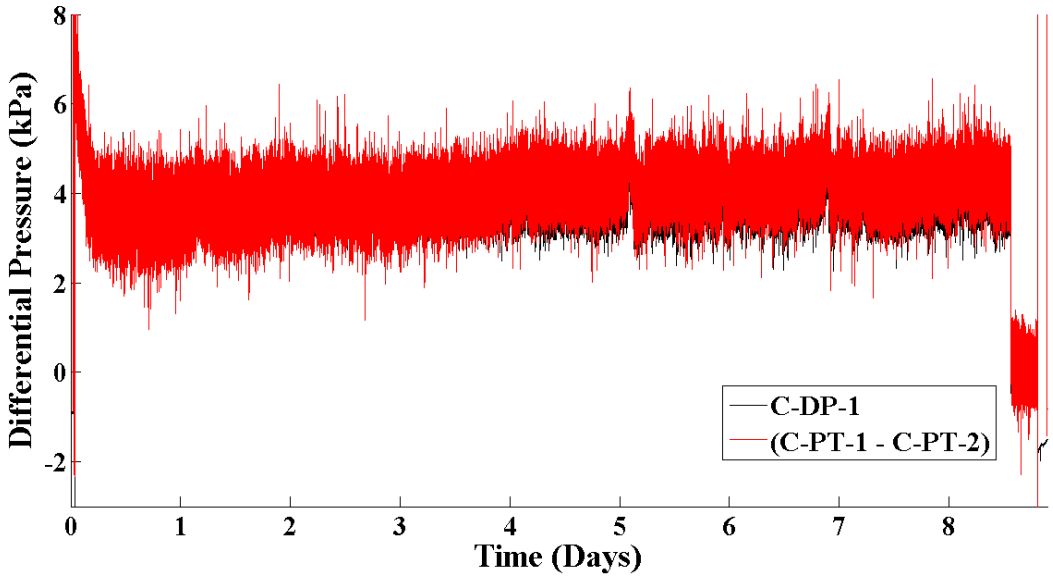

Figure A.11: Variation of differential pressure during the collection of Effluent Sample No. 8.

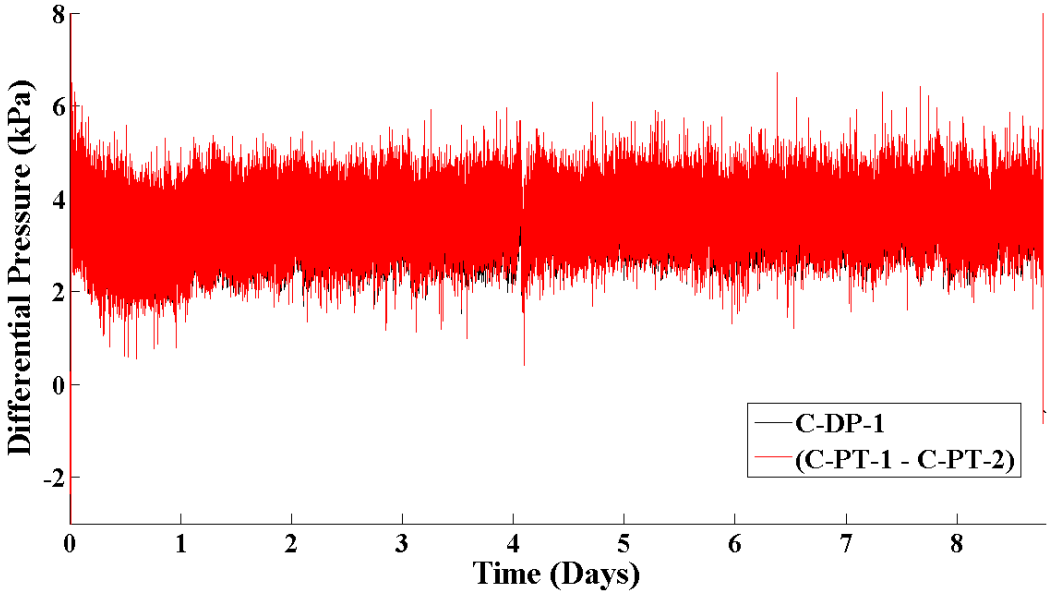

Figure A.12: Variation of differential pressure during the collection of Effluent Sample No. 9.

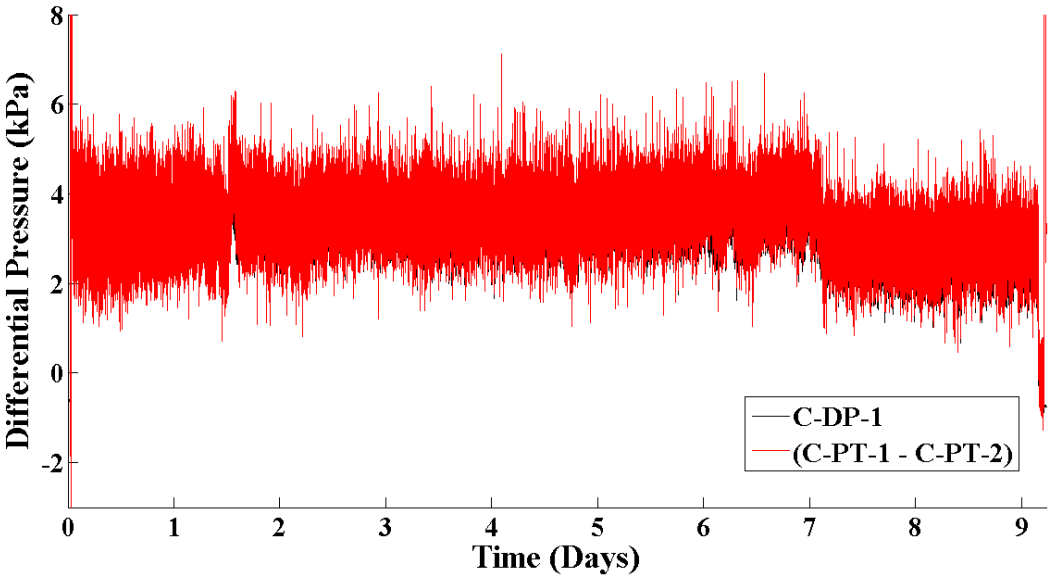

Figure A.13: Variation of differential pressure during the collection of Effluent Sample No. 10.

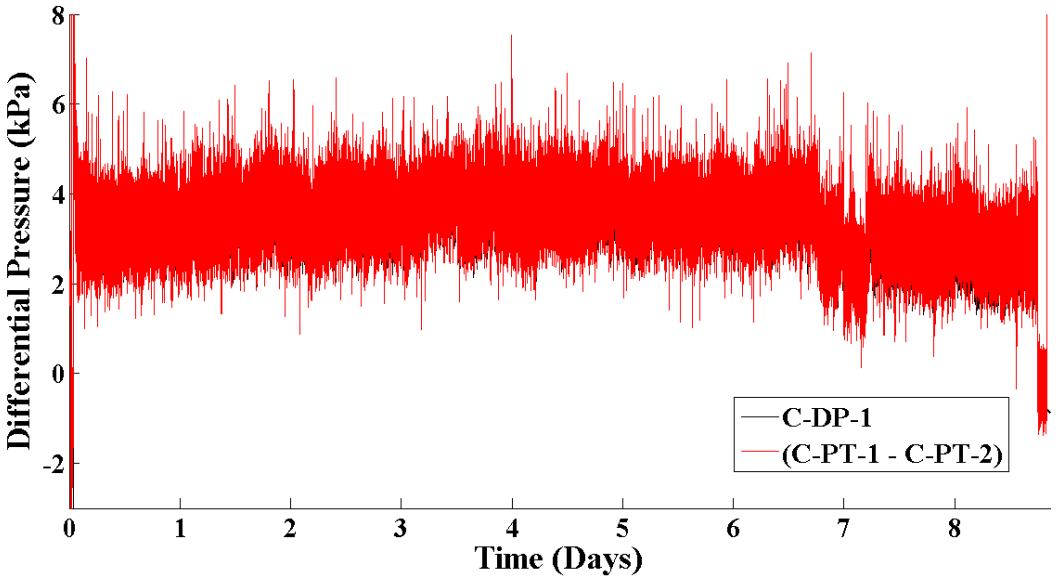

Figure A.14: Variation of differential pressure during the collection of Effluent Sample No. 11.

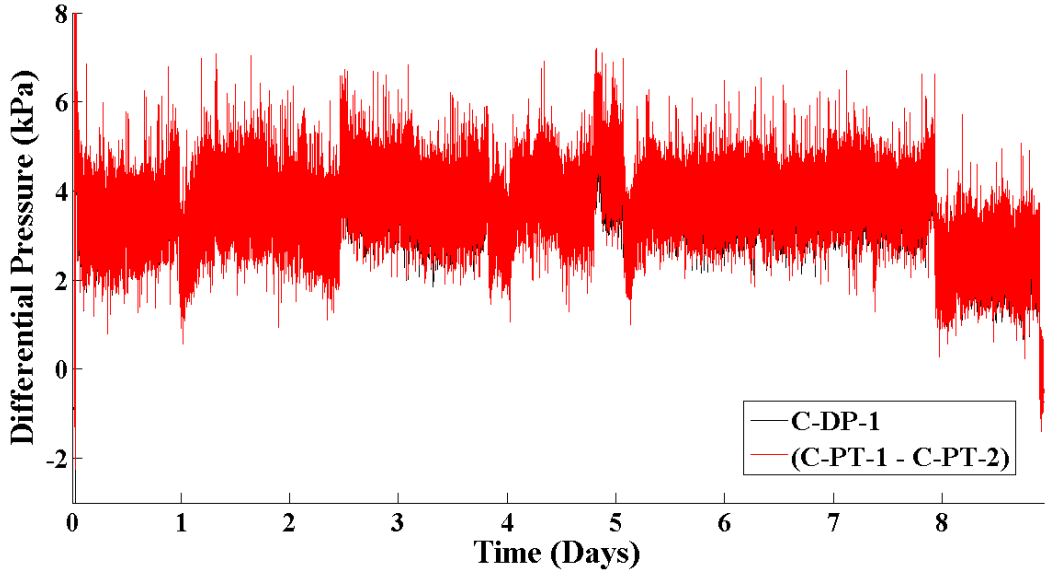

Figure A.15: Variation of differential pressure during the collection of Effluent Sample No. 12.

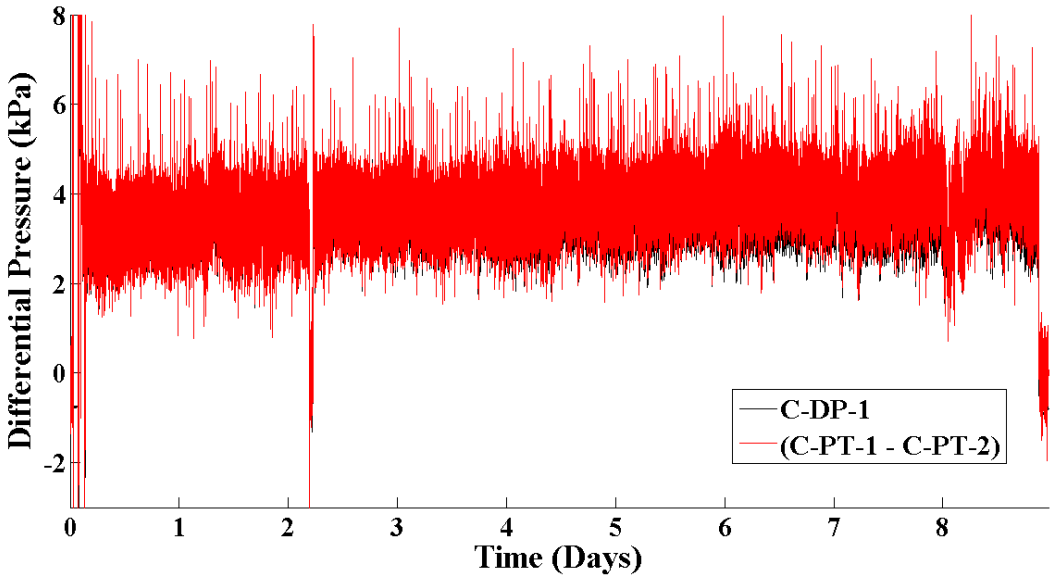

Figure A.16: Variation of differential pressure during the collection of Effluent Sample No. 13.

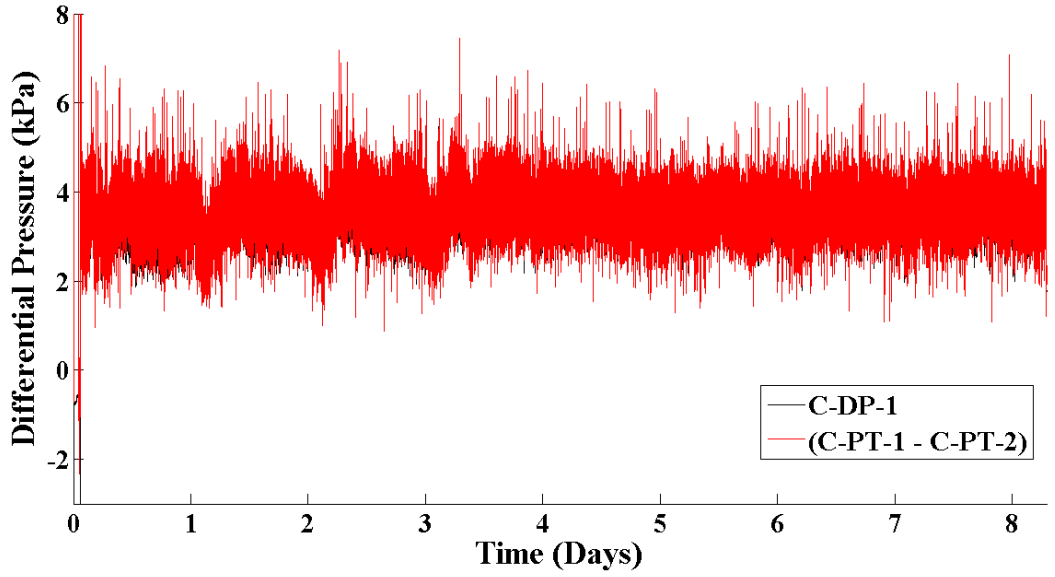

Figure A.17: Variation of differential pressure during the collection of Effluent Sample No. 14.

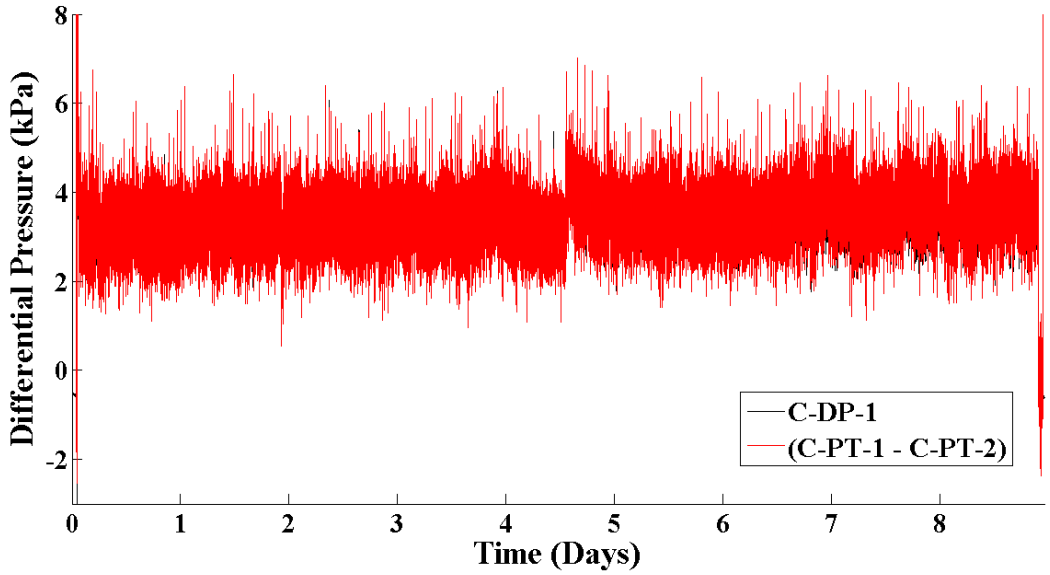

Figure A.18: Variation of differential pressure during the collection of Effluent Sample No. 15.

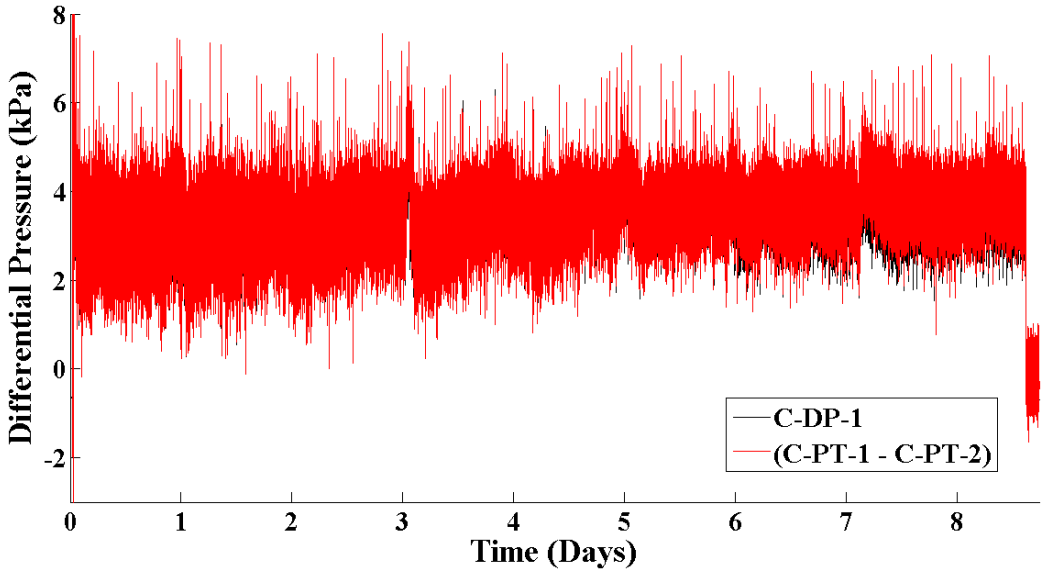

Figure A.19: Variation of differential pressure during the collection of Effluent Sample No. 16.

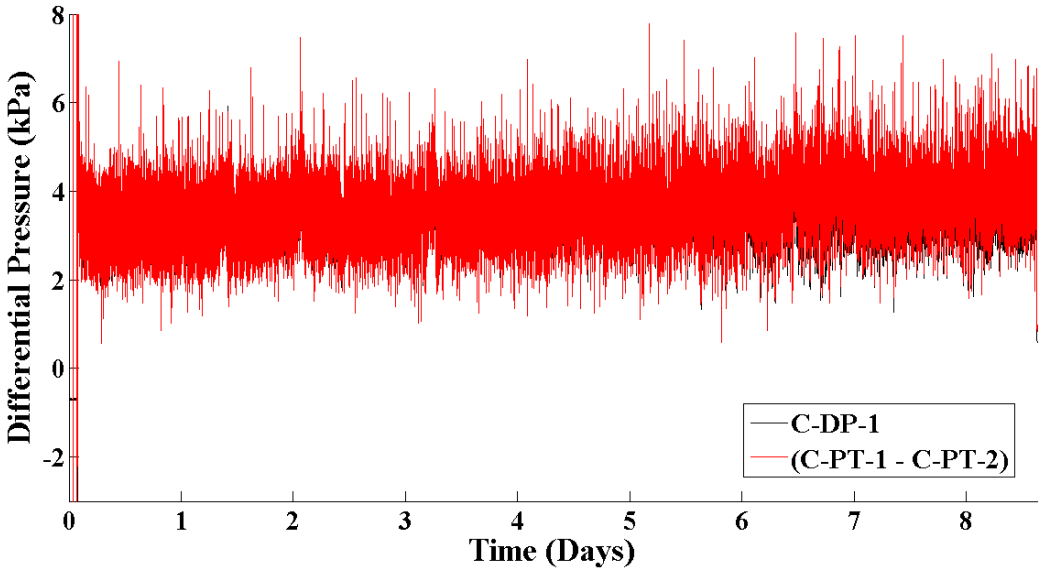

Figure A.20: Variation of differential pressure during the collection of Effluent Sample No. 17.

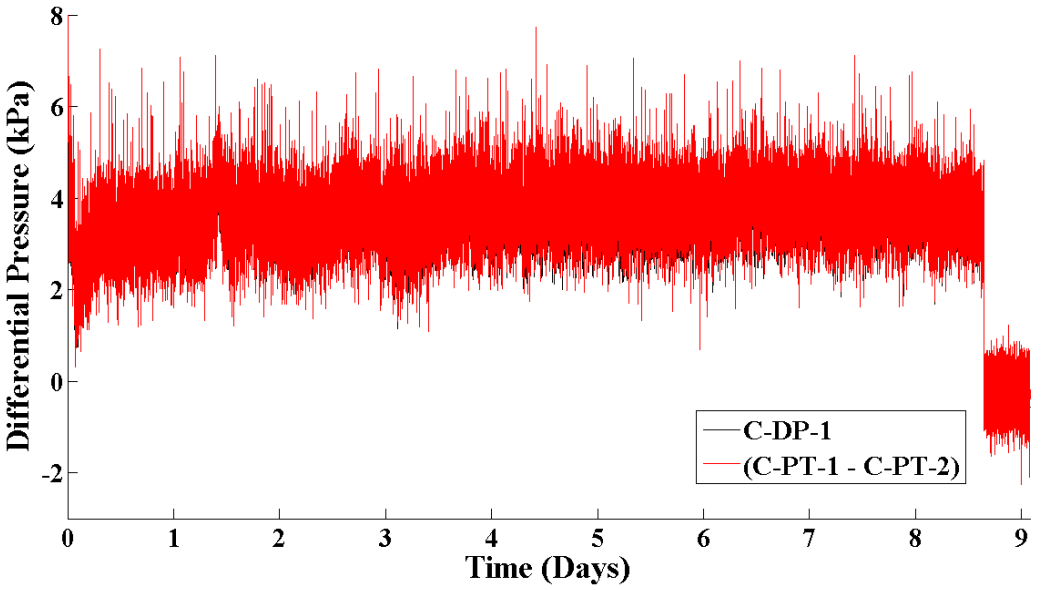

Figure A.21: Variation of differential pressure during the collection of Effluent Sample No. 18.

B.1 Thermocouples

B.1.1 Calibration of Thermocouples

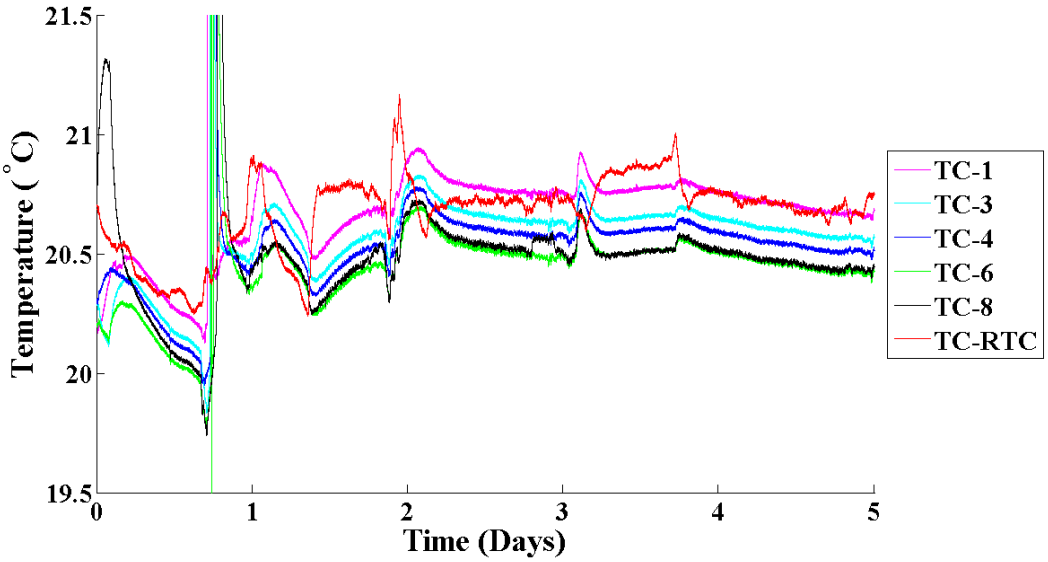

Figure B.1: Variation of room temperature and temperature at different locations inside the core holder during water flooding experiments.

Water flooding experiment was considered as the base for calibration of T type thermocouples. It had been assumed that during water flooding experiments, the thermocouple installed inside the core holder ports as well as the room temperature thermocouple should give the same reading since the innoculum required for coal bio-conversion was not injected to the coal pack at that time. Hence, ideally there should not be any chemical reactions occurring inside the core holder due to flooding of degassed water into the coal core.

The period between 4 to 4.5 days during water flooding experiment was found to be stable and so the average of the temperature readings during that period was calculated for each thermocouples. The amount of offset from the calculated average value of each *in-situ* thermocouples was determined with respect to the average value of the outside or room temperature thermocouple. The calculated offset values for each *in-situ* thermocouples were then added to the temperature readings obtained during each sample collection period in order to obtain the corrected value

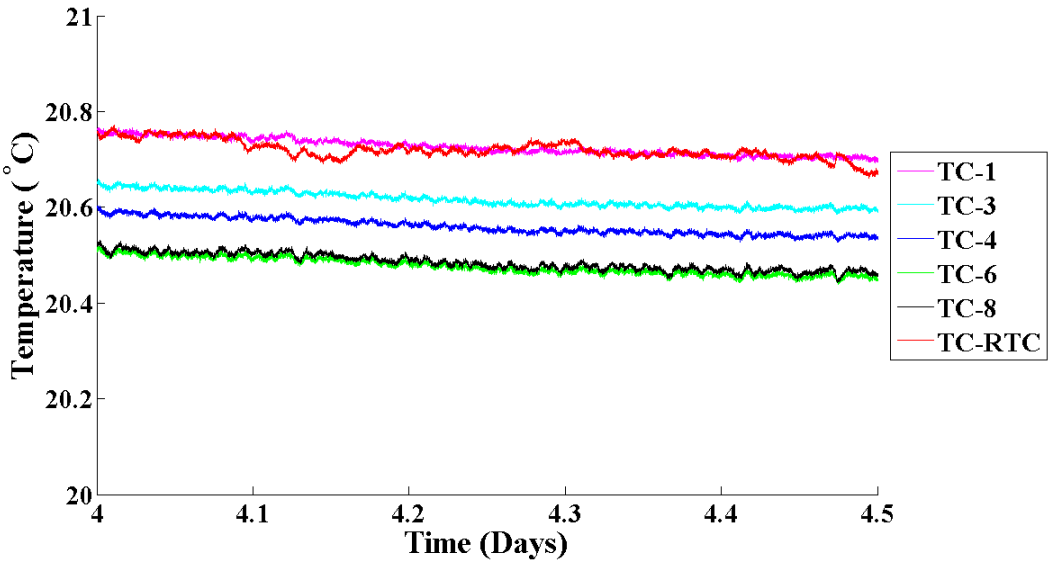

Figure B.2: Variation of room temperature and temperature at different locations inside the core holder during water flooding experiments for a time span of 12 hours.

of temperature.

B.1.2 Variation of uncorrected temperature readings obtained from different thermocouples for all the sampling points

This section provides the variation of temperature readings obtained from thermocouples for each sample without any calibration during the collection of subsequent effluent samples.

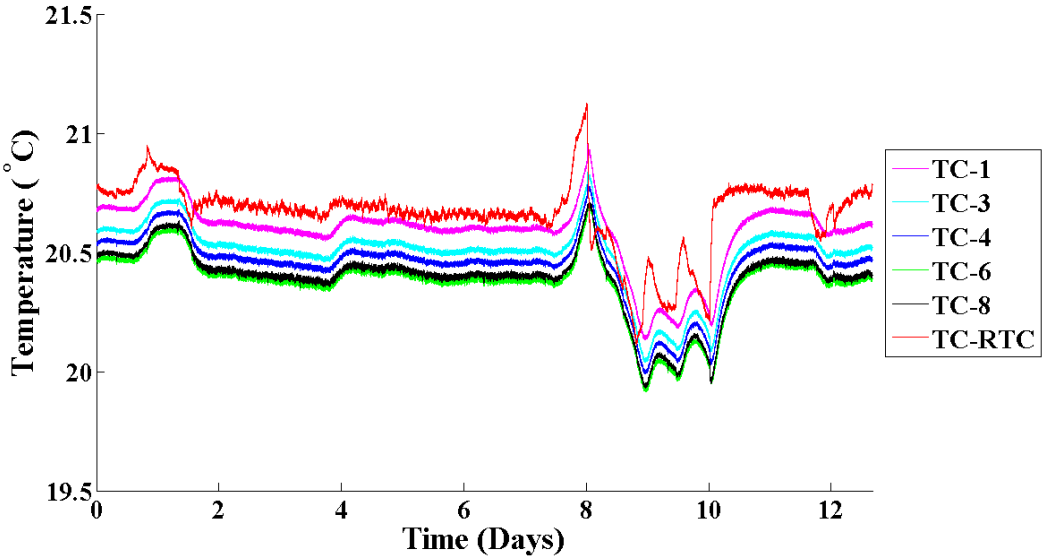

Figure B.3: Variation of room temperature and uncorrected *in-situ* temperatures at different locations inside the core holder during the collection of Effluent Sample No. 1.

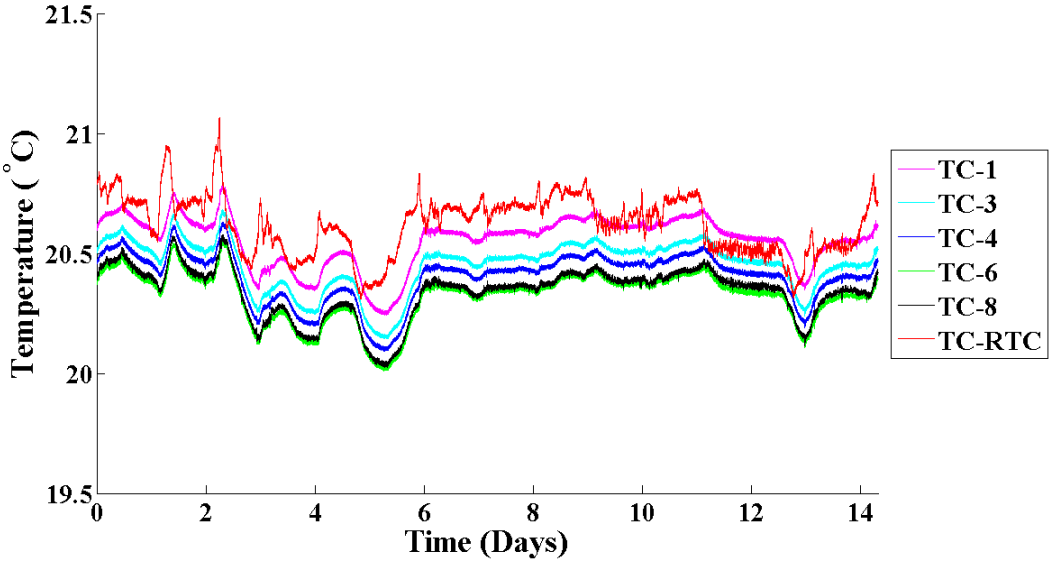

Figure B.4: Variation of room temperature and uncorrected *in-situ* temperatures at different locations inside the core holder during Sample No. 2.

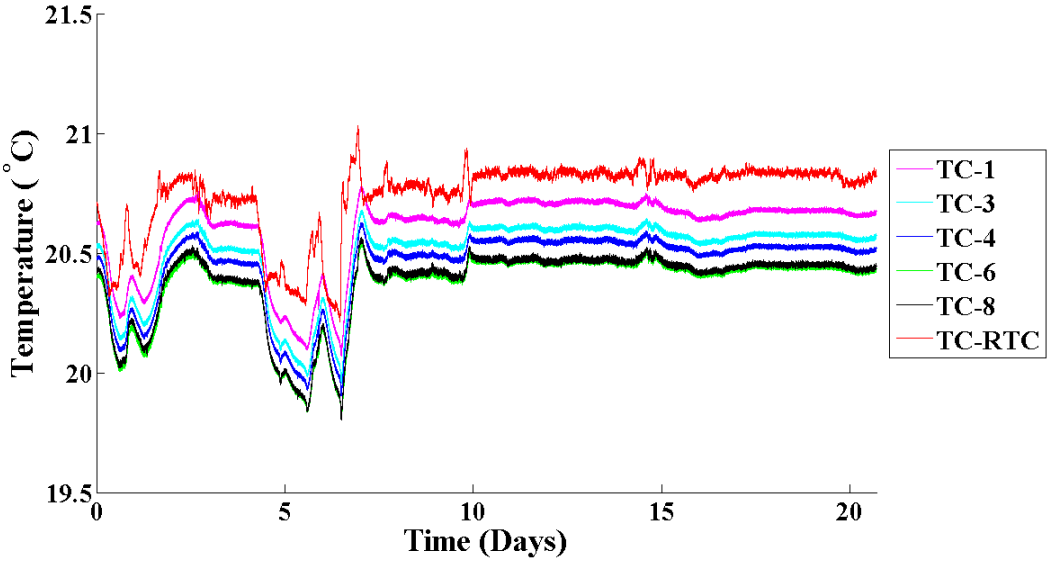

Figure B.5: Variation of room temperature and uncorrected *in-situ* temperatures at different locations inside the core holder during Sample No. 3.

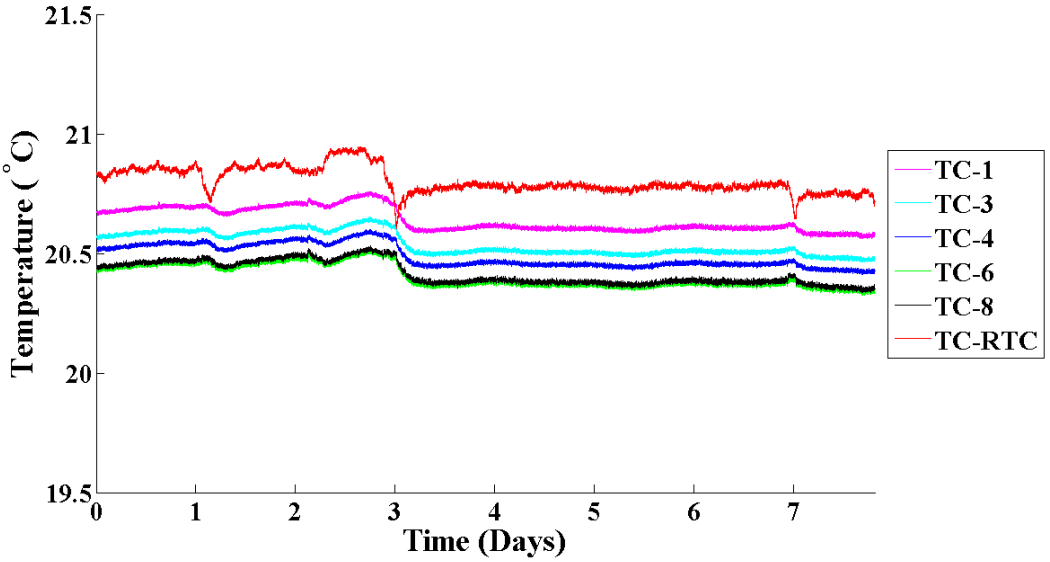

Figure B.6: Variation of room temperature and uncorrected *in-situ* temperatures at different locations inside the core holder during Sample No. 4.

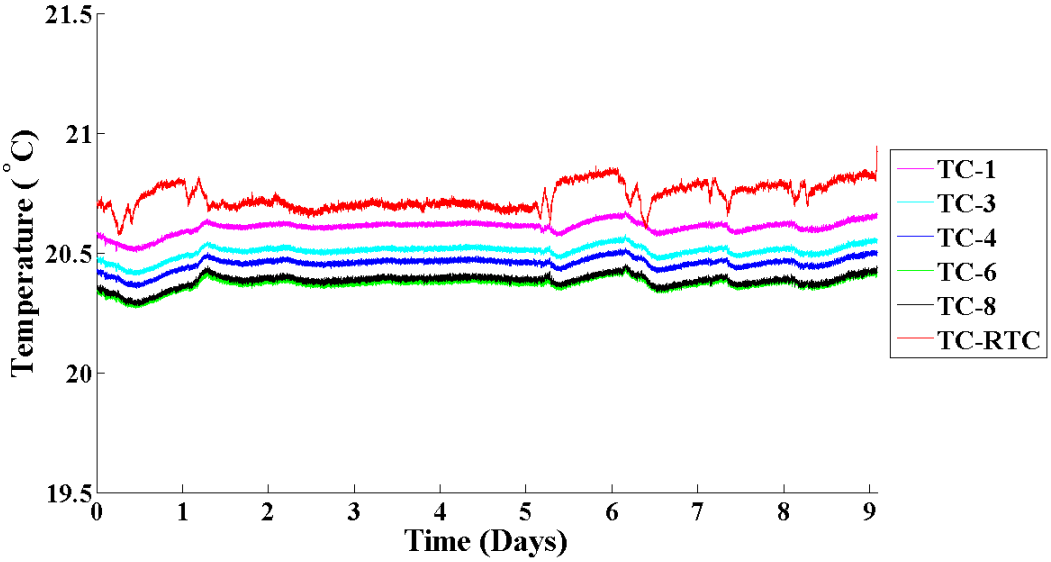

Figure B.7: Variation of room temperature and uncorrected *in-situ* temperatures at different locations inside the core holder during Sample No. 5.

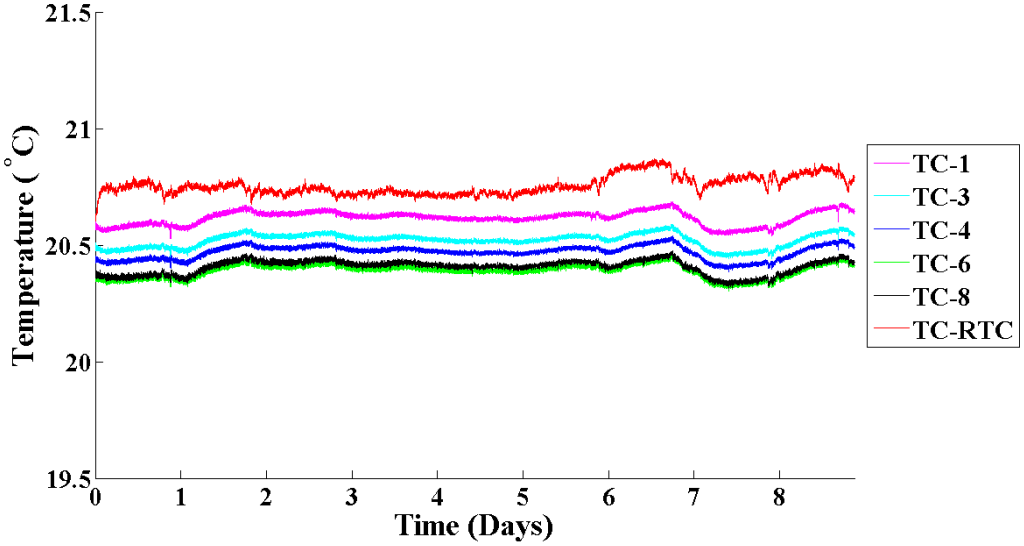

Figure B.8: Variation of room temperature and uncorrected *in-situ* temperatures at different locations inside the core holder during Sample No. 6.

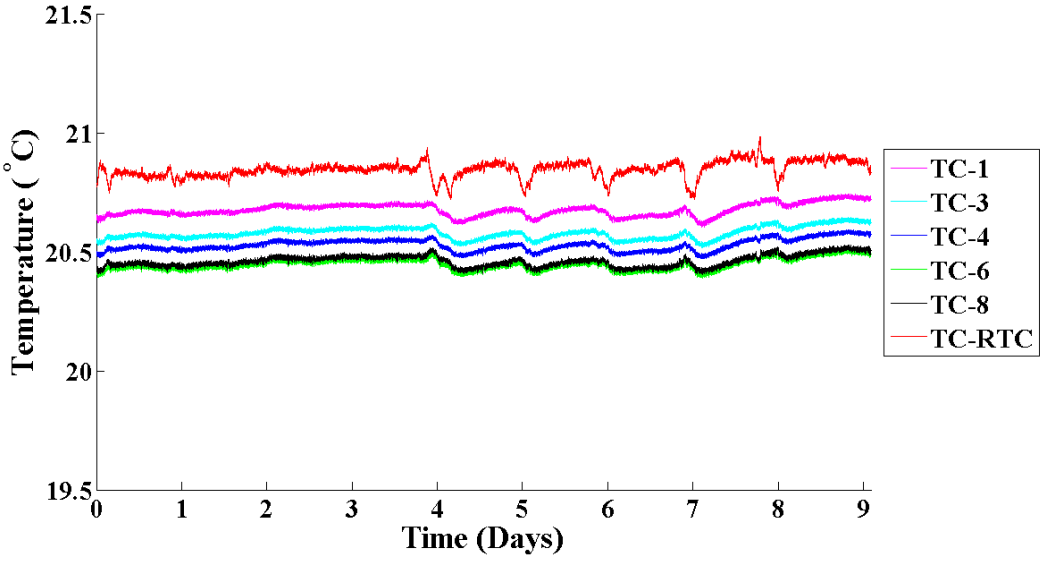

Figure B.9: Variation of room temperature and uncorrected *in-situ* temperatures at different locations inside the core holder during Sample No. 7.

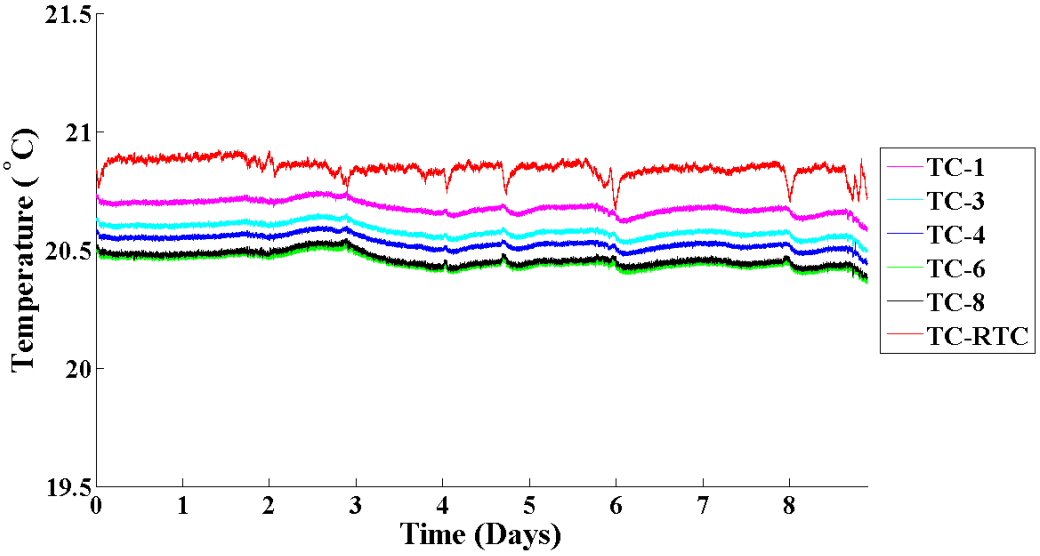

Figure B.10: Variation of room temperature and uncorrected *in-situ* temperatures at different locations inside the core holder during Sample No. 8.

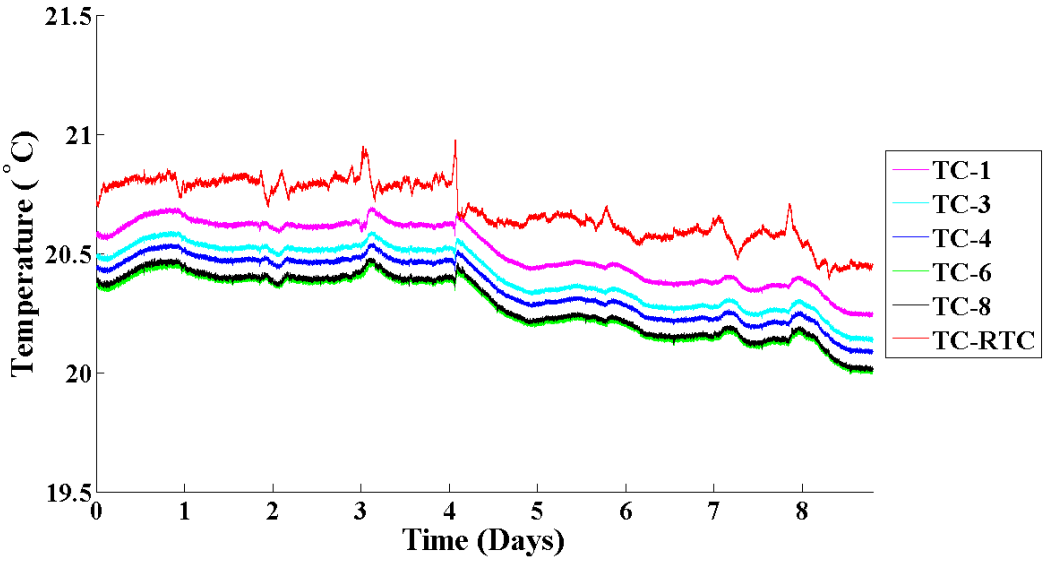

Figure B.11: Variation of room temperature and uncorrected *in-situ* temperatures at different locations inside the core holder during Sample No. 9.

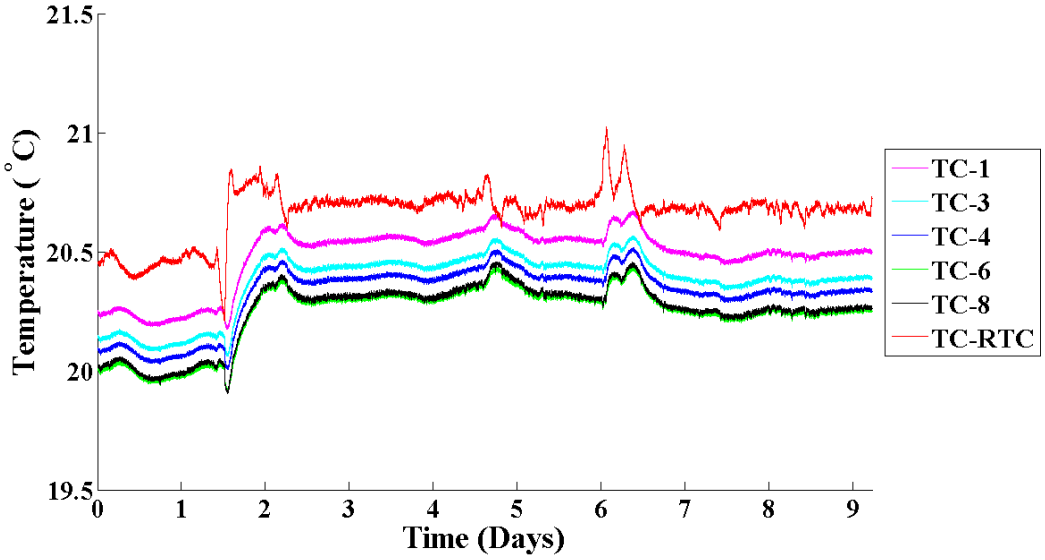

Figure B.12: Variation of room temperature and uncorrected *in-situ* temperatures at different locations inside the core holder during Sample No. 10.

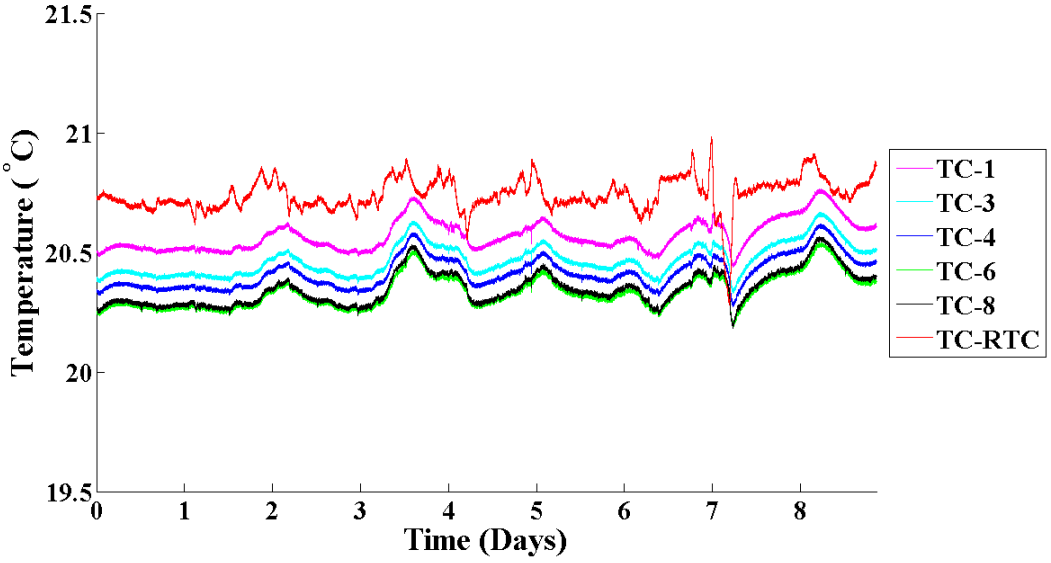

Figure B.13: Variation of room temperature and uncorrected *in-situ* temperatures at different locations inside the core holder during Sample No. 11.

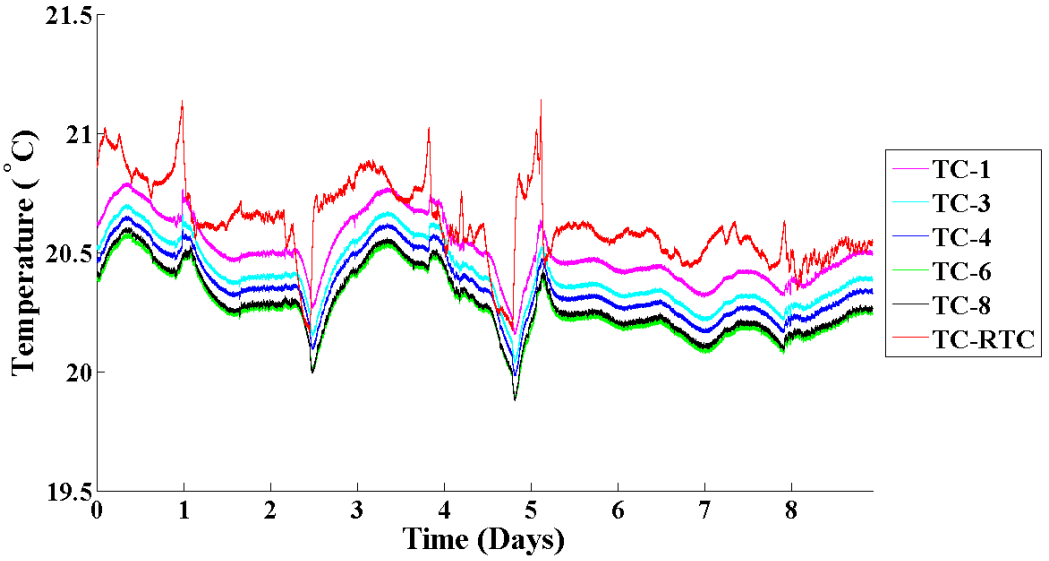

Figure B.14: Variation of room temperature and uncorrected *in-situ* temperatures at different locations inside the core holder during Sample No. 12.

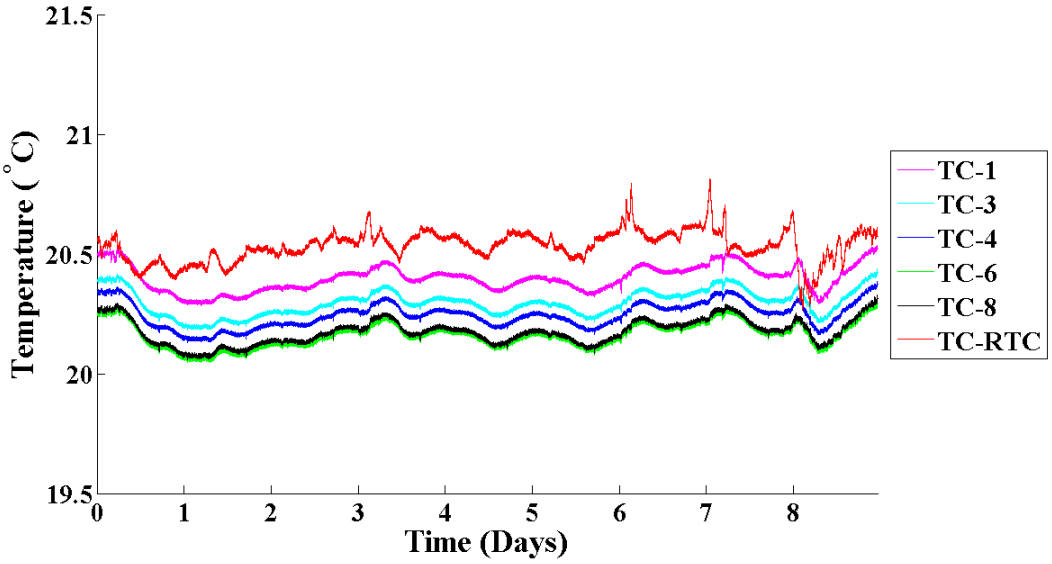

Figure B.15: Variation of room temperature and uncorrected *in-situ* temperatures at different locations inside the core holder during Sample No. 13.

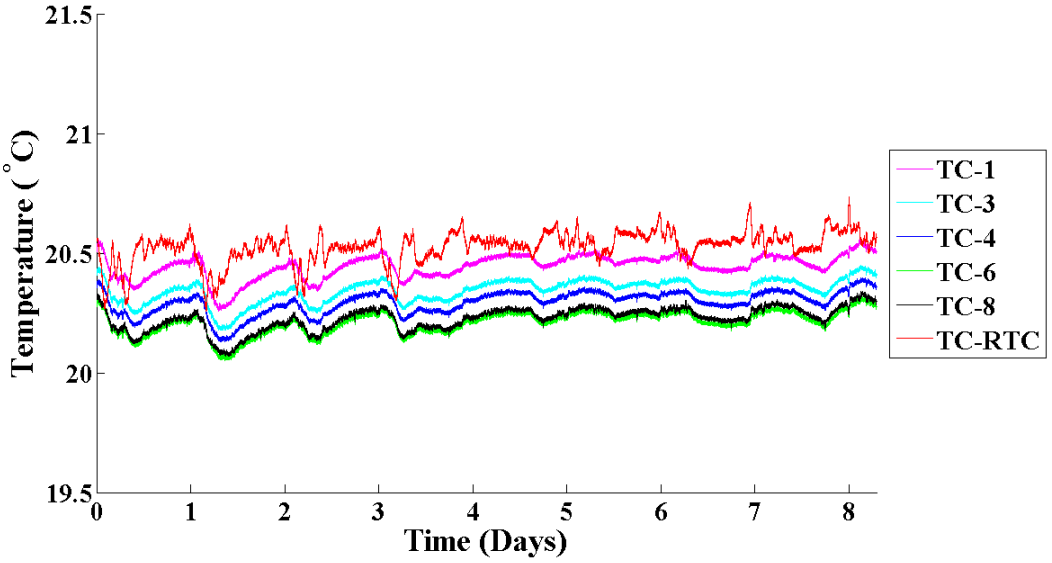

Figure B.16: Variation of room temperature and uncorrected *in-situ* temperatures at different locations inside the core holder during Sample No. 14.

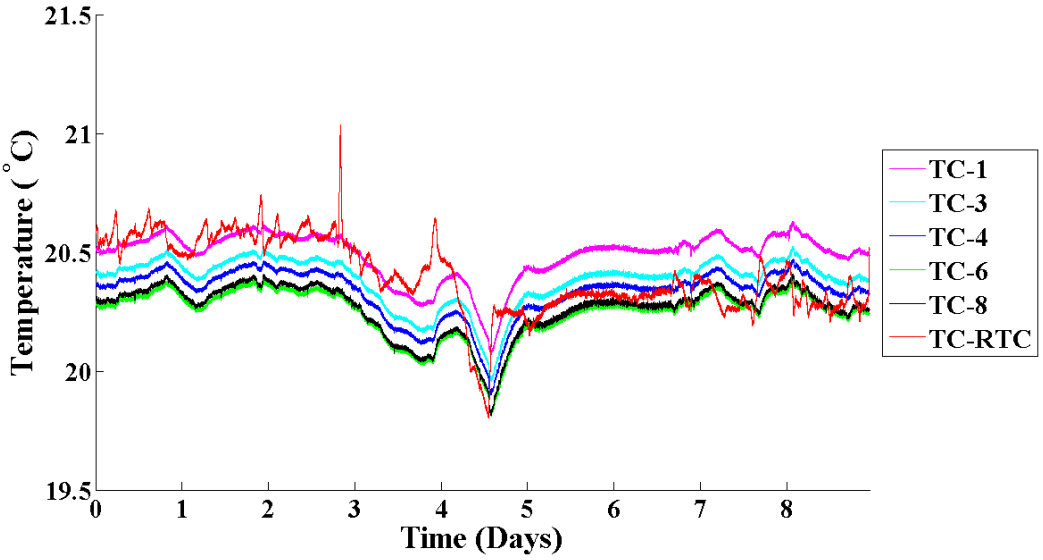

Figure B.17: Variation of room temperature and uncorrected *in-situ* temperatures at different locations inside the core holder during Sample No. 15.

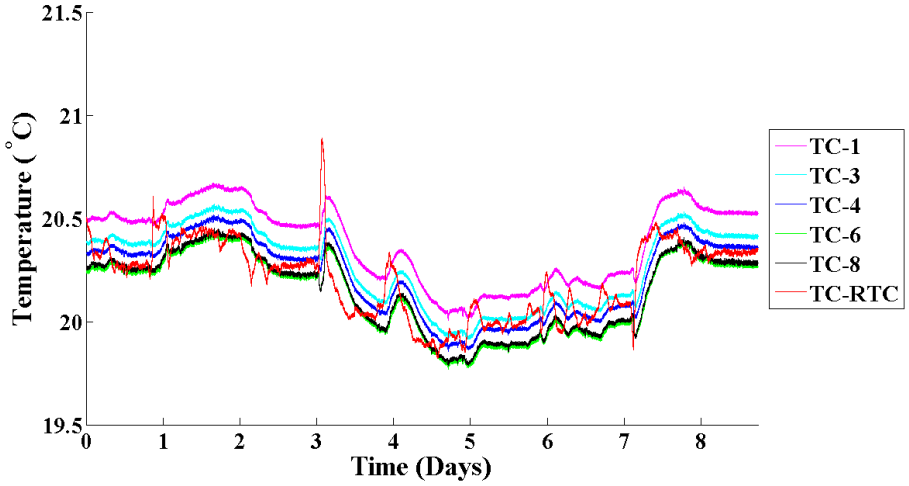

Figure B.18: Variation of room temperature and uncorrected *in-situ* temperatures at different locations inside the core holder during Sample No. 16.

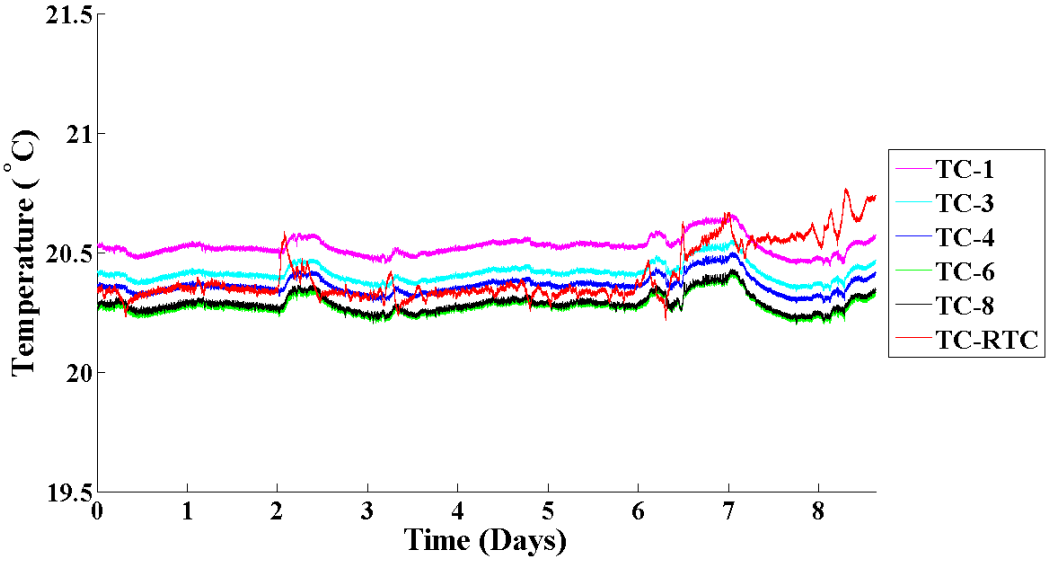

Figure B.19: Variation of room temperature and uncorrected *in-situ* temperatures at different locations inside the core holder during Sample No. 17.

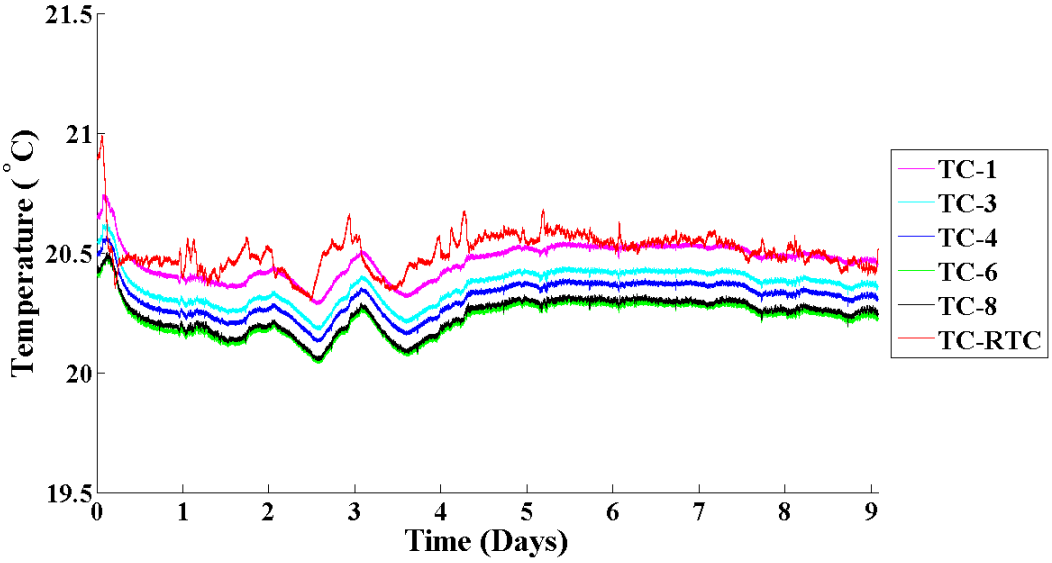

Figure B.20: Variation of room temperature and uncorrected *in-situ* temperatures at different locations inside the core holder during Sample No. 18.

B.1.3 Variation of corrected temperature readings obtained from different thermocouples for all the sampling points

This section provides the variation of temperature readings obtained from thermocouples after considering calibration into account during the collection of subsequent sampling points.

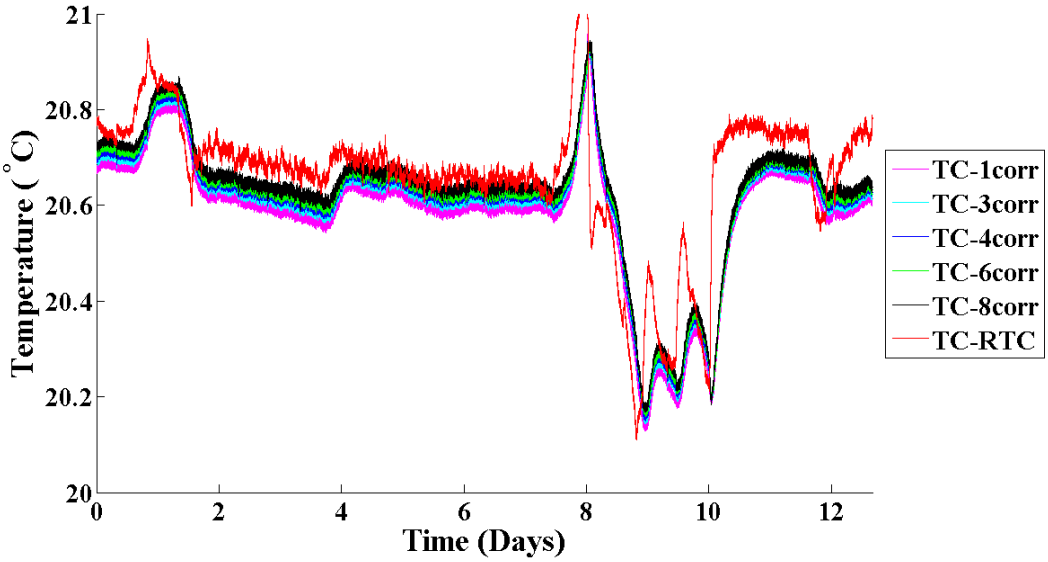

Figure B.21: Variation of room temperature and corrected *in-situ* temperatures at different locations inside the core holder during Sample No. 1.

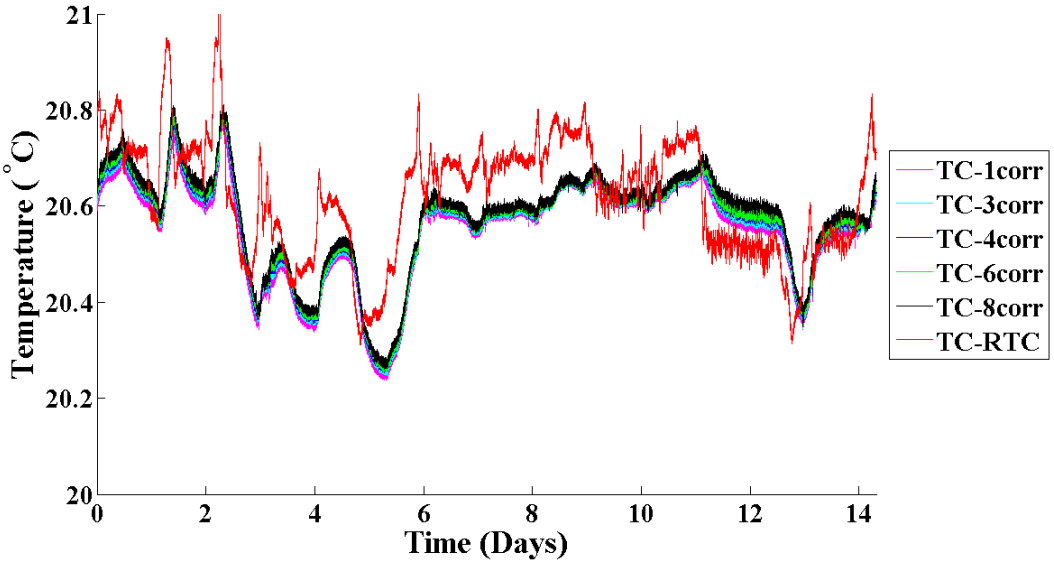

Figure B.22: Variation of room temperature and corrected *in-situ* temperatures at different locations inside the core holder during Sample No. 2.

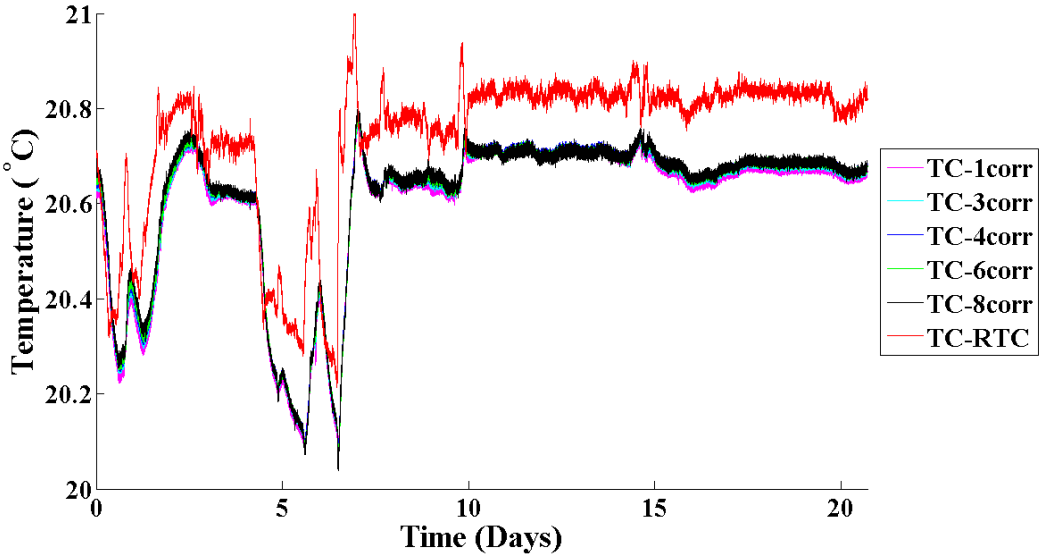

Figure B.23: Variation of room temperature and corrected *in-situ* temperatures at different locations inside the core holder during Sample No. 3.

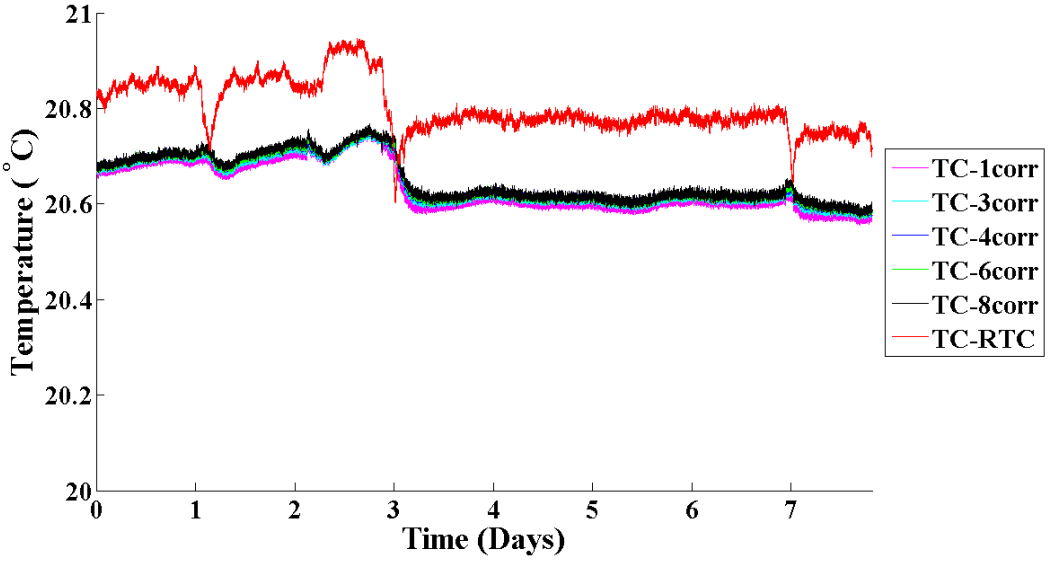

Figure B.24: Variation of room temperature and corrected *in-situ* temperatures at different locations inside the core holder during Sample No. 4.

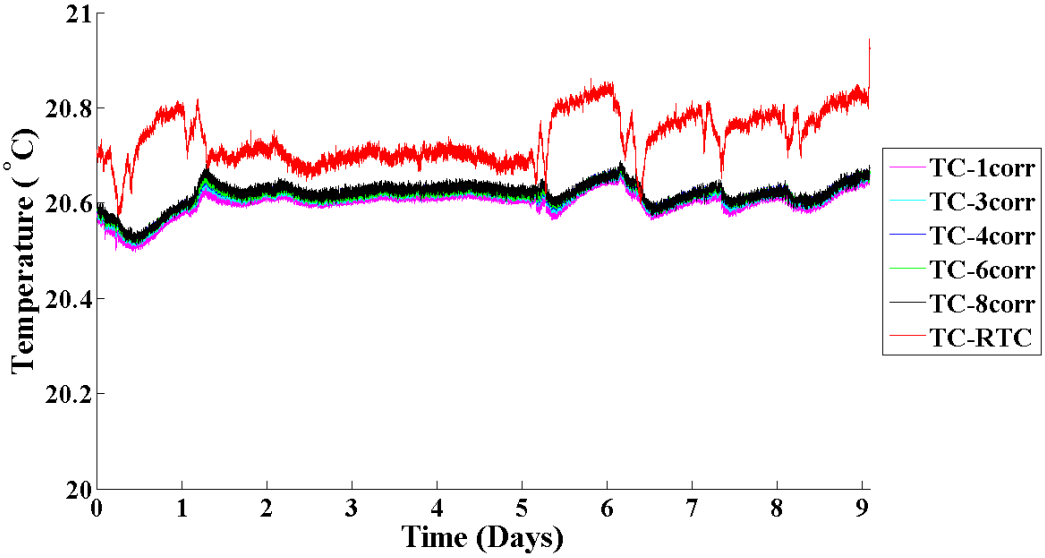

Figure B.25: Variation of room temperature and corrected *in-situ* temperatures at different locations inside the core holder during Sample No. 5.

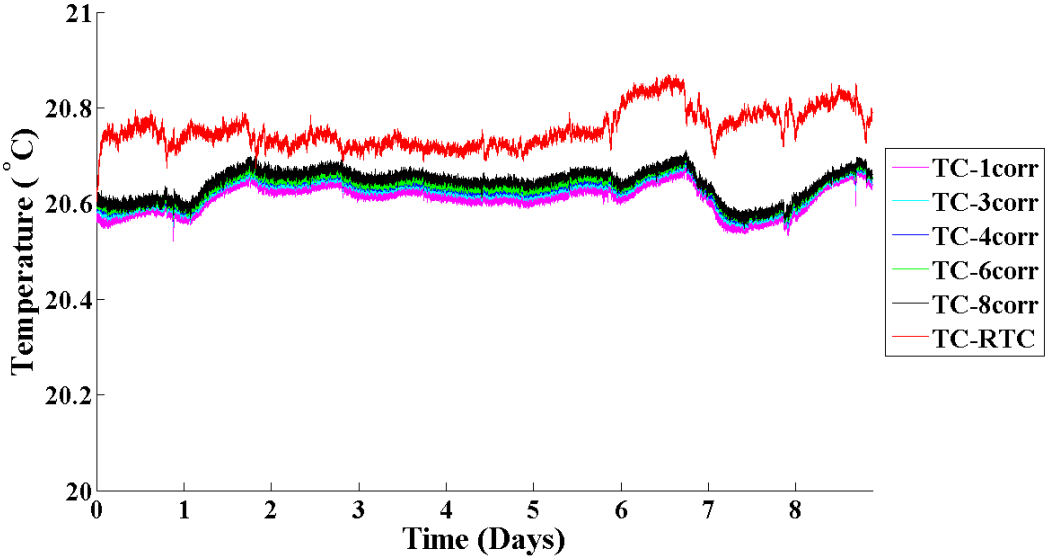

Figure B.26: Variation of room temperature and corrected *in-situ* temperatures at different locations inside the core holder during Sample No. 6.

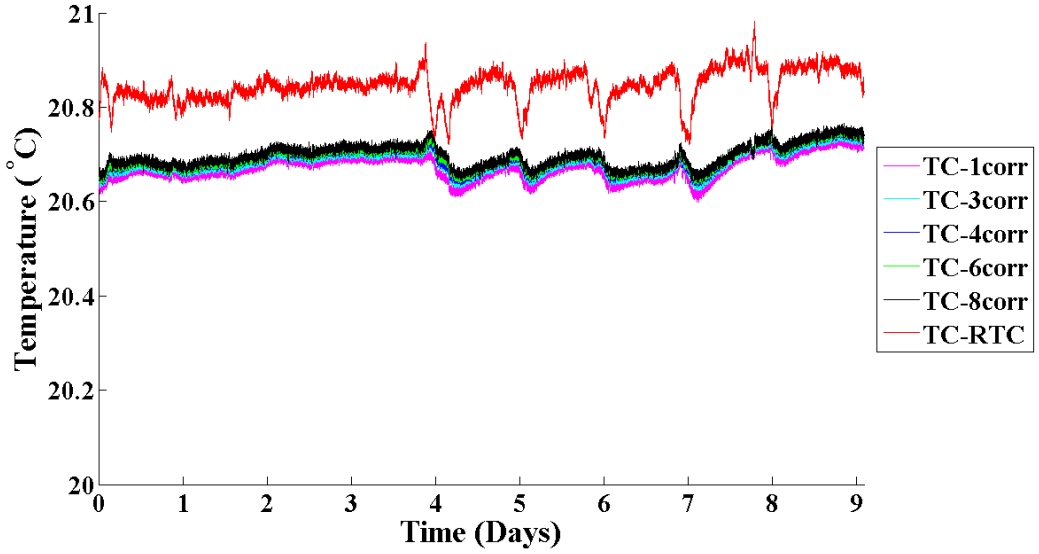

Figure B.27: Variation of room temperature and corrected *in-situ* temperatures at different locations inside the core holder during Sample No. 7.

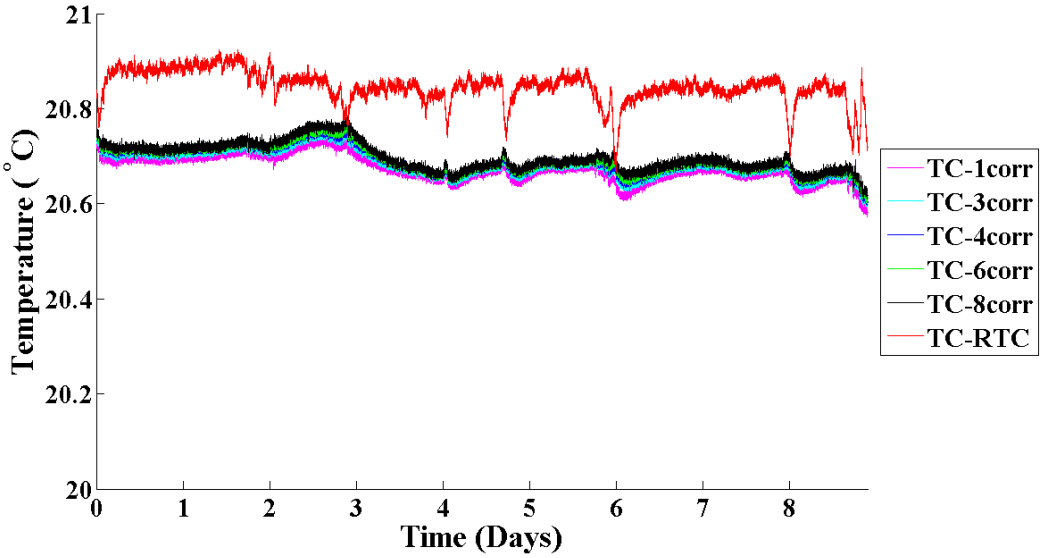

Figure B.28: Variation of room temperature and corrected *in-situ* temperatures at different locations inside the core holder during Sample No. 8.

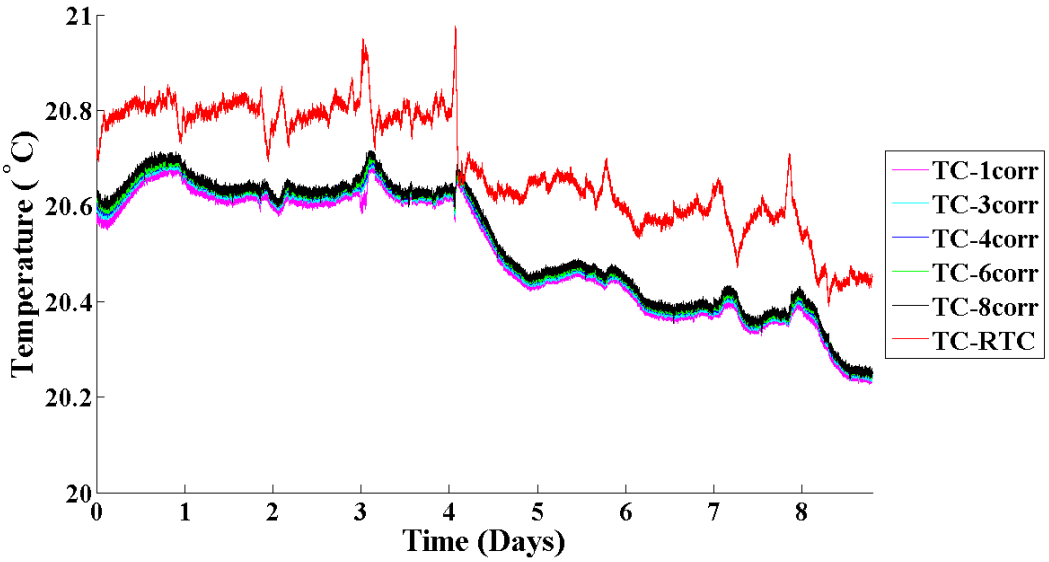

Figure B.29: Variation of room temperature and corrected *in-situ* temperatures at different locations inside the core holder during Sample No. 9.

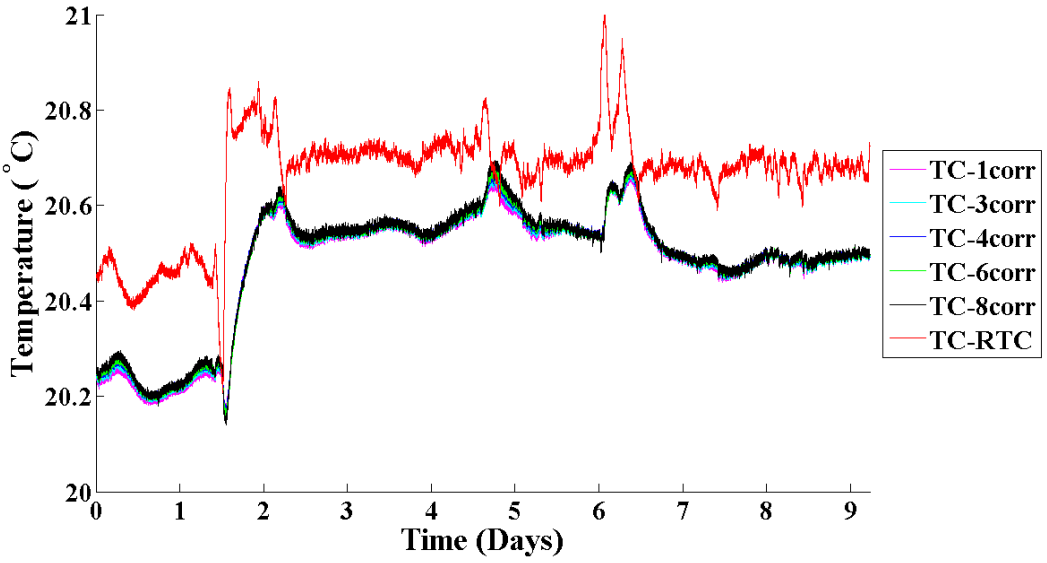

Figure B.30: Variation of room temperature and corrected *in-situ* temperatures at different locations inside the core holder during Sample No. 10.

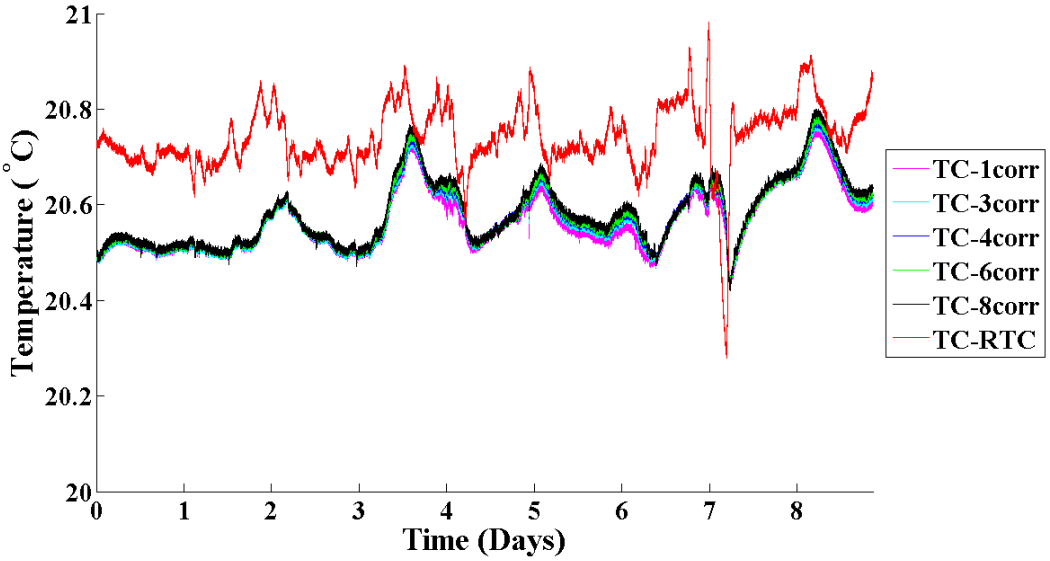

Figure B.31: Variation of room temperature and corrected *in-situ* temperatures at different locations inside the core holder during Sample No. 11.

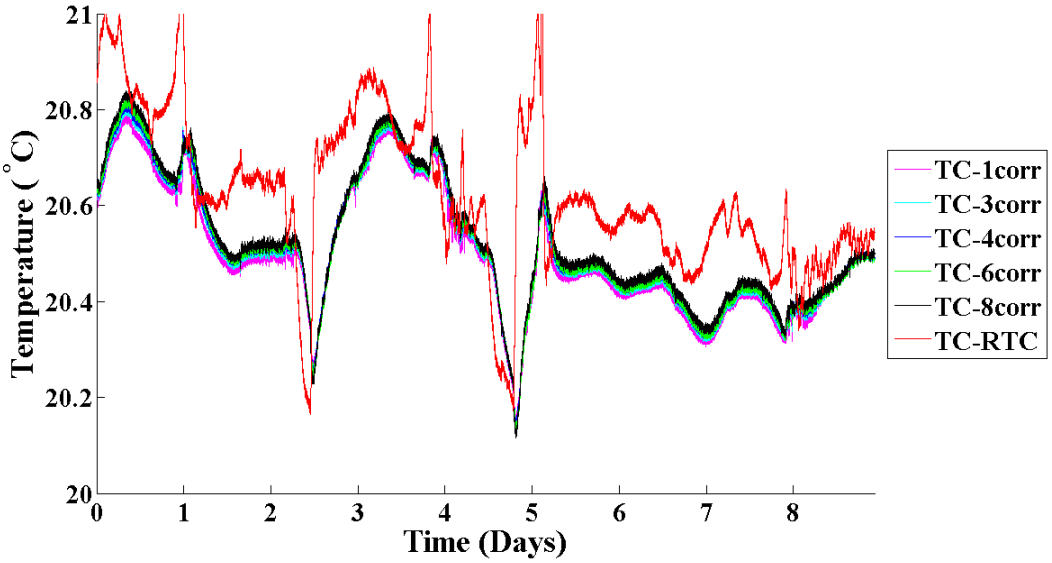

Figure B.32: Variation of room temperature and corrected *in-situ* temperatures at different locations inside the core holder during Sample No. 12.

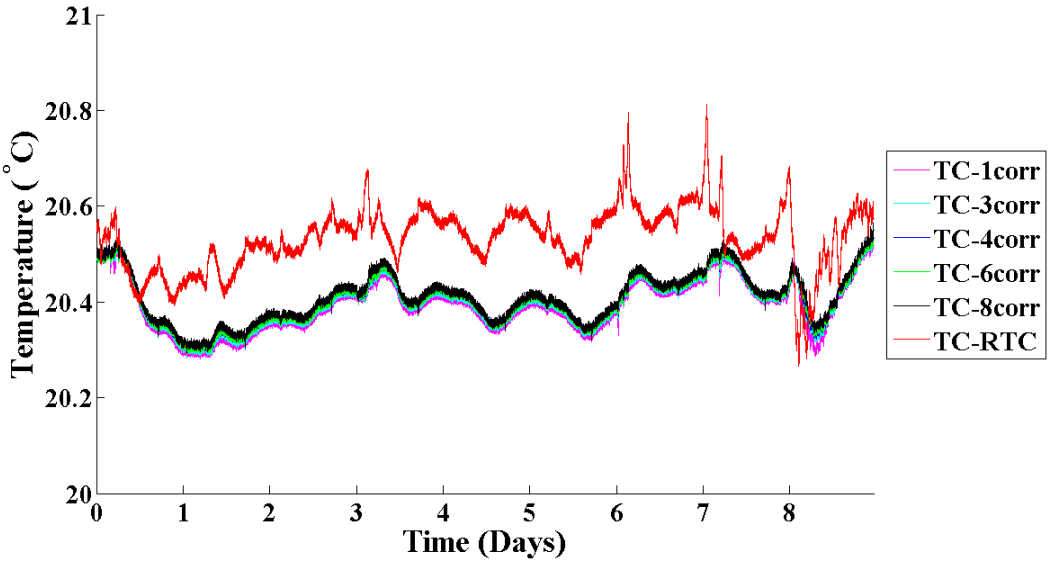

Figure B.33: Variation of room temperature and corrected *in-situ* temperatures at different locations inside the core holder during Sample No. 13.

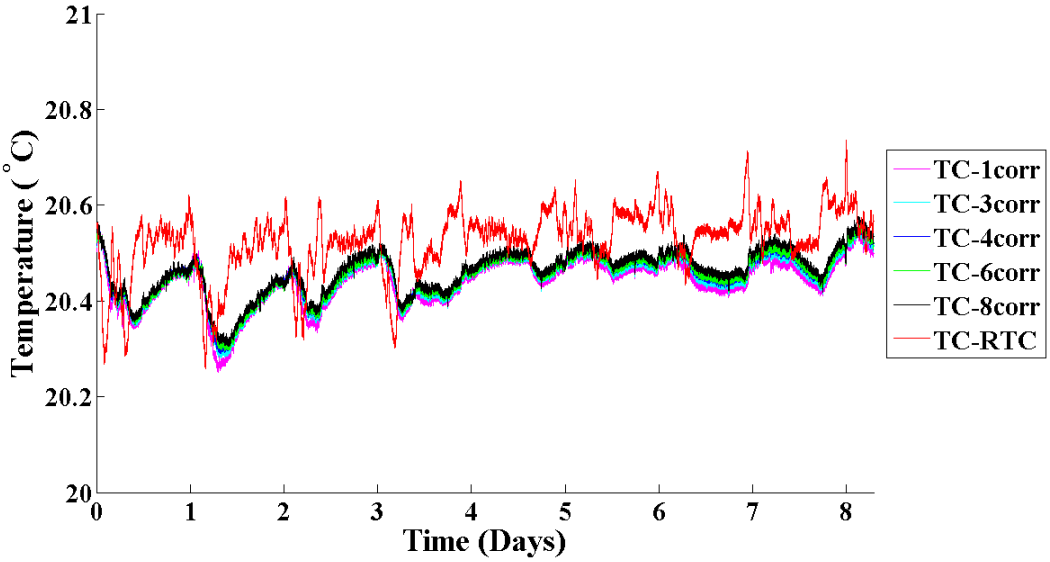

Figure B.34: Variation of room temperature and corrected *in-situ* temperatures at different locations inside the core holder during Sample No. 14.

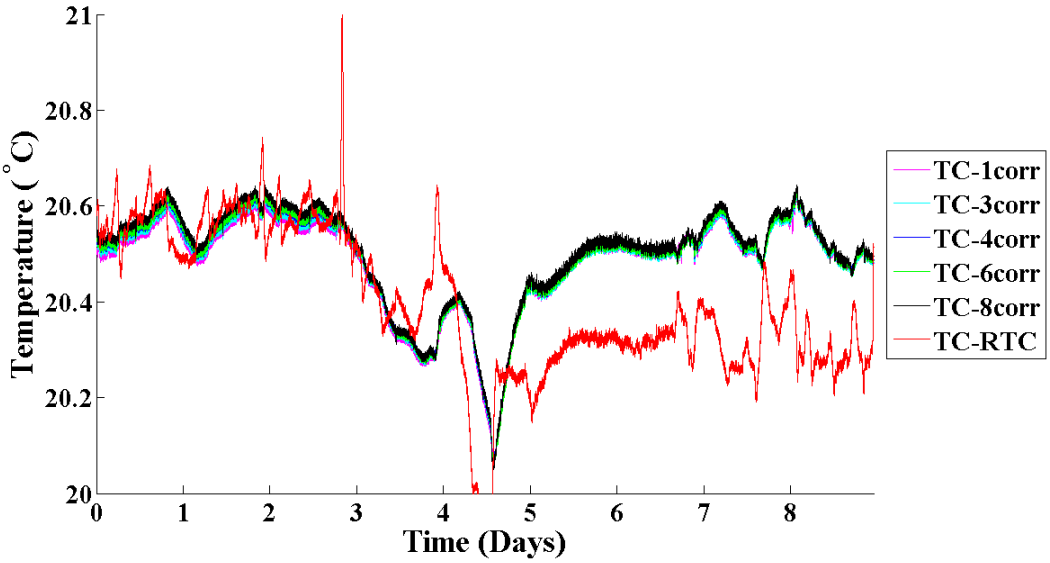

Figure B.35: Variation of room temperature and corrected *in-situ* temperatures at different locations inside the core holder during Sample No. 15.

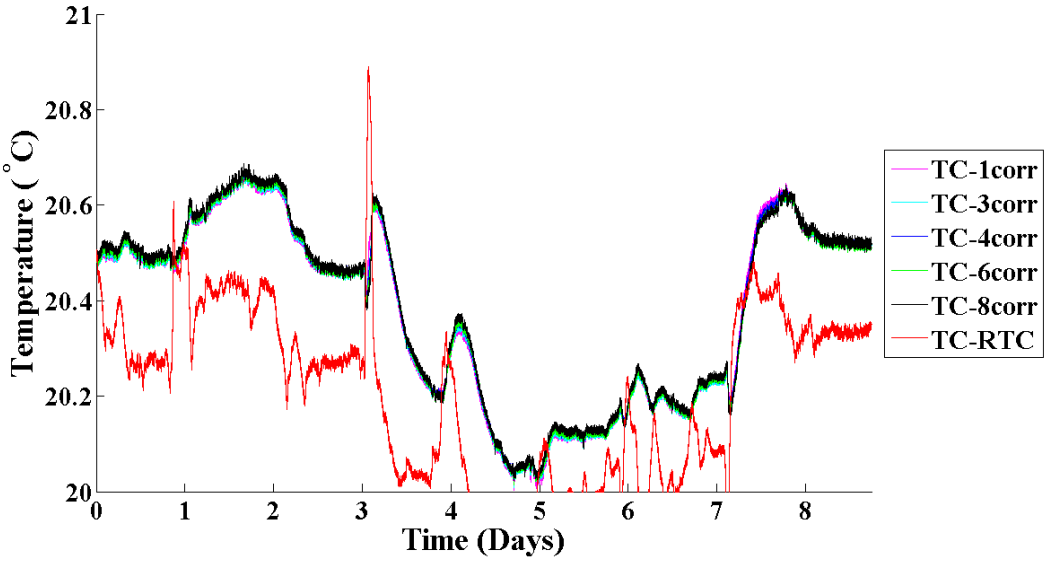

Figure B.36: Variation of room temperature and corrected *in-situ* temperatures at different locations inside the core holder during Sample No. 16.

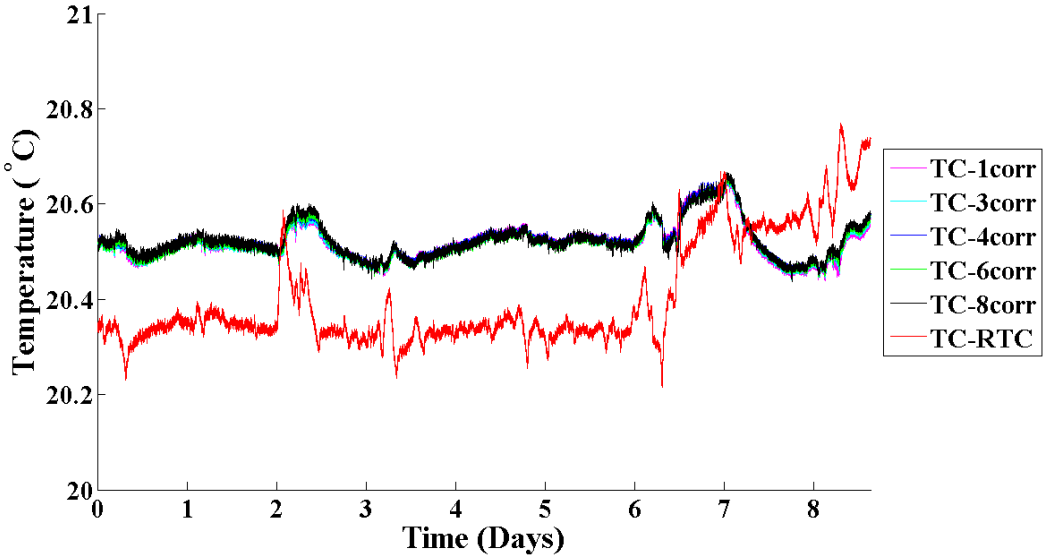

Figure B.37: Variation of room temperature and corrected *in-situ* temperatures at different locations inside the core holder during Sample No. 17.

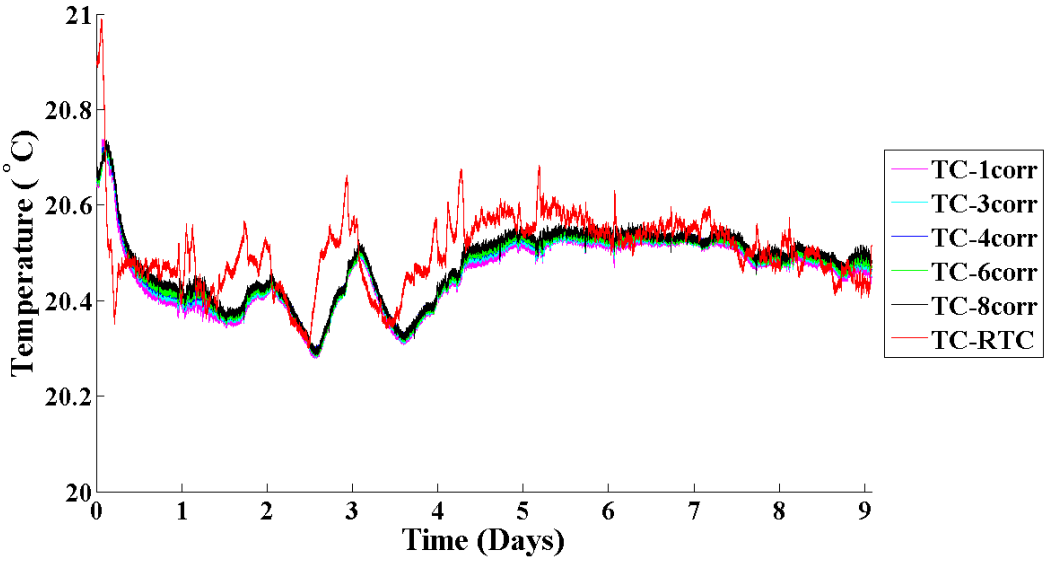

Figure B.38: Variation of room temperature and uncorrected *in-situ* temperatures at different locations inside the core holder during Sample No. 18.

C.1 Gas Measurements

C.1.1 Preparation of calibration standards of gases

CH_4 and CO_2 standards were prepared in 12.5 ml vials with a PTFE septum. The vials were evacuated at first and the pressure inside the vial was measured by means of a ram pressure gauge. The percentage of vacuum achieved inside the vial was calculated from the pressure-vacuum chart. In reality, we cannot achieve 100% vacuum and so the volume of air remaining inside the vial after evacuation was calculated which was referred as V_{air}. Calculations were performed based on the remaining volume of air (V_{air}) inside the vial for making a standard with a known volume percentage.

Making of CH_4 standards

Calibration standards for CH_4 were made for 5.02%, 10.17%, 15.09%, 20% and 30.08% by volume respectively. The required volume of CH_4 to be added for making a standard with known percentage volume was calculated using the equation below:

$$\text{CH}_4\ (\%) = \frac{\text{volume of CH}_4\ (\text{ml})}{\text{volume of CH}_4\ (\text{ml}) + \text{V}_{air}\ (\text{ml})} \times 100 \qquad (\text{C.1})$$

The gas sample from each standard vials were injected into a methane GC (5700A Model) for three times and the peak area obtained after each injection was recorded. The average of the obtained peak areas pertaining to a particular standard were taken. Parameters related to making of CH_4 standards have been shown in Table C.1.1. Variation of volume(%) of CH_4 with the average peak area was fitted linearly to produce the required calibration curve. The calibration equation for methane measurements is stated below:

$$\text{CH}_4\ (\%) = 2.33 \times 10^{-5} \times \text{ average peak area} + 0.9989 \qquad (\text{C.2})$$

Making of CO_2 standards

Calibration standards for CO_2 were made for 4.84%, 9.94%, 20%, 39.95% and 60% by volume respectively. The required volume of CO_2 to be added for making

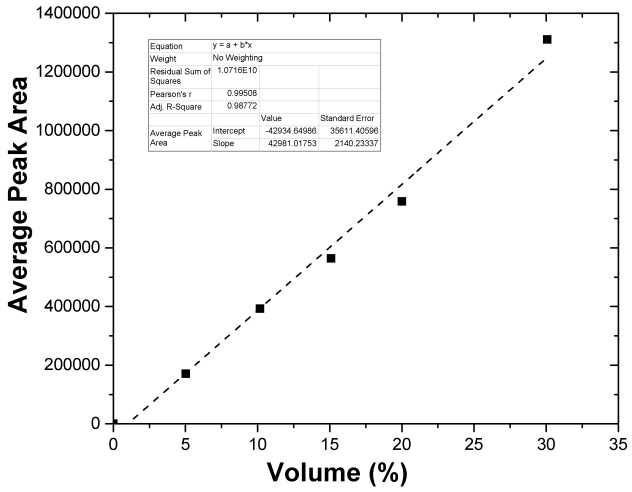

Figure C.1: Calibration curve of CH_4

Table C.1: The volume of CH_4 (ml) added into 12.5 ml vials, volume (%) of CH_4, volume of air remaining inside the vial after evacuation and the obtained peak areas for making of CH_4 calibration standards

CH_4 added (ml)		0.14	0.3	0.51	0.66	1.14
V_{air} (ml)		2.65	2.65	2.87	2.64	2.65
$CH_4(\%)$		5.02	10.17	15.09	20	30.08
Peak Area	Trial i	172750	396610	566940	768620	1313900
	Trial ii	170680	393560	562740	754040	1319500
	Trial iii	169610	387780	562480	751230	1298600
	Average	171013.3333	392650	564053.3333	757963.3333	1310666.67

a standard with known percentage volume was calculated using the equation below:

$$CO_2\ (\%) = \frac{\text{volume of } CO_2\ (\text{ml})}{\text{volume of } CO_2\ (\text{ml}) + V_{air}\ (\text{ml})} \times 100 \qquad (C.3)$$

The gas sample from each standard vials were injected into a carbon dioxide GC (5890 Model) for three times and the peak area obtained after each injection was recorded. The average of the obtained peak areas pertaining to a particular standard were taken. Parameters related to making of CO_2 standards have been shown in Table C.1.1. Variation of volume(%) of CO_2 with the average peak area was fitted linearly to produce the required calibration curve. The calibration equation for

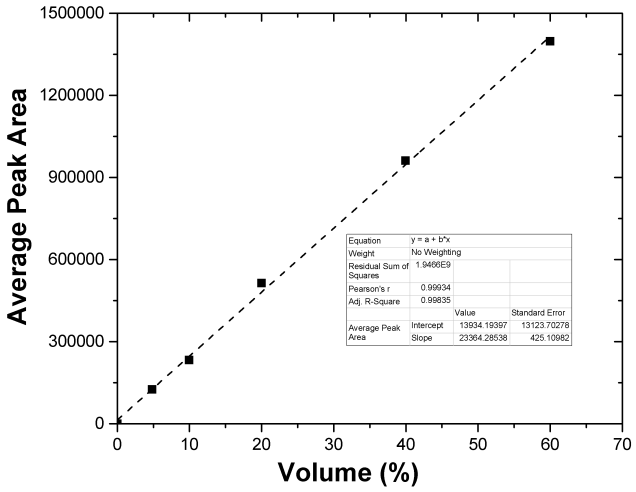

Figure C.2: Calibration curve of CO_2

Table C.2: The volume of CO_2 (ml) added into 12.5 ml vials, volume (%) of CO_2, volume of air remaining inside the vial after evacuation and the obtained peak areas for making of CO_2 calibration standards

CO_2 added (ml)		0.14	0.31	0.73	1.75	3.9
V_{air} (ml)		2.75	2.81	2.92	2.63	2.6
CO_2(%)		4.84	9.94	20	39.95	60
Peak Area	Trial i	116777	241546	487412	957040	1123134
	Trial ii	118108	235977	543824	959071	1149519
	Trial iii	141268	221598	510057	968078	1235557
	Average	125384.3333	233040.3333	513764.3333	961396.3333	1169403.333

carbon dioxide measurements is stated below:

$$CO_2\ (\%) = 4.28 \times 10^{-5} \times \text{ average peak area} - 0.5964 \qquad (C.4)$$

C.1.2 Gas Measurements

Two methods were used for the gas measurements. Method 1 referred to the case when the peak area obtained after gas injection into a GC was within the calibration limit. Method 2 referred to the case when the peak area obtained was out of the range of calibration of the GC.

Method 1

In method 1, the volume of gas from the tedlar bag,also referred as V_{td} was directly transferred into a previously evacuated 12.5 ml vial by means of a sterile syringe. Percentage of vacuum in the vial and therefore the volume of air remaining inside (V_{air}) was noted down before the gas was injected into the vial. The gas sample from 12.5 ml vial was directly injected into a GC for three times and the average peak area for the trials were obtained. Volume(%) of CH_4 and CO_2 can be obtained from the average peak area by using Eqs. C.2 and C.4 respectively. Samples 1 to11 and from 16 to 18

Method 2

In method 2, the gas from the tedlar bag was transferred to a previously evacuated 12.5 ml vial. The peak area was obtained by injection of the gas sample from the vial into a GC and if the peak area was out of the calibration range, another dilution of the collected gas sample was made. Generally 10% dilution was made. The quantity of gas needed to occupy 10% by volume in a second evacuated vial was calculated at first. The calculated amount of gas from the first vial was transferred to the second vial and the GC analysis was performed. Dilution technique was mostly employed for quantification of methane. The obtained peak area was then multiplied by 10 and the calibration equation for methane was used to get the volume(%) of CH_4.

C.1.3 Solubility correction

The quantity of CH_4 and CO_2 (ml) dissolved in the effluent have been shown in Table C.1.3. The temperature used for calculating the dissolved quantity of gases was 20°C.

Table C.3: Quantity of CH_4 and CO_2 dissolved in 100 ml of core flooding effluent samples.

Sample No	Dissolved CH_4 (ml)	Dissolved CO_2 (ml)
1	0.067	3.88
2	0.132	16.78
3	0.107	5.83
4	0.064	8.47
5	0.053	1.86
6	0.171	19.13
7	0.27	44.7
8	0.151	25.72
9	0.611	37.48
10	0.701	13.52
11	1.086	24.57
12	1.879	24.43
13	1.001	42.96
14	0.718	38.68
15	0.706	42.64
16	1.328	39.45
17	1.044	41.34
18	1.109	56.41

D.1 Error Calculations

D.1.1 Error Analysis

Three kinds of error have been computed for the gas generation data corresponding to each sampling point which are stated below in the subsequent subsections. Finally, the root mean square of the errors have been taken for computing the total error associated with each sampling point. The total errors are added while calculating the cumulative production of the gases. The errors associated with each sampling point for CH_4 have been shown in Table D.4. The errors associated with each sampling point for CO_2 have been shown in Table D.5.

Standard deviation and the associated error

Standard deviation and mean of the peak areas corresponding to each sample was computed at first. Standard deviation was either added or subtracted to each peak area obtained in a set of three trials for each sampling point. Addition was done when the peak area value was above the mean peak area in each sampling point. Substraction operation was performed when the peak area value was below the average peak area value associated with each sampling point. Finally, the mean of the new set of peak areas were taken and the volume(%) of the gases were computed using Eqs. C.2 and C.4 for CH_4 and CO_2 respectively. The error associated with the standard deviation was calculated by evaluating the difference in the volume(%) values obtained considering with and without standard deviations.

Measurement error

The gases from the tedlar bag were taken out by means of a 10 ml syringe. The least count of the syringe was 1 ml. Half of the least count value (i.e. 0.5 ml) was added to the value of the collected gas volume in order to get a modified gas collection data for each sampling point . The error was computed by evaluating the difference in the volume of the gases (CH_4 and CO_2) obtained considering with and without least count. Volume(%)of the gases obtained using using Eqs. C.2 and C.4 were kept constant while calculating the error.

Calibration error

The least count of the syringes used for preparing the gas standards were considered for computing the calibration error. The least count of the used syringes were added to the volume of gases added to a 12.5 ml vial for preparing the standards. The modified volume(%) of the gases were computed using Eqs. C.1 and C.3. Calibration curves for CH_4 and CO_2 were modified. Calibration error was calculated by evaluating the difference in the volume(%) values obtained considering with and without the corrected calibration curve.

The corrected calibration equation for methane measurements is stated below.

$$CH_4\ (\%) = 2.33 \times 10^{-5} \times \text{ average peak area} + 1.183 \qquad (D.1)$$

The corrected calibration equation for carbon dioxide measurements is stated below.

$$CO_2\ (\%) = 4.28 \times 10^{-5} \times \text{ average peak area} - 0.3798 \qquad (D.2)$$

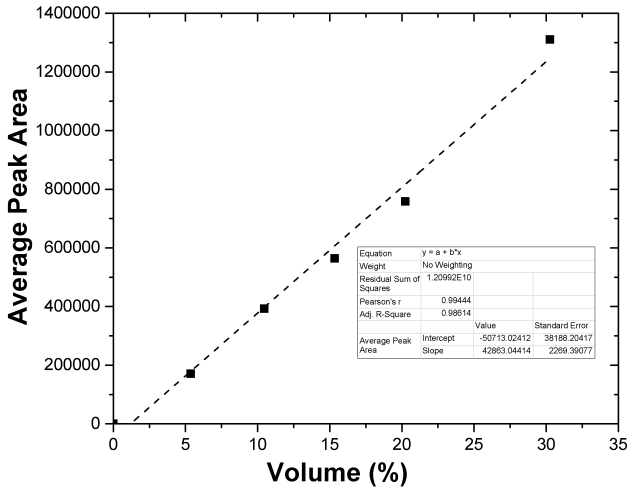

Figure D.1: Corrected Calibration curve of CH_4

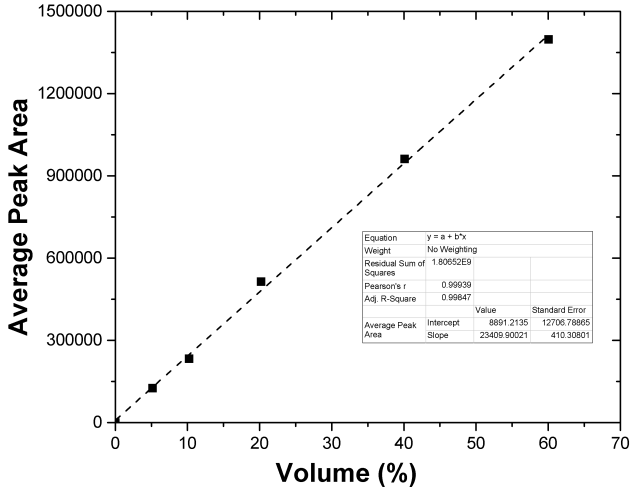

Figure D.2: Corrected Calibration curve of CO_2

Table D.4: Uncertainty in the measurements of CH_4 production.

Sample No.	Average Peak Area	Standard Deviation Error $\pm$ μmol/gm-coal	Measurement Error $\pm$ μmol/gm-coal	Calibration Error $\pm$ μmol/gm-coal	Total Error $\pm$ μmol/gm-coal
1	36598.33	9.487×10^{-6}	5.812×10^{-4}	1.802×10^{-3}	0.0011
2	113426.6667	2.7×10^{-5}	1.143×10^{-3}	1.037×10^{-3}	0.00089
3	83780	3.77×10^{-5}	9.26×10^{-4}	4.52×10^{-4}	0.0006
4	32866.333	1.804×10^{-5}	5.54×10^{-4}	5.59×10^{-4}	0.00045
5	20728.33	5.96×10^{-6}	4.65×10^{-4}	5.63×10^{-4}	0.00042
6	160200	1.16×10^{-4}	1.49×10^{-3}	7.34×10^{-4}	0.00096
7	278660	2.96×10^{-4}	2.35×10^{-3}	1.18×10^{-3}	0.0015
8	136833.33	1.767×10^{-4}	1.313×10^{-3}	8.392×10^{-4}	0.0009
9	2555.7	1.7×10^{-4}	5.31×10^{-3}	1.955×10^{-3}	0.0033
10	799492.6	5.21×10^{-4}	6.08×10^{-3}	1.71×10^{-3}	0.0037
11	2961933.33	n/a	0.0094	n/a	0.0094
12	2188566.7	1.11×10^{-3}	0.016	2.37×10^{-3}	0.0094
13	1146433.33	7.15×10^{-4}	8.69×10^{-3}	2.07×10^{-3}	0.0052
14	809483.33	8.89×10^{-4}	6.23×10^{-3}	1.64×10^{-3}	0.0038
15	795673.33	1.13×10^{-3}	6.13×10^{-3}	1.7×10^{-3}	0.0037
16	1534800	2.51×10^{-3}	0.011	2.69×10^{-3}	0.0067
17	1197300	7.37×10^{-4}	9.06×10^{-3}	1.81×10^{-3}	0.0054
18	1274033.33	3.3×10^{-4}	9.62×10^{-3}	2.25×10^{-3}	0.0057

Table D.5: Uncertainty in the measurements of CO_2 production.

Sample No.	Average Peak Area	Standard Deviation Error $\pm$ μmol/gm-coal	Measurement Error $\pm$ μmol/gm-coal	Calibration Error $\pm$ μmol/gm-coal	Total Error $\pm$ μmol/gm-coal
1	110047.6667	2.075×10^{-3}	0.0314	1.961×10^{-3}	0.0182
2	429592	5.72×10^{-4}	5.58×10^{-3}	9.71×10^{-4}	0.0033
3	158474.3333	2.26×10^{-4}	1.94×10^{-3}	4.8×10^{-4}	0.0012
4	223835	3.9×10^{-4}	2.82×10^{-3}	6×10^{-4}	0.0017
5	59983	8.03×10^{-5}	6.18×10^{-4}	6.28×10^{-4}	0.00051
6	487770	1.814×10^{-3}	6.36×10^{-3}	6.95×10^{-4}	0.0038
7	1121300	2.77×10^{-3}	0.015	7.08×10^{-4}	0.0088
8	651356.67	1.323×10^{-3}	8.558×10^{-3}	7.057×10^{-4}	0.005
9	942468.33	1.87×10^{-3}	0.012	1.19×10^{-3}	0.007
10	353179.28	2×10^{-3}	4.05×10^{-3}	1.34×10^{-3}	0.0027
11	622509	3.43×10^{-3}	8.17×10^{-3}	1.035×10^{-3}	0.0052
12	619121.33	3.1×10^{-3}	8.12×10^{-3}	1.25×10^{-3}	0.0051
13	1078242.67	3.57×10^{-3}	0.014	1.03×10^{-3}	0.0084
14	972429.67	6.15×10^{-4}	0.013	9.56×10^{-4}	0.0075
15	1070305.33	3.53×10^{-3}	0.014	9.18×10^{-4}	0.0084
16	991368	9.72×10^{-4}	0.013	1.3×10^{-3}	0.0076
17	1038027.67	1.2×10^{-3}	0.014	8.69×10^{-4}	0.0081
18	1411308	2.74×10^{-3}	0.019	8.31×10^{-4}	0.0111